To the Graduate Council:

I am submiting herewith a thesis written by Thomas C. Morse entitled "Characterization of Particle Collection Efficiency in an Ionizing Wet Scrubber." I have examined the final copy of this thesis for form and content and recommend that it be accepted in partial fulfillment of the requirements for the degree of Master of Science, with a major in Environmental Engineering.

Wayne T. Davis, Major Professor

We have read this thesis
and recommend its acceptance:

Accepted for the Council:

Associate Vice Chancellor and
Dean of The Graduate School

CHARACTERIZATION OF PARTICLE COLLECTION EFFICIENCY IN AN IONIZING WET SCRUBBER

A Thesis
Presented for the
Master of Science
Degree
The University of Tennessee, Knoxville

Thomas C. Morse
December 1996

DEDICATION

I dedicate this thesis to my father, William Morse, who once told me that "people never have time to do anything right the first time, but they always seem to have time to go back and fix it later." He taught me that anything worth doing is worth doing right the first time. That philosophy has made me the person I am today, and for that, I am extremely grateful.

ACKNOWLEDGEMENTS

I would like to take this opportunity to express my gratitude and appreciation to Dr. Wayne T. Davis, my major professor. Without his guidance, patience, and unending pursuit of perfection, this project would not have been successful. I would also like to thank Dr. Terry Miller, and Dr. James Smoot for serving on my committe.

It is also necessary to thank a former fellow graduate student, Sunil Abraham, and fellow graduate student, Vincent Adams, for their help with the many hours of data collection and data analysis.

A word of thanks to Ken, Sherman, and Clarence in the Civil and Environmental Engineering shop for their help with the setup and maintenance of the pilot plant.

A special word of thanks is also in order for Bob Rehberg at the Kingston Steam Plant, operated by TVA in Kingston, TN, for providing the flyash used during testing.

Last, but certainly not least, I must thank my dear wife Heather for her never ending support and for putting up with all of the late nights and early mornings.

Funding for the research was provided by Lockheed Martin Energy Systems, Inc.

ABSTRACT

The primary objectives of this study were to characterize and quantify the particle collection efficiency of an ionizing wet scrubber (IWS). The system tested consisted of a cross-flow packed bed pre-scrubber, an ionizer, and a second cross-flow packed bed scrubber in series.

The penetration of the system was studied as a function of particle diameter, gas flowrate, and packing media used in the scrubbers. Studies were conducted at gas flowrates of 500, 900 and 1100 ft^3/min (specific collector areas of 62.6, 34.8 and 28.5 respectively), for particle diameters ranging from 0.118 - 5.0 microns. Three types of packing were studied.

Three equations were developed as a function of specific collector area to describe the behavior of the IWS, which consists of an ionizer and a packed bed in series. The models have the following forms:

IWS: 62.6 SCA (For d_p= 0.075 - 3.2μ ; d_a=0.12 - 5.0μ)

$$Pt_{(62.6)IWS} = \exp\left[-\left(-0.48\, d_p^{\,2} + 3.07\, d_p + 2.02\right)\right] \times \left[0.006199\, d_a^{\,3} - 0.060103\, d_a^{\,2} + 0.011302\, d_a + 0.77037\right]^{(L/8)}$$

IWS: 34.8 SCA (For d_p= 0.075 - 3.2μ ; d_a=0.12 - 5.0μ)

$$Pt_{(34.8)IWS} = \exp\left[-\left(-0.43\, d_p^{\,2} + 2.60\, d_p + 1.20\right)\right] \times \left[0.006199\, d_a^{\,3} - 0.060103\, d_a^{\,2} + 0.011302\, d_a + 0.77037\right]^{(L/8)}$$

IWS: 28.5 SCA (For d_p= 0.075 - 3.2μ ; d_a=0.12 - 5.0μ)

$$Pt_{(28.5)IWS} = \exp [- (-0.66\ d_p^2 + 2.93\ d_p + 0.74)]$$

$$\times\ [0.006199\ d_a^3 - 0.060103\ d_a^2 + 0.011302\ d_a + 0.77037]^{(L/8)}$$

where Pt is the fractional penetration, d_p is the physical diameter of the particle in microns, d_a is the aerodynamic diameter of the particle in microns, and L is the depth of wetted packing in the direction of gas flow in feet.

TABLE OF CONTENTS

1. INTRODUCTION 1

2. LITERATURE REVIEW 3

2.1 PARTICLE COLLECTION IN A PACKED BED 4

2.2 ELECTROSTATICS 10

2.3 ELECTROSTATIC PRECIPITATION 17

2.4 IMAGE FORCE ATTRACTION 37

2.5 THE IONIZING WET SCRUBBER 41

3. PILOT PLANT SETUP, OPERATION, AND TESTING METHODS 47

3.1 PILOT PLANT SETUP 47

3.2 PILOT PLANT OPERATION 54

3.3 SAMPLING METHOD 59

3.4 SAMPLING LOCATIONS 63

3.5 SUMMARY OF TESTS CONDUCTED 64

4. RESULTS AND DISCUSSION 67

4.1 PARTICLE COLLECTION EFFICIENCY 67

4.2 PREDICTIVE MODEL FOR PARTICLE COLLECTION EFFICIENCY 73

5. CONCLUSIONS 122

BIBLIOGRAPHY 126

APPENDICES 128

VITA 186

LIST OF TABLES

Table		Page
2-1.	Ionization energies for various gases	29
2-2.	Comparison of measured efficiency and predicted efficiency using the Deutsch-Anderson and Matts-Ohnfeldt models	35
2-3.	Summary of overall mass collection efficiency	43
3-1.	Physical characteristics of Tellerettes packing media	50
3-2.	Operating voltage as a function of time under baseline operating conditions	55
3-3.	Operating voltage as a function of time under dry pre-scrubber and dry plate conditions	56
3-4.	Summary of tests	65
4-1.	Correlation coefficients as a function of k and SCA	110
B-1.	Test numbers and operating conditions, 500 acfm	139
B-2.	Summary of penetrations for various tests, 500 acfm	141
B-3.	Test numbers and operating conditions, 700 acfm	144
B-4.	Summary of penetrations for various tests, 700 acfm	145
B-5.	Test numbers and operating conditions, 900 acfm	146
B-6.	Summary of penetrations for various tests, 900 acfm	149
B-7.	Test numbers and operating conditions, 1100 acfm	154

B-8. Summary of penetrations for various tests, 1100 acfm.....156

C-1. Results of EPA Method V tests.....162

C-2. Summary of overall mass collection efficiency as measured by an OPC.....165

D-1. Results of fluorescent sphere tests..... 170

E-1. Determination of dust loading at 900 acfm..... 173

F-1. Mass carryover at p1wp2w and 900 acfm..... 178

F-2. Mass carryover at p1w35p2w and 900 acfm..... 178

G-1. Results of droplet carryover measurements..... 184

LIST OF FIGURES

Figure		Page
2-1.	Penetration as a function of particle diameter at 900 acfm	5
2-2.	Effect of gas flowrate through wetted packed beds	7
2-3.	Effect of liquid flowrates through packed beds at 900 acfm	8
2-4.	Inlet and outlet counts as a function of channel number on OPC	11
2-5.	Collection of dioctyl phthalate aerosol particles on spherical collector	13
2-6.	Relationship between penetration, velocity, and particle charge	15
2-7.	Particle collection efficiency of electrostatic spray droplet scrubber as a function of particle size	16
2-8.	ESP discharge electrodes	19
2-9.	Cross section of a typical single stage ESP	20
2-10.	An electron avalanche	22
2-11.	Corona discharge in ionizing section of pilot plant	25
2-12.	Schematic showing collection of charged particle	33
2-13.	Comparison of predictive electrostatic models	36
2-14.	Schematic of typical IWS system	38
2-15.	Image force attraction	40
2-16.	Particle size dependent penetration for cascade impactor and EASA results	44
3-1.	Pilot plant system	48

3-2. Schematic of pilot plant 49

3-3. Types of Tellerettes studied 51

3-4. Voltage vs time for ionizer 57

4-1. Measured penetrations at p1w35p2w for SCA of 34.8 69

4-2. Measured penetrations at p1w35p2w for SCA of 62.6, 34.8 and 28.5 71

4-3. Penetration vs particle diameter for several packing at p1wp2w for 900 acfm 74

4-4. Penetration vs particle diameter for several packing at p1w35p2w for SCA of 34.8 75

4-5. Measured penetrations vs particle diameter at p1wp2w for 500, 900 and 1100 acfm 78

4-6. Measured and predicted penetrations (based on a form of Abraham's model) at p1wp2w 82

4-7. Measured and predicted penetrations for p1wp2w at particle diameters from 0.118 - 5.0 microns 84

4-8. Measured and predicted penetrations (based on polynomial model) for p1wp2w at particle diameters from 0.118 - 5.0 microns 85

4-9. Measured penetrations for p1w35p2w at SCA of 62.6, 34.8 and 28.5 87

4-10. Measured penetrations for p1w35p2w at SCA of 62.6, 34.8 and 28.5. Data affected by droplet carryover excluded 88

4-11. Calculated penetrations of ionizer at SCA of 62.6, 34.8 and 28.5 90

4-12. Comparison of Deutsch-Anderson (DA) type and Matts-Ohnfeldt (MO) type models to calculate penetrations for ionizer at SCA of 34.8 94

4-13. General DA effective, theoretical, and individual calculated migration velocities as a function of physical particle diameter 99

4-14. Predicted and calculated ionizer penetrations using the general DA effective migration velocity equation at SCAs of 62.6, 34.8 and 28.5 101

4-15. DA 62.6 SCA effective, individual calculated and theoretical migration velocities 103

4-16. DA 34.8 SCA effective, individual calculated and theoretical migration velocities 104

4-17. DA 28.5 SCA effective, individual calculated and theoretical migration velocities 105

4-18. Predicted and calculated penetrations of ionizer using the DA SCA-specific effective migration velocity equations 106

4-19. General MO effective and individual migration velocities as a function of physical particle diameter 109

4-20. Predicted and calculated ionizer penetrations using the general MO effective migration velocity equation at SCAs of 62.6, 34.8 and 28.5 111

4-21. MO 62.6 SCA effective and individual calculated migration velocities 113

4-22. MO 34.8 SCA effective and individual calculated migration velocities 114

4-23. MO 28.5 SCA effective and individual calculated migration velocities 115

4-24. Predicted and calculated penetrations of the ionizer using the MO SCA-specific effective migration velocity equation....116

4-25. Predicted vs calculated penetrations for ionizer using DA SCA-specific effective migration velocity equations....118

4-26. Predicted vs calculated penetrations for ionizer using MO SCA-specific effective migration velocity equations....119

A-1. Calibration curve for gas flowrate in pilot plant....133

A-2. Calibration curve for optical particle counter....134

A-3. Particle size distribution of flyash....135

G-1. Inlet and outlet counts vs channel number for 0.5 - 5.0 micron particles at p1w35p2w, 2" Type-R Tellerettes, no dust feed into inlet....185

NOMENCLATURE

A	area of collecting electrode, ft^2
acfm	actual cubic feet per minute
APC	Air Pollution Control
CFR	Code of Federal Regulations
D	dielectric constant, *dimensionless*
d_a	aerodynamic diameter, *m or microns*
D.C.	Direct Current
DOE	Department of Energy
DOP	Dioctyl Phthalate
d_p	physical diameter of particle, *m or microns*
d_r	relative gas density, *dimensionless*
dscf	dry standard cubic feet
EASA	Electric Aerosol Size Analyzer
E_{avg}	average field strength, *volts/m*
E_c	corona onset field strength, *volts/m*
E_c	charging field strength, *volts/m*
E_p	collecting field strength, *volts/m*
EPA	Environmental Protection Agency
ε_o	free-space permitivity
E_s	sparking field strength, *volts/m*
ESP	Electrostatic Precipitator
η_o	overall collection efficiency, *fraction or %*
f	smoothness factor, *dimensionless*
F	electrostatic force, *N*
F_d	viscous force, *N*
fps	feet per second
FRP	Fiberglass Reinforced Plastic
ft	feet
g	gram
GBF	Granular Bed Filter
gpm	gallons per minute
gr	grains
HEPA	High Efficiency Particle Air Filter
ID	Induced Draft
IWS	Ionizing Wet Scrubber
K_c	Cunningham Correction Factor, *dimensionless*
L	depth of wetted packing, *m or ft*
L	wire-to-plate spacing, *m*
l	liter
lb	pound
MCA	Multi-Channel Analyzer

mg	milligram
MMD	Mass Mean Diameter, *m or microns*
MSE	Mean Square Error
μ_g	gas viscosity, kg/m-s
ω	migration velocity, *m/s*
O.D.	outside diameter
ω_e	effective migration velocity, *m/s*
ω_k	effective Matts-Ohnfeldt migration velocity, *m/s*
OPC	Optical Particle Counter
ORNL	Oak Ridge National Laboratory
P	pressure, *atm*
P_o	standard pressure, *1 atm*
PSL	Poly-Styrene Latex
Pt	fractional penetration
q	water flowrate (*gpm*) per unit volume (ft^3) of packing
q_s	saturation charge, *coulombs*
Q	gas flowrate, ft^3/min
ρ_p	particle density, g/cm^3 *or* kg/m^3
ROI	Region of Interest
r_w	radius of discharge electrode, *m*
s	second
SCA	Specific Collector Area, *plate area* (ft^2) *per 1000 acfm of gas treated*
σ^2	variance, *dimensionless*
T	absolute temperature, *K*
T_o	standard absolute temperature, *298 K*
TSCA	Toxic Substances Control Act
TVA	Tennessee Valley Authority
V_{avg}	average voltage, *volts*
V_c	critical voltage, *volts*

INTRODUCTION

The Toxic Substances Control Act (TSCA) Incinerator located in Oak Ridge, TN, is operated by the Department of Energy (DOE) as a means of thermally destructing both hazardous and low-level radioactive waste. The incinerator operates under a Tennessee Department of Environment and Conservation (TDEC) air permit and RCRA Part B permit.

As part of a national strategy to reduce source emissions from hazardous waste combustors, the Environmental Protection Agency (EPA) is suggesting that facilities implement Maximum Achievable Control Technology (MACT) standards to reduce particulate emissions. The MACT standards are technology based standards which establish emission limits based on the performance of the top twelve percent of all hazardous waste combustion facilities. The emission range for particulate matter from the top twelve performers is 0.005-0.0086 gr/dscf, corrected to 7% O_2.

The current particulate emission limit at the TSCA facility located in Oak Ridge is 0.08 gr/dscf. Particulate emission data taken during the 1989 trial burn at the facility show an average emission rate of 0.025 gr/dscf. However, the EPA has suggested that the particulate emission limit at the hazardous waste incineration facilities will be lowered to 0.015 - 0.03 gr/dscf. Therefore, there is concern that the Oak Ridge facility will not be able to meet the new emission limits using the current particulate control system.

The TSCA facility currently uses a venturi scrubber, followed by a packed bed and two ionizing wet scrubbers (IWS) in series as a means of acid gas and particulate control. In anticipation of the required lower emission limits, feasibility studies were implemented. A pilot plant system was constructed to simulate the air pollution control (APC) at the TSCA facility. The pilot plant, which is described in greater detail in the literature review, consisted of a packed bed scrubber and an IWS in series, which operated at gas flowrates from 500-1300 acfm. Initial studies were performed on the packed bed scrubbers in order to characterize their particle collection efficiencies as a function of particle diameter and gas flowrate through the system. An empirical model was then developed which describes the penetration of the packed beds as a function of particle diameter and gas flowrate. Through testing and modeling, the effect of electrostatic collection of particles on the penetration was also quantified and incorporated into a predictive model. The predictive model can be used to estimate the penetration of the system as a function of particle size, gas flowrate, and depth of packing, and provides some insight as to the collection mechanisms of the system. Other data collected from the system is currently being analyzed in an effort to develop a better, more comprehensive model.

2. LITERATURE REVIEW

The ionizing wet scrubber (IWS) is an air pollution control device commonly used for acid gas and particulate control at incinerators. Limited data on the IWS is available in terms of particulate collection efficiency. In order to gain a better insight and understanding of the particle collection mechanisms, it was necessary to break the system into components and study each of these components separately.

As a part of this effort, Abraham (1996) studied the particle collection efficiency of packed beds and developed an empirical model which can be used to predict the collection efficiency of packed beds typically used in ionizing wet scrubbers. His research is reviewed in order to develop an understanding of the particle collection mechanisms present in the packed beds.

Abraham's work is followed by a review of electrostatic particle collection and electrostatic precipitation. This forms the foundation for particle collection which occurs in the ionizing section of the IWS. A review of image force attraction is also presented.

This chapter concludes by presenting evaluations and pilot test results reported on systems that used the IWS as a pollution control device.

2.1 PARTICLE COLLECTION IN A PACKED BED

Packed beds are typically used in industry for acid gas control. Limited data are available on the particle collection efficiency of packed bed scrubbers. Abraham (1996) studied the particle collection efficiency of two packed bed scrubbers in series, and developed an empirical model to estimate the efficiency of these scrubbers based on the density of the particles collected, the water flow rate per unit surface area of packing, and the length of the packed bed. The packed beds contained 2 inch type-R Tellerettes® packing.

The following sections will discuss the results of Abraham's work in order to develop a solid foundation in understanding the particle collection mechanisms present in packed bed systems.

2.1.1 Effect of Particle Size on Collection Efficiency

As reported by Abraham (1996), particles with an aerodynamic diameter less than 2 microns are not removed in the packed bed systems. However, above 2 microns, particle removal efficiency increases with an increase in the particle size. This is illustrated in Figure 2-1. These results are in agreement with the results of Johnstone and Roberts (1949) who reported that the effects of impaction were minimal for particle sizes less than 2 microns.

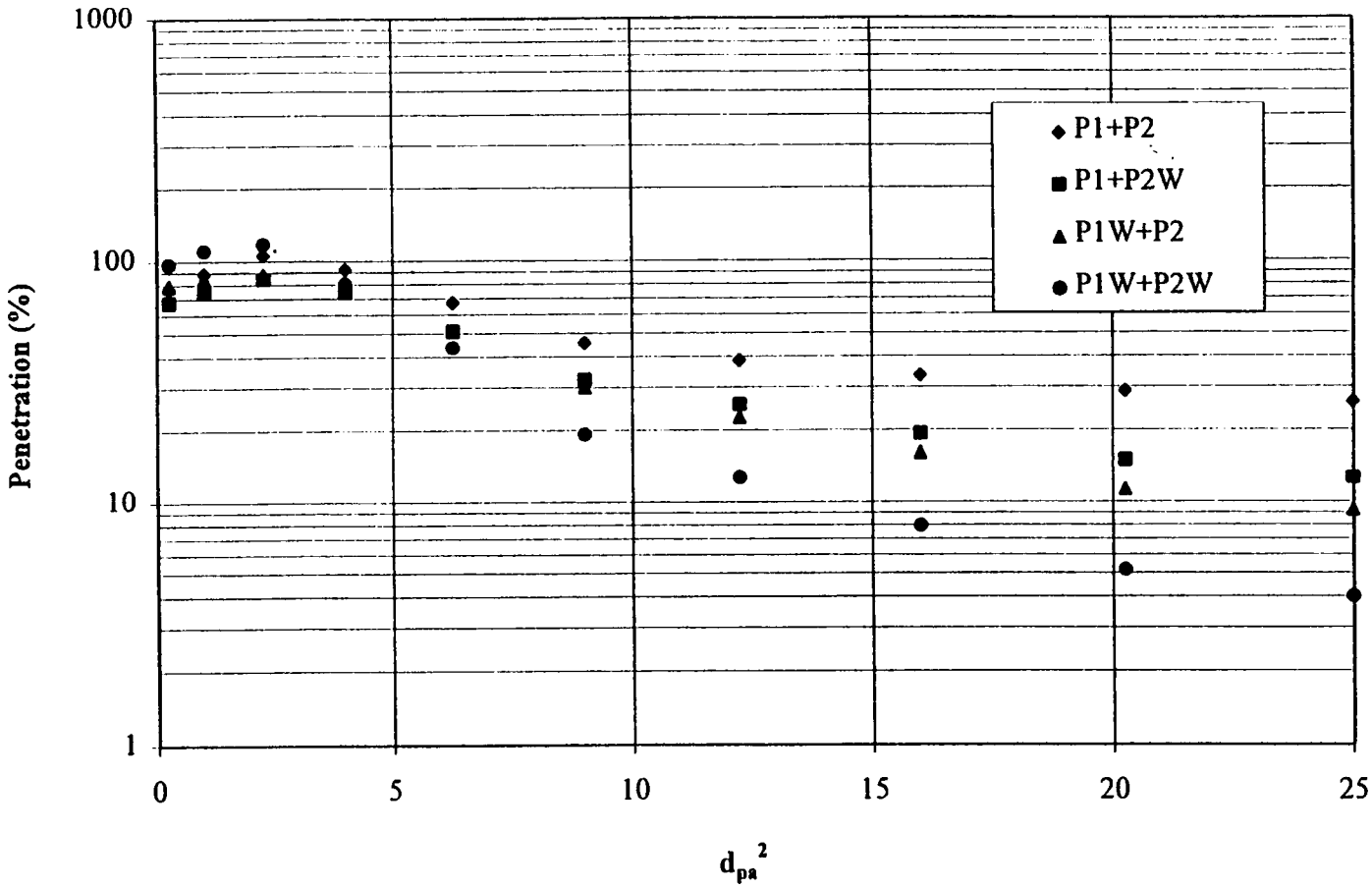

Figure 2-1. Penetration as a function of particle diameter at 900 acfm.

Source: Abraham, Sunil. M.S. Thesis, University of Tennessee, Tennessee (1996).

2.1.2 Effect of Gas Velocity through Wet Packed Beds

Inertial impaction was considered to be the dominant mechanism of particle collection in the packed bed scrubbers. The inertial impaction parameter is directly proportional to the velocity of the gas stream through the packed beds. Therefore, a higher velocity would indicate a higher inertial impaction parameter, and a lower penetration.

Figure 2-2 shows the relationship between the penetration and the gas flowrate through the packed beds for 2, 3, 4, and 5 micron particles. As indicated, the gas velocity has relatively little effect on the penetration. This may be due to increased reentrainment or increased droplet carryover at higher gas flow rates.

2.1.3 Effect of Water Flow Rate through Packed Beds

As indicated in Figure 2-3, at a constant gas flow rate of 900 acfm through the packed beds, the penetration of a given particle size decreases as the flowrate of the scrubbing liquor through the packed beds increases. Abraham (1996) noted that typical models which evaluate scrubber performance often disregard the effect of liquor flow rate through the system. However, the liquor flowrate appears to be an important parameter in particle collection efficiency.

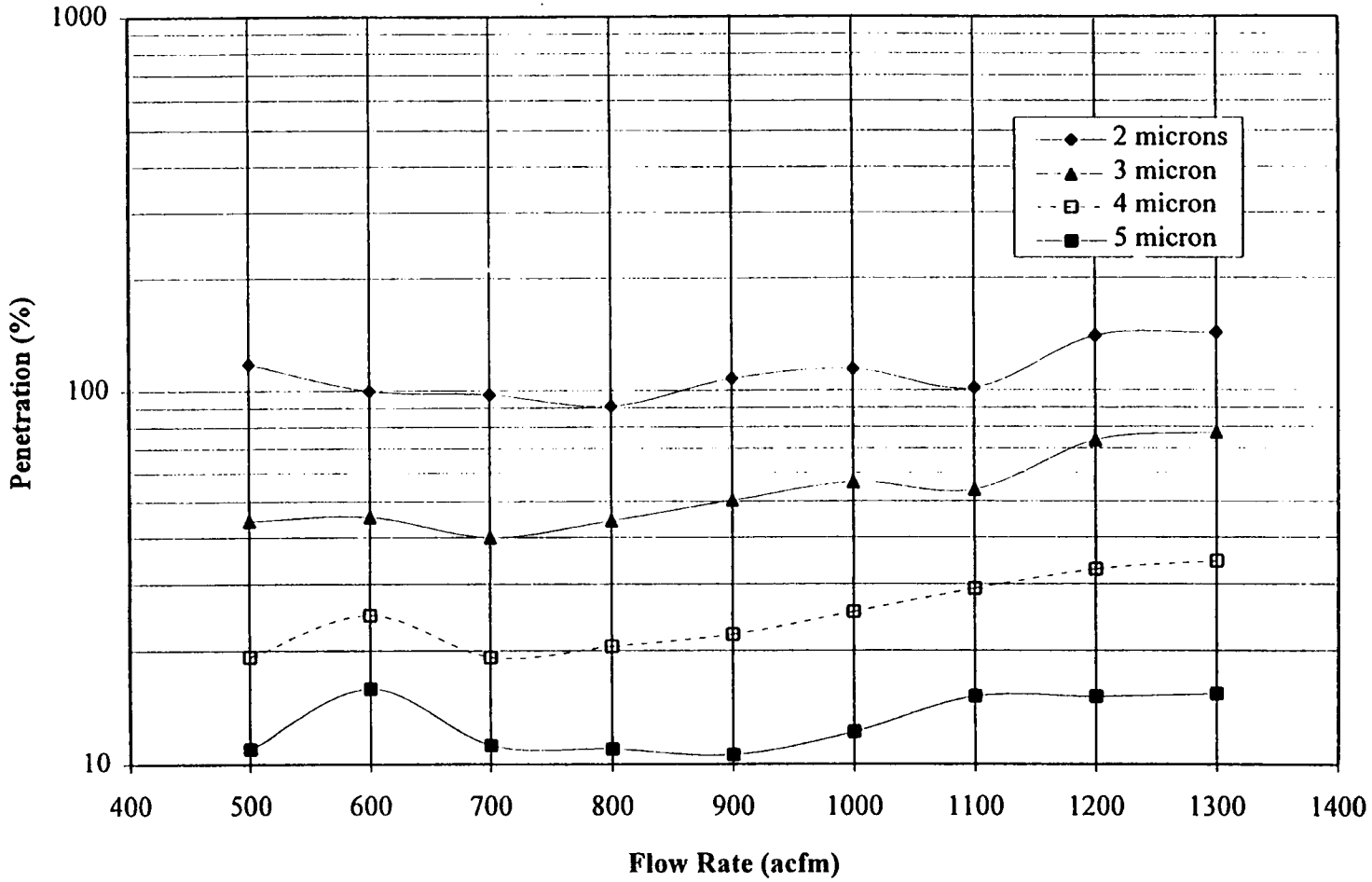

Figure 2-2. Effect of gas flowrate through wetted packed beds.

Source: Abraham, Sunil. M.S. Thesis, University of Tennessee, Tennessee (1996).

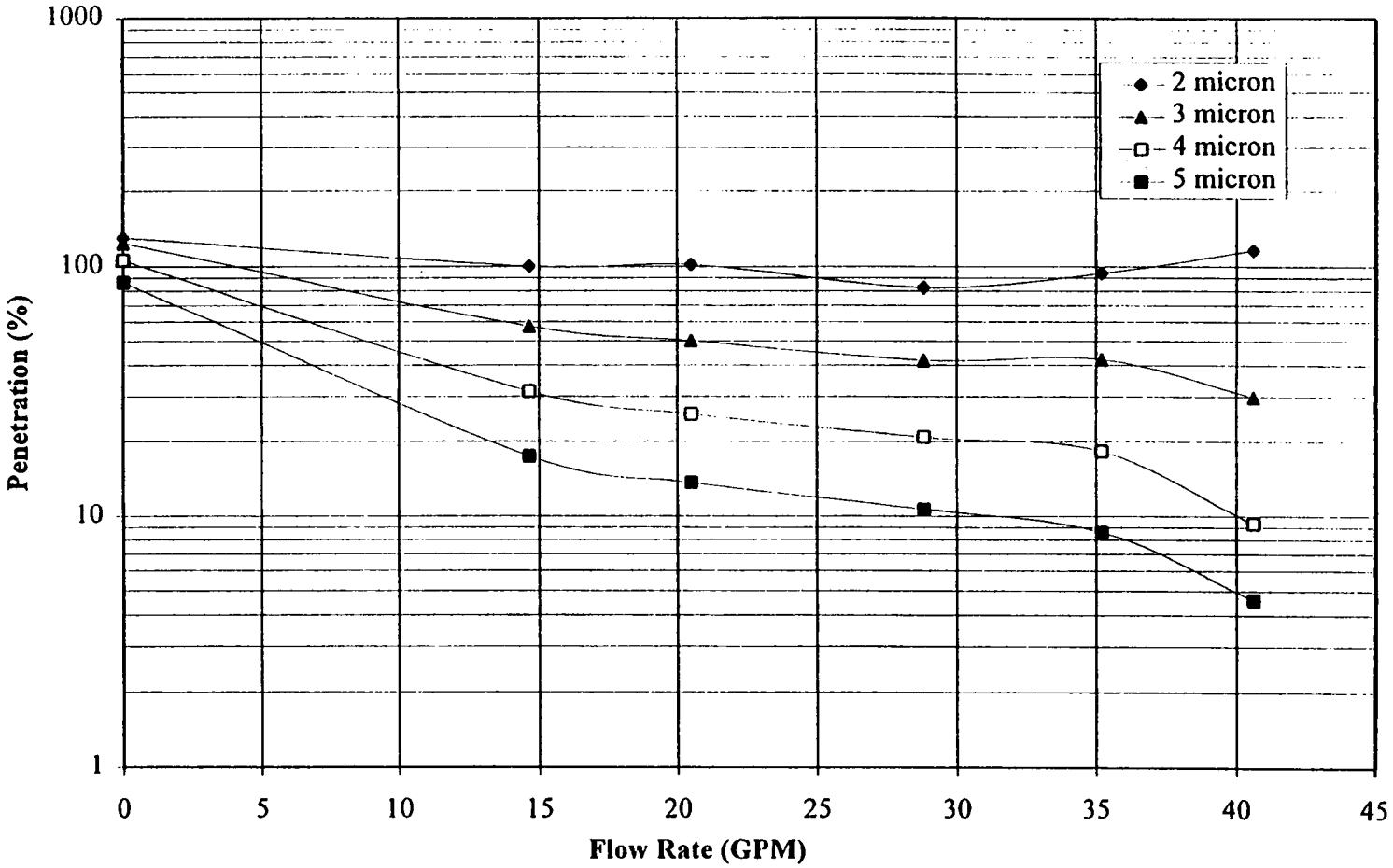

Figure 2-3. Effect of liquid flowrates through packed beds at 900 acfm.

Source: Abraham, Sunil. M.S. Thesis, University of Tennessee, Tennessee (1996).

2.1.4 Predictive Model for Particle Collection Efficiency in Packed Beds

Abraham (1996) developed an empirical model to predict the particle collection efficiency of packed bed scrubbers using 2" Type-R Tellerettes® as the packing media. The model was developed based on previous relationships which were developed by Calvert for scrubbing devices. The basic premise behind the model is that the particle collection efficiency of the packed bed scrubbers is a function of the aerodynamic particle diameter, and to a lesser extent, the liquid flow rate per unit volume of packing. The following relationship, as developed by Abraham, can be used to predict the particle collection efficiency of a packed bed containing 2" Type-R Tellerette® packings

$$Pt(\%) = 100 * \left[\exp\left(-1.57 * 10^{10} \rho_p q^{0.57} d_p^2 L\right)\right] * 1.01 \qquad (2\text{-}1)$$

where $Pt(\%)$ is the percent penetration, ρ_p is the density of the particle in kg/m^3, q is the flow rate of scrubber liquor in (m^3/s) per unit area of packing (m^2), d_p is the particle diameter in meters, and L is the length of the packed bed in meters.

Abraham (1996) also studied the Whitby theory for efficiency due to inertial impaction on fibrous filters, modeling the filaments of the Tellerettes® as filter fibers. His results indicate that the Whitby approach overpredicts the efficiency for particles less than 4.5 microns, and underpredicts efficiency for particles larger than 4.5 microns. Therefore, the empirical model shown above is considered to be the best approach to predict the efficiency at the present time.

2.1.4.1 Limitations of Predictive Model

Figure 2-1 indicates that penetration is greater than 100 percent for particles between 0.5 and 1.5 microns. This may be a result of the growth of particles in the system which are less than 0.5 microns due to moisture in the packed beds or agglomeration in the system. The high penetration may also be contributed to droplet carryover from the wet packed beds. Figure 2-4 shows the results of a test performed with an optical particle counter (OPC) at a location downstream of the packed beds with no dust loading to the system. As indicated, a substantial number of counts exists between the size range of 0.5 to 1.5 microns. Abraham (1996) also noted that penetrations greater than 100 percent were observed when both of the packed beds were dry but dust was fed into the system. This suggests that particles below 2 microns agglomerate in the packed beds and form particles with a maximum size of 2 microns. Therefore, the empirical model developed by Abraham is only effective at predicting collection efficiencies for particles larger than 2.0 microns.

2.2 ELECTROSTATICS

Electrostatics can have a strong impact on particle collection efficiency, especially at small particle sizes. Even when small particles approach collectors at distances where inertial impaction, diffusion, or interception would not be appropriate mechanisms of collection, electrostatic forces may overcome the inertial and viscous forces and cause the particles to migrate to the collector surface and be collected.

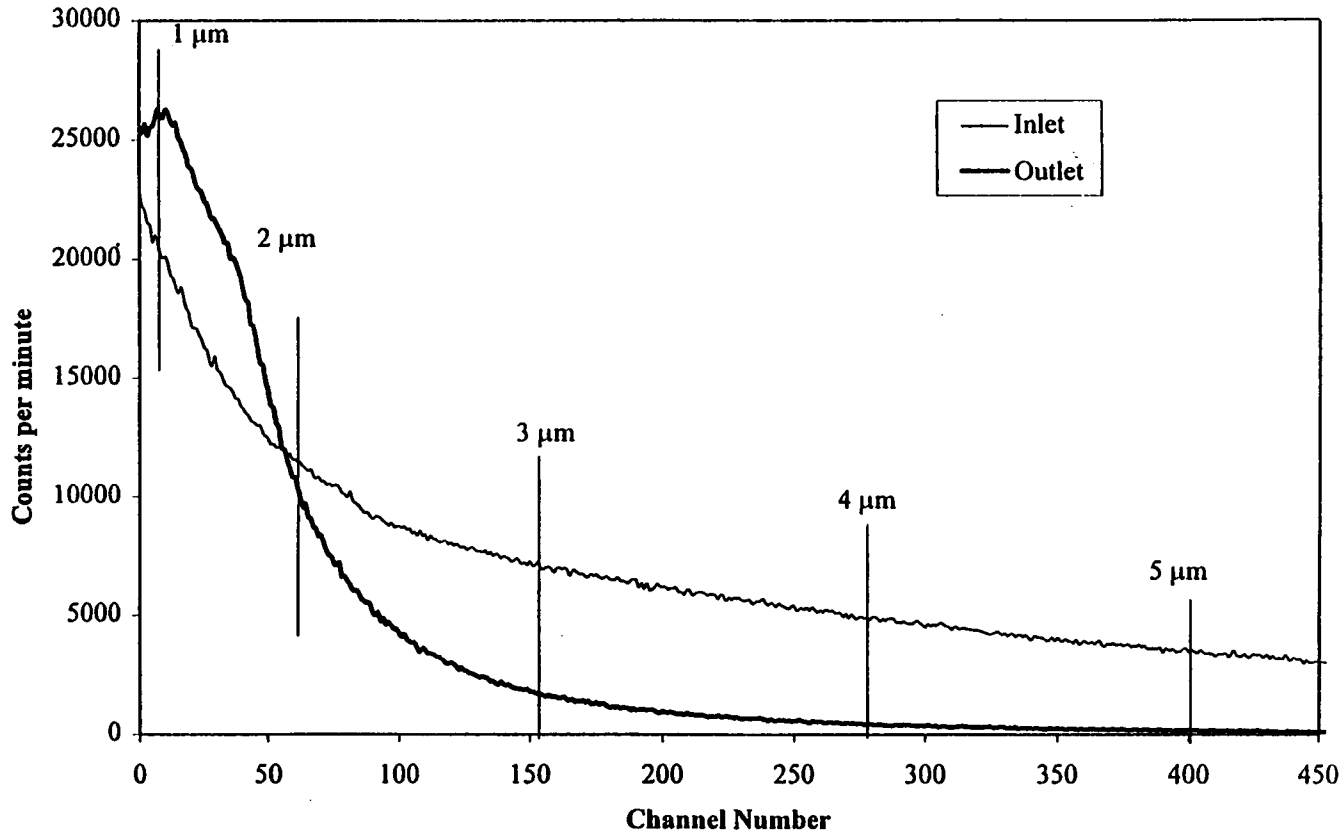

Figure 2-4. Inlet and outlet counts as a function of channel number on OPC.

Source: Abraham, Sunil. M.S. Thesis, University of Tennessee, Tennessee (1996).

Particles may become charged in many ways. Some particles have a natural charge created by radiation and photoionization. Other particles may become charged as a result of friction between the particle and a moving gas stream, or a neutral particle may develop a charge after colliding with a charged particle. Situations exist when the collectors may also be charged. In general, there are five cases which describe the electrostatic relationships which exist between particles and collectors. These cases are described by Nielsen and Hill (1976) as follows

1. the coulombic force between a charged particle and a charged collector
2. the electrical image force between a charged particle and a neutral collector
3. the electrical image force between a neutral particle and a charged collector
4. the force of a charged particle in the presence of a neutral collector by a uniform external electric field directed parallel to the flow field
5. the electric dipole interaction force between a neutral particle and a neutral collector, both bodies being polarized by a uniform external electric field directed parallel to the flow field

Separating these relationships and developing equations to describe the collection efficiency as a function of each is very complicated. Kraemer and Johnstone (1955) solved the equations of motion for some of the cases and discussed the collection efficiency of each case as a function of the collection parameter. As shown in Figure 2-5, their results indicate that the highest collection efficiency occurs when both the particle and the collector are charged.

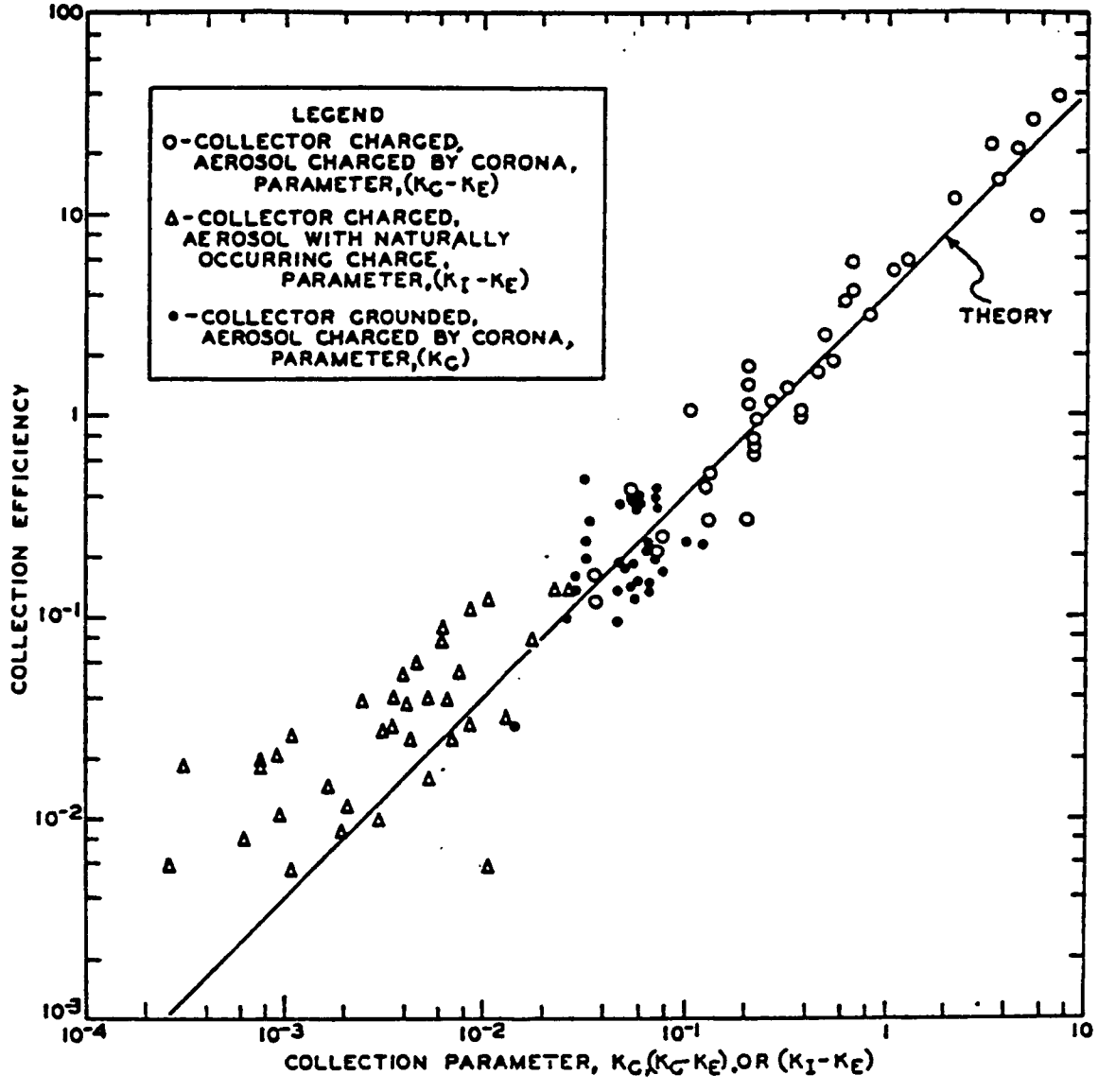

Figure 2-5. Collection of dioctyl phthalate aerosol particles on spherical collector.

Source: Kraemer, Herbert F., and H. F. Johnstone. "Collection of Aerosol Particles in the Presence of Electrostatic Fields." *Industrial and Engineering Chemistry* 47, No. 12, (1955): 2426-2434.

Goyer et al (1953) discuss the effects of electrostatically charged DOP aerosols on filtration efficiency. The results indicate that the filtration efficiency increases as the average particle charge increases. As shown in Figure 2-6, at a velocity of 28 cm/s, the average decrease in penetration is 20.3% of the penetration of uncharged particles, and at a velocity of 2.7 cm/s, the average decrease in penetration is 45.2%. It is important to note that the effect of electrostatics increases as the particles size decreases since the number of charges per unit area of droplet increases as the particle size decreases.

Pilat (1975) conducted tests on DOP aerosol particles at the University of Washington electrostatic scrubber pilot plant in which a corona discharge was used to create negatively charged particles, and inductive charging was used to create positively charged water droplets. His results show that the overall particle collection efficiency increased from 68.8% at uncharged conditions to 93.6% at charged conditions for 1.05 micron particles. The overall collection efficiency for a 0.3 micron particle increased from 35% at uncharged conditions to 87% at charged conditions. These results are shown in Figure 2-7. Sumiyoshitani et al (1984) also studied the collection of dust particles in an air stream by a charged water droplet. They report that if the droplet and dust particles are charged oppositely, the attractive Coulomb force promotes dust collection by the droplet.

Calvert and Yung (1979) studied the effects of electrostatic augmentation of a granular bed filter (GBF) on the overall particle collection efficiency. Collection efficiency increased from 25%, when neither the particles or the bed was charged, to 61%

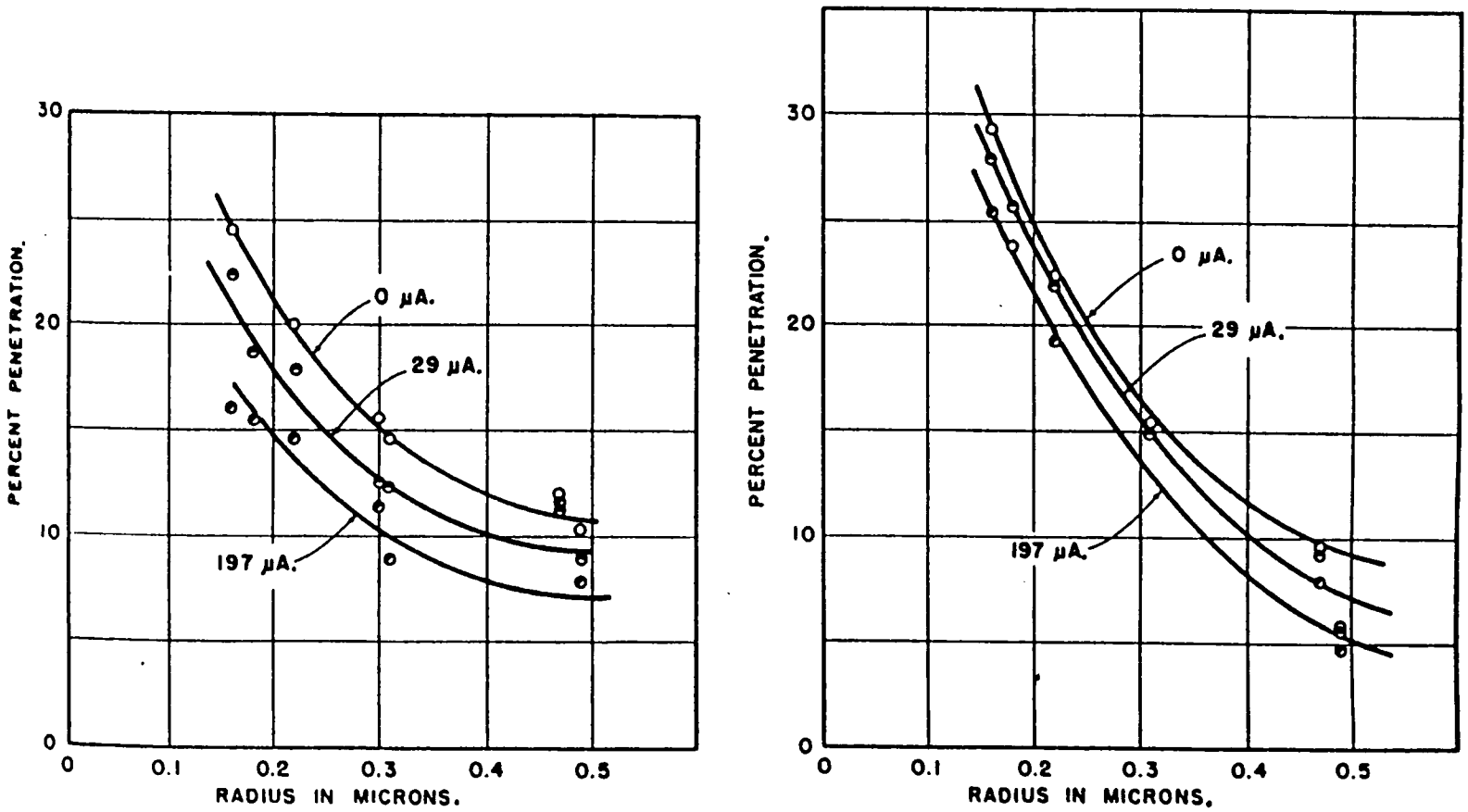

Figure 2-6. Relationship between penetration, velocity, and particle charge. (a) filtration of charged DOP, linear velocity = 2.52 cm/s (b) filtration of charged DOP, linear velocity = 28.01 cm/s.

Source: Goyer, Guy G., et al. "Filtration of Monodisperse Electrically Charged Aerosols." *Journal of Physics and Chemistry* 58 (1954): 137-142.

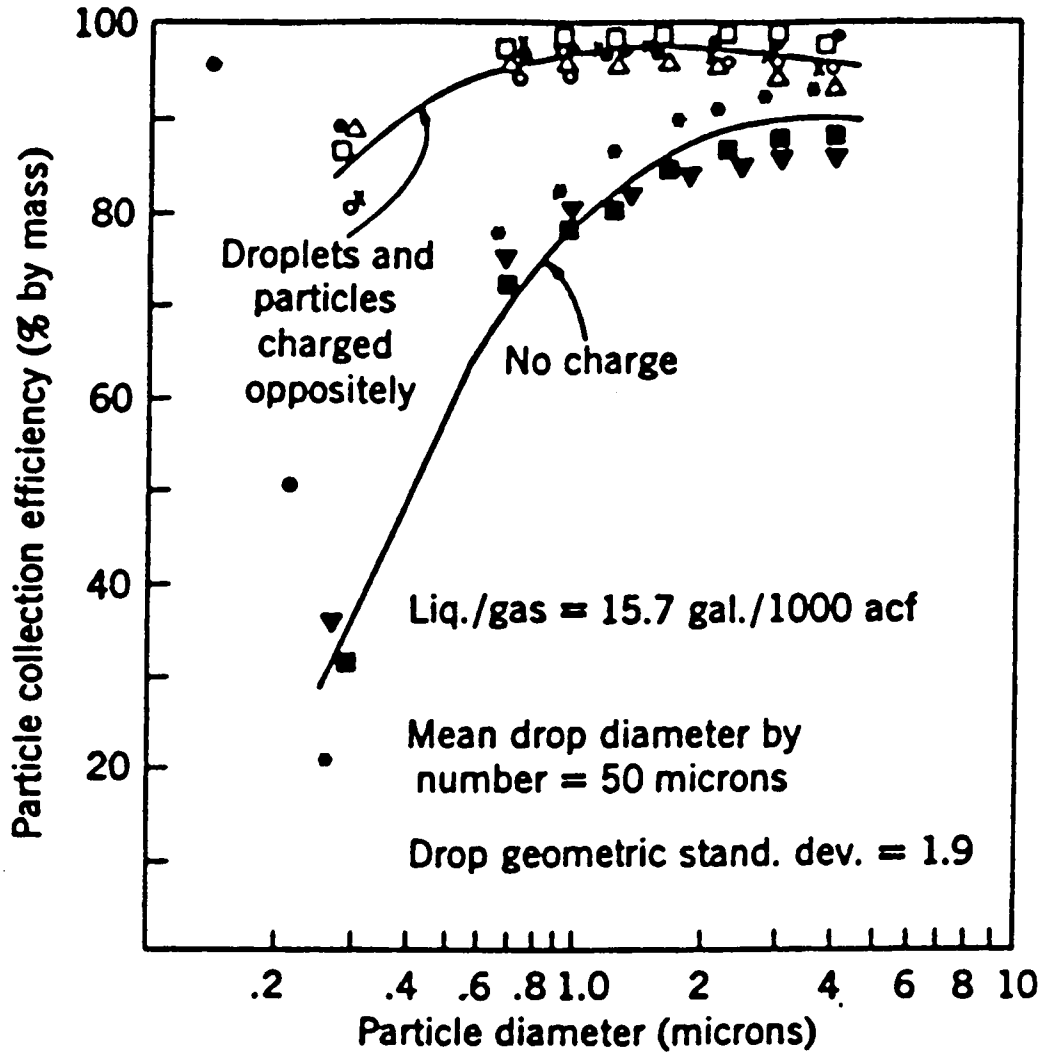

Figure 2-7. Particle collection efficiency of electrostatic spray droplet scrubber as a function of particle size.

Source: Pilat, Michael J., "Collection of Aerosol Particles by Electrostatic Droplet Spray Scrubbers." *Journal of the Air Pollution Control Association* 25, (1975): 176-178..

when the particles were charged and the bed was grounded. They also report that by polarizing the bed but not charging the particles, the collection efficiency increases with increasing applied voltage across the bed. For 1 micron particles, collection efficiency increased from 25% to 90% when the applied voltage was increased from 0 V to 11.4 kV.

The most common method of particulate collection using electrostatic forces occurs in electrostatic precipitation. The next section discusses the principles of operation of electrostatic precipitation and presents models which are useful in predicting the collection efficiency of electrostatic precipitators.

2.3 ELECTROSTATIC PRECIPITATION

According to Stern (1977), the interest of using electrostatic precipitation to control emissions in the industrial sector can be traced back to the work of Cottrell in the early 1900's. Cottrell first used an electrostatic precipitator (ESP) to control sulfuric acid emissions from a copper smelting process. He later applied the method to the collection of metal oxides and non-ferrous metal collection.

Oglesby and Nichols (1978) report that the largest single application of ESPs, both in numbers and the volume of gas treated, is in the removal of flyash from the combustion gases at electric power utilities. ESPs are unique in that the forces used to collect the particles in the gas stream are essentially applied only to the particles and not the entire gas stream. This reduces the amount of energy required to effectively clean the gas stream, as compared to other types of collection equipment. Since electrical forces,

as opposed to mechanical forces, are used to clean the gas stream, the pressure drop in an ESP is relatively low compared to other mechanical devices such as venturi scrubbers or fabric filters. The pressure drop across an ESP may be on the order of 1-2 inches of water, while that of a fabric filter may be 4-6 inches of water, and that of a venturi may be 10-100 inches of water.

An electrostatic precipitator consists of a series of parallel plates, parallel wires and plates, or wires suspended axially in a tube. The first two types are referred to as plate-type ESPs, with the parallel wire and plate being the most common, while the latter is referred to as a tube-type ESP. The wires are typically discharge electrodes, and are charged negatively, while the plates are typically collection electrodes and are charged positively. When a high voltage is applied across the wires and plates, an electric field is created. Particles passing through the field become charged and then migrate towards the collection plates where they are collected. The discharge electrodes take on many different configurations, from smooth round wires to spiked tubes. Figure 2-8 illustrates several types of discharge electrodes. A typical arrangement of an ESP is shown in Figure 2-9.

In wet ESPs, the collection plates are continually flushed or sprayed with water. This removes particles which collect on the plates and prevents particulate buildup. The water film also enhances gas absorption, and reduces particle reentrainment. Fresh makeup water is used in wet ESPs to compensate for evaporation and to reduce the concentration of absorbed gases in the water. In dry ESPs, the collected particles are

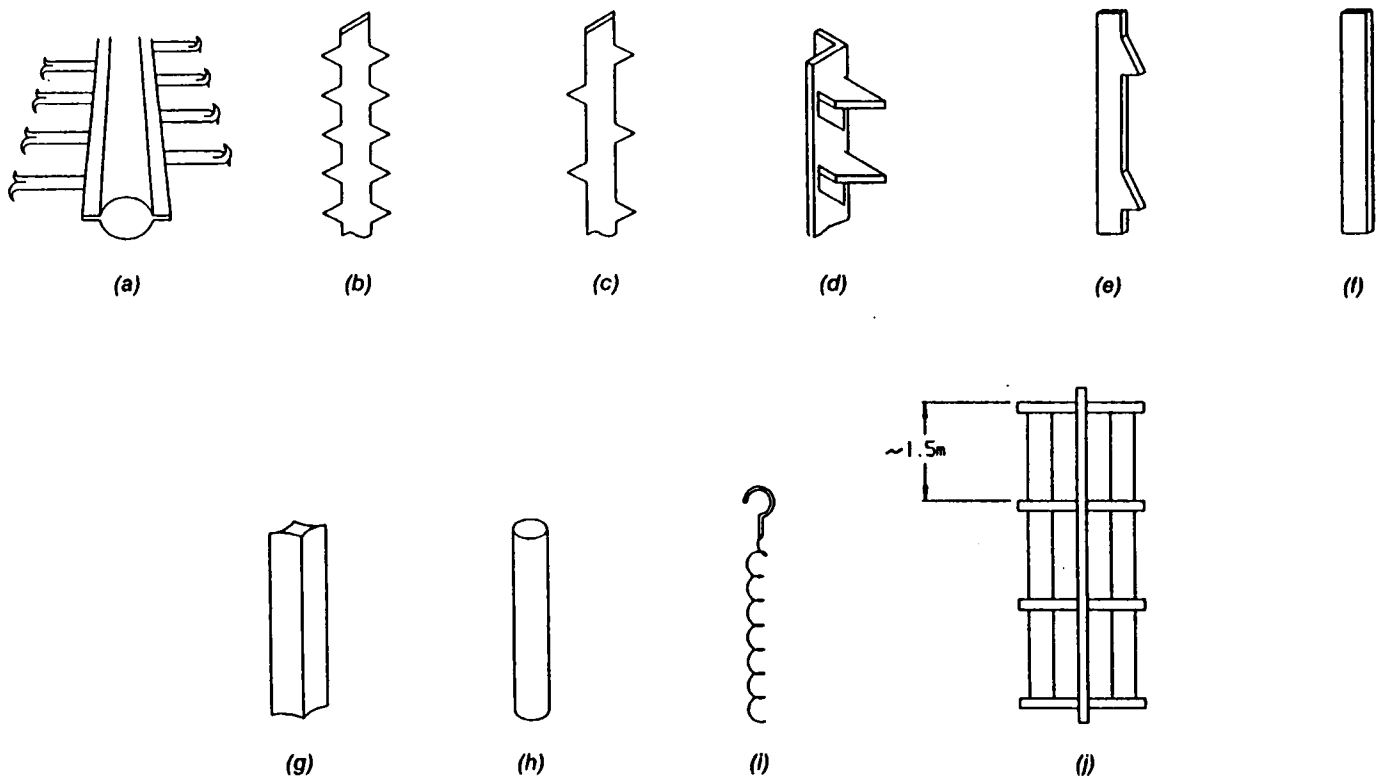

Figure 2-8. ESP discharge electrodes: (a) rolled tubing pipe with spiked emitters (b) parallel spikes (c) alternate spikes (d) punched spike (e) spiked bar (f) flat bar (g) star bar (h) round bar (i) coiled wire (j) square twisted rods

Source: Hesketh, Howard E., *Air Pollution Control: Traditional and Hazardous Air Pollutants*, Technomic Publishing Company, Lancaster, PA, (1991).

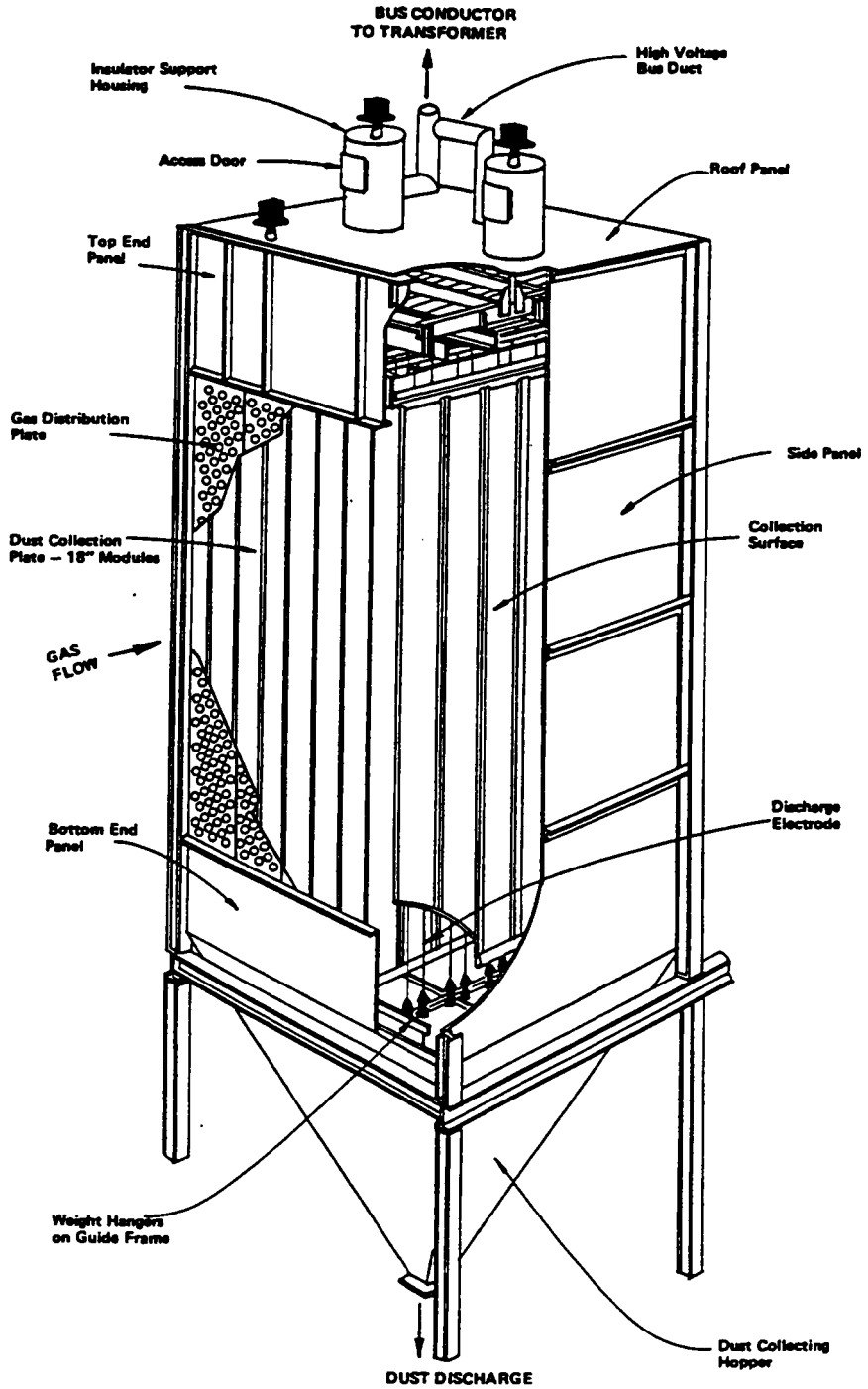

Figure 2-9. Cross-section of a typical single stage ESP.

Source: Hesketh, Howard E., *Air Pollution Control: Traditional and Hazardous Air Pollutants*, Technomic Publishing Company, Lancaster, PA, (1991).

allowed to build up and form layers on the collection plates. At given time intervals, rappers are actuated which sharply strike the plates and cause the dust layer to dislodge and fall into the bottom of the ESP and collect in a hopper. Reentrainment of particles is more common in dry ESPs since some of the particles separate from the falling dust layer and become reentrained in the flue gas.

2.3.1 Principles of Operation

Wark and Warner (1981) discuss three mechanisms which are required for electrostatic particulate collection to occur in an ESP. These mechanisms consist of gas ionization, the charging of particulates in the gas stream, and the migration and ultimate collection of the charged particles on the collection surface. Oglesby and Nichols (1978) provide an in-depth description of these three mechanisms.

2.3.1.1 Gas Ionization

Gas ionization occurs when a high voltage is applied across two electrodes. These electrodes may consist of parallel plates, small diameter parallel wires and plates, or small diameter wires suspended axially in a tube. The discharge electrodes are generally charged negatively, while the collector electrodes are electrically grounded. When a high voltage is applied across the discharge and collector electrodes, a non-uniform electric field is created. This electric field is high near the discharge electrode and rapidly decreases with increased distance from the electrode. Some gas molecules in the flue gas stream are ionized due to natural radiation, therefore, free electrons and positive gas ions

are present in the gas stream. When these free electrons pass through the electric field, they are rapidly accelerated away from the discharge electrode, while the positive ions are accelerated towards the discharge electrode. As the electrons move across the gas stream, they collide with neutral gas molecules and strip electrons from the outer shell of these molecules. The newly freed electrons are also rapidly accelerated in the field and available to collide with the neutral gas molecules, thus continuing the process. This process of creating free electrons and positive gas ions is known as the electron avalanche and is show schematically in Figure 2-10.

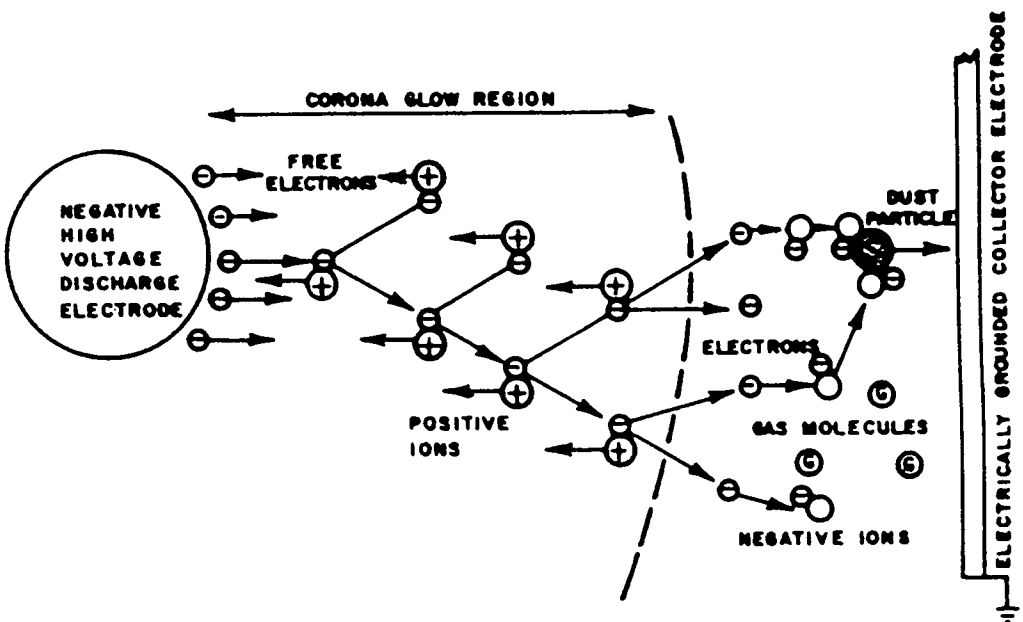

Figure 2-10. An electron avalanche.

Source: Hesketh, Howard E., *Air Pollution Control: Traditional and Hazardous Pollutants*, Technomic Publishing Company, Lancaster, PA, (1991).

As the strength of the electric field decreases, the acceleration of the electrons decreases, the momentum of the electrons decreases, and the ability of the free electrons to strip electrons from the neutral gas molecules decreases. Therefore, the electron avalanche occurs only within a very close proximity to the discharge electrode since the electric field is very high in this region. The process of ionization of gas molecules by high energy electrons in the region of a strong electric field is referred to by Cooper and Alley (1994) as a corona.

A minimum field is required to produce a self-sustaining electron avalanche and form a corona. This field is referred to as the corona onset field. For a wire and parallel plate precipitator with smooth wires, Turner et al (1992) report this field strength as

$$E_c = 3.126 \times 10^6 \left[d_r + 0.0301 \left(\frac{d_r}{r_w} \right)^{0.5} \right] \qquad (2\text{-}2)$$

where

$$d_r = \text{relative gas density} = \frac{T_o P}{T P_o} \qquad (2\text{-}3)$$

and E_c is the corona onset field at the wire surface in V/m, T_o is 298 K, P_o is 1 atm, T is the gas stream temperature in K, P is the gas stream pressure in atm, and r_w is the radius of the discharge electrode in m. A corona emits a characteristic glow which appears as bright purple "tufts" around the discharge electrode. Turner et al (1992) report that a field strength of 0.6 times the value of E_c is required to produce the "tuft" corona as shown in Figure 2-11, for wires of normal or typical smoothness. A smoothness

correction factor can be incorporated into equation 2-2, to yield the following equation

$$E_c = 3.126 \times 10^6 \left[d_r + 0.0301 \left(\frac{d_r}{r_w} \right)^{0.5} \right] \mathrm{f} \qquad (2\text{-}4)$$

where f is the smoothness correction factor with a value of 0.6 for smooth wires.

By integrating the critical electric field from the wire to the plate, the minimum voltage, or critical voltage, required to obtain this electric field can be determined. Current will not flow until the critical voltage is reached. The critical voltage can be determined by the following equation

$$V_c = E_c r_w \ln\left(\frac{4L}{\pi r_w} \right) \qquad (2\text{-}5)$$

where V_c is the critical voltage in volts, L is the distance between the wire and the plate in m, and all other variables are as defined previously.

The voltage in the precipitator can be increased until sparking (spark-over) occurs. The strength of electric field at which spark-over occurs is estimated by Turner et al (1992) as

$$E_s = 6.3 \times 10^5 \left(\frac{273P}{T} \right)^{1.65} \qquad (2\text{-}6)$$

where E_s is the sparking field strength in V/m, T is the absolute temperature in K, and P is the gas pressure in atm. Hesketh (1991) suggests that the greatest amount of power that can be delivered during ESP operation is the area under a voltage-time curve where the voltage is just below the spark-over voltage. Most control systems on ESPs have a

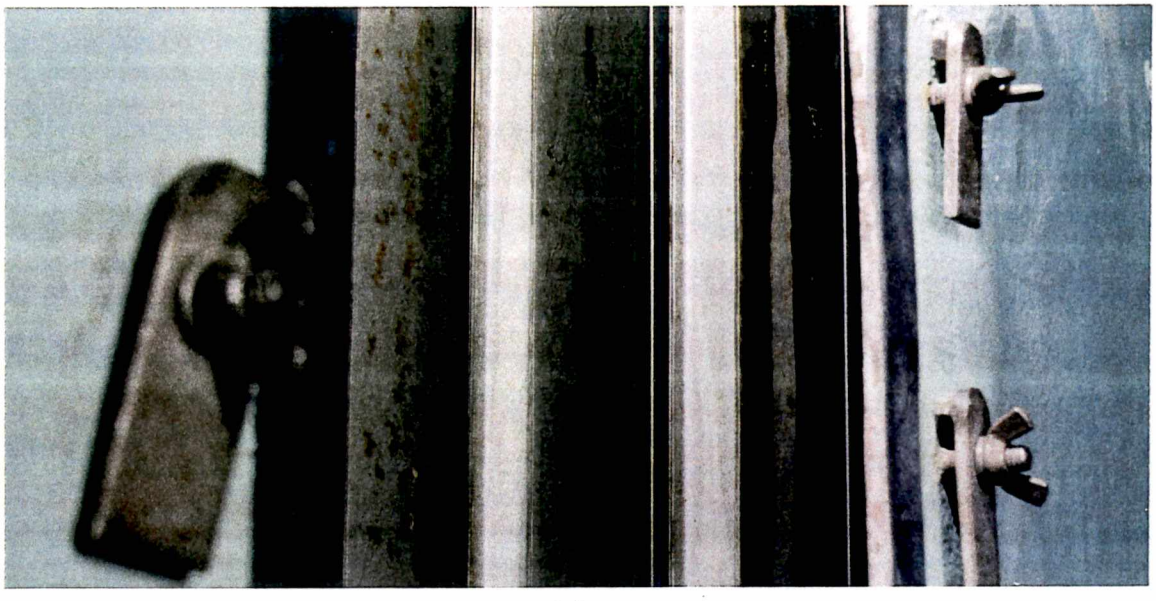

(a)

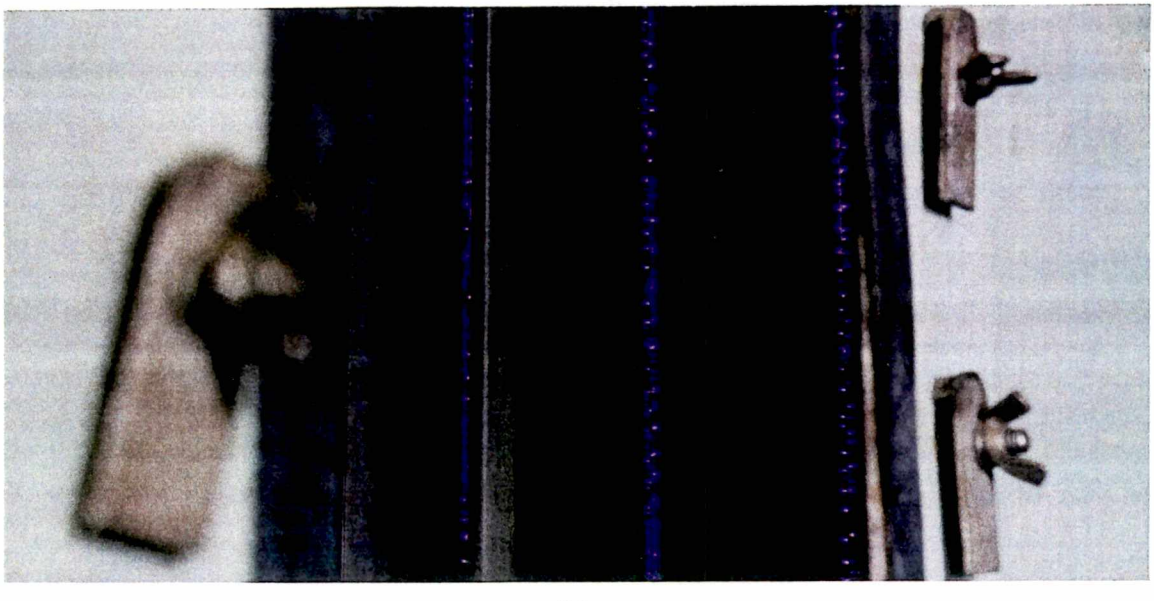

(b)

Figure 2-11. Corona discharge in ionizing section of pilot plant: (a) wetted parallel plates and wires, ionizer is not operating (b) "tuft" corona around the discharge electrode at average operating voltage of 31.1 kV.

spark-rate controller which continually adjusts the operating voltage to a value just below the spark-over voltage in order to supply the greatest amount of power to the ESP. When the spark rate exceeds a preset value, the controller causes the voltage to drop momentarily and then ramp back up to the operating value. This reduces excessive spark-over.

Turner et al (1992) suggest that the electric field strength is strongest along a line from the wire to the plate, and is approximated very well, except very near the wire, by the following equation

$$E_{avg} = \frac{V_{avg}}{L} \tag{2-7}$$

where E_{avg} is the average field strength in V/m, V_{avg} is the average voltage at the average field strength, and L is the distance between the wire and plate in m.

2.3.1.1.1 Sample Calculation for a Typical Industrial ESP

The following example illustrates typical operating values of industrial ESPs. The conditions of the flue gas and ESP are as follows

Flue gas temperature	400 F
Wire to plate spacing	0.10 m
Wire diameter	0.00254 m
Velocity of flue gas	1.6 m/s

The corona onset field was determined by equation 2-4 as follows

From equation 2-3, the relative gas density was determined as

$$d_r = \frac{T_o P}{T P_o} = \frac{293K(1atm)}{477.6K(1atm)} = 0.61$$

then

$$E_c = 3.126 \times 10^6 \left[d_r + 0.0301 \left(\frac{d_r}{r_w} \right)^{0.5} \right] \text{f}$$

$$E_c = 3.126 \times 10^6 \left[0.61 + 0.0301 \left(\frac{0.61}{\left(\frac{0.00254m}{2} \right)} \right)^{0.5} \right] \times 0.6 = 2.4 \times 10^6 \text{ V/m}$$

The corona starting voltage was determined by equation 2-5 as follows

$$V_c = E_c r_w \ln\left(\frac{4L}{\pi r_w} \right) = \left(2.4 \times 10^6 V/m \right) \left(\frac{0.00254m}{2} \right) \ln\left(\frac{4(0.10m)}{\pi \left(\frac{0.00254m}{2} \right)} \right) = 14 \text{ kV}$$

The sparking field strength was determined by equation 2-6

$$E_s = 6.3 \times 10^5 \left(\frac{273P}{T} \right)^{1.65} = 6.3 \times 10^5 \left(\frac{273K(1atm)}{477.6K} \right)^{1.65} = 2.5 \times 10^5 \text{ V/m}$$

The voltage at which spark-over occurs was determined by equation 2-7, and substituting the sparking field strength for E_{avg}

$$V_{avg} = E_{avg} L = \left(2.5 \times 10^5 V/m \right) (0.10m) = 25 \text{ kV}$$

2.3.1.1.2 Factors Affecting the Ionization Process

Several factors affect the ionization process, including the strength of the electric field. The strength of the electric field affects the acceleration of the electrons through the gas stream. Increasing the strength of the electric field increases the acceleration of the electrons, thus increasing the momentum of the electrons, and increasing the probability of gas ionization. The strength of the electric field is, in turn, affected by the radius of the discharge electrode, and the density of the gas as indicated by equations 2-4 and 2-6.

The ionization energy of a gas molecule is the minimum amount of energy required to remove an electron from the molecule. Therefore, the ionization energies of the gas molecules present are important in determining if a given gas molecule will lose an electron upon collision with an accelerated electron. Table 2-1 shows the ionization energies for some typical gases. Electrons are more easily stripped from gas molecules which have the lowest ionization energies. Thus, the composition of the gas stream plays an important role in the ionization process.

The temperature and pressure of the gas stream also play an important role in the ionization process since they affect the density, and therefore, the mean free path of the electrons. As the mean free path decreases, the momentum of the electrons decreases, thereby decreasing the probability of ionization. Thus, under conditions of increased pressure or decreased temperature, an increased electric field is required for ionization.

Table 2-1. Ionization energies for various gases.

Gas	Ionization Potential, V
Hydrogen	15.4
Nitrogen	15.5
Oxygen	12.2
Carbon monoxide	14.1
Carbon dioxide	13.7
Water vapor	12.6
Nitrogen oxides	
nitric oxide	9.5
nitrogen dioxide	11.0
nitrous oxide	12.9
Sulfur dioxide	13.1

Source: Oglesby Jr., Sabert, and Grady B. Nichols. *Electrostatic Precipitation.* Marcel Dekker, Inc., New York, NY, p. 18, 1978

2.3.1.2 Particle Charging

The second mechanism required for electrostatic precipitation is particle charging. Oglesby and Nichols (1978) explain that particle charging occurs when the electrons which exit the corona region of the discharge electrode enter the quiescent region of the precipitator and encounter electronegative gas molecules. Collisions between these electronegative gas molecules and the electrons result in the capture of the electrons and the creation of negatively charged gas ions. The gas ions migrate towards the grounded collection electrode, creating a current. The magnitude of the current is dependent upon the strength of the electric field and the ion mobility. Ion mobilities are dependent on the mass and concentration of ions. Since these ions migrate at a velocity that is less than the

velocity of the electrons before capture, a space charge is established between the corona glow region and the collection electrode.

As the negative gas ions migrate perpendicular to the flow of the gas stream, they follow the electric field lines. When these ions contact particles in the gas stream, they lose their charge to these particles, resulting in negatively charged particles. Cooper and Alley (1994) refer to this type of charging as field charging. Field charging is most effective for particles larger than 1 micron in diameter, while particles less than 0.2 micron in diameter are charged most effectively by diffusional charging. Diffusional charging occurs when gas ions and particles in the gas stream collide with each other due to random motion. However, Turner et al (1992) report that diffusion charging and field charging occur simultaneously on all particles.

The amount of charge a particle may hold, the saturation charge, is limited by the particle diameter, the dielectric constant of the particle, and the strength of the charging field. Wark and Warner (1981) determine the saturation charge to be

$$q_S = p\pi\varepsilon_o E_c d_p^2 \tag{2-8}$$

where

$$p = \frac{3D}{D+2} \tag{2-9}$$

and p typically lies between 1.50 and 3.0 for many types of dust, q is the limiting charge, D is the dielectric constant of the particulate, ε_o is the free-space permitivity, E_c is the strength of the charging field, and d_p is the physical diameter of the particle.

2.3.1.3 Migration and Collection of Particles

The third mechanism of electrostatic particulate collection is the migration and collection of the charged particles on the surface of the collector. This occurs because the negatively charged particles are acted upon by the force of the electric field. Sears et al (1987) describe the relationship between a charged particle and the force acting on that particle as follows

$$F = qE \tag{2-10}$$

where F is the force due to the electric field (electrostatic force) in Newtons, q is the charge on the particle in Coulombs, and E is the electric field in V/m.

Wark and Warner (1981) report that the viscous force on a particle in the Stokes' regime, where Reynolds number lies between 10^{-4} and 0.5, is represented as

$$F_d = \frac{3\pi\mu_g d_p \omega}{K_c} \tag{2-11}$$

where F_d is the force on the particle, μ_g is the viscosity of the gas, d_p is the physical diameter of the particle, ω is the migration velocity of the particle, and K_c is the Cunningham correction factor. Assuming that forces of inertia and gravity are negligible,

the electrostatic force may be set equal to the viscous force, and the following equation for the migration velocity of charged particles in an electric field can be determined.

$$\omega = \frac{p\varepsilon_o E_c E_p d_p K_c}{3\mu_g} \qquad (2\text{-}12)$$

where E_p is the strength of the collecting field and all other terms are as defined previously. In a typical industrial electrostatic precipitator, the charging and collecting fields are equal since both the charging and collection occur in the same zone between the wires and the plates.

The migration velocity describes the velocity at which a given charged particle in the gas stream approaches a collection surface, and plays an important role in determining whether or not the particle is collected on the surface of the collector. If the time which it takes the charged particle to migrate from the position in the gas stream at the time it is charged to the collection electrode, is less than the time it takes for the particle to travel in the direction of the gas stream and exit the region between the charging and collecting electrodes, then the particle may be collected. Therefore, as described by Kraemer and Johnstone (1955), collection efficiency is enhanced with low relative velocities between the charged particles in the gas stream and the collecting surface. This is illustrated in Figure 2-12.

Upon reaching the collection electrode, if the adhesive, cohesive, and electrostatic forces are strong enough to hold the particle to the collection electrode to prevent

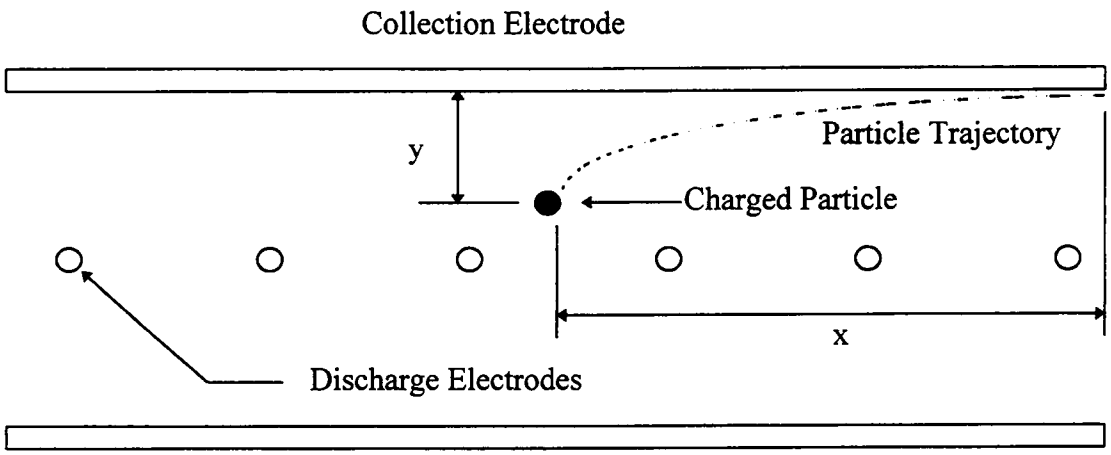

Figure 2-12. Schematic showing collection of charged particle. If the particle migrates distance y towards the collecting plates before it travels distance x in the gas stream, then the particle will be collected.

reentrainment of the particle back into the gas stream, and particle bounce does not occur, the particle will be collected.

Since the assumptions of ideal flow, perfectly spherical particles, uniform electric field, uniform particle distribution in the gas stream, and negligible reentrainment of particles rarely exist, an effective migration velocity, ω_e, may be determined empirically.

2.3.2 Electrostatic Precipitation Models

Lawless and Sparks (1985) indicate that the Deutsch-Anderson (DA) model was the first model developed to evaluate ESP performance. The DA model is one of the most popular and commonly used models. It is based on the specific collector area

(SCA) of the ESP and the effective migration velocity. SCA is defined as the square feet of plate area per 1,000 acfm of gas treated.

$$Pt = \exp\left(-\omega_e \times \frac{A}{Q}\right) \tag{2-13}$$

where

$$SCA = \frac{A}{Q}\,(1000) \tag{2-14}$$

and Pt is the mass fractional penetration, ω_e is the effective migration velocity, A is the area of the collecting electrode, and Q is the gas flow rate. Lawless and Sparks (1985) also discuss a modified DA model which is know as the Matts-Ohnfeldt (MO) model. This model accounts for the variations of particle size distributions for ESPs of nearly equivalent size.

$$Pt = \exp\left[-\left(\omega_k \times \frac{A}{Q}\right)^k\right] \tag{2-15}$$

where ω_k is the effective MO migration velocity, and k is an exponential factor which is commonly 0.5 for fly ash, but varies for different particles.

Lawless and Sparks (1985) also present the Cooperman (CC) model, the Robinson (MR) model, the Research Triangle Institute (RTI) model, and the Southern Research Institute (SRI) model. The Cooperman model is similar to the Deutsch-Anderson and Matts-Ohnfeldt models in that all of the effects of particle collection are expressed in terms of a migration velocity. The other models attempt to account for the non-ideal circumstances which are present in electrostatic precipitators, such as sneakage

and rapping reentrainment. These more complex models require more detailed information about the system operating conditions and particle sizes, which may be difficult to obtain. Comparisons show that the Matts-Ohnfeldt model yields results as accurate as the Deutsch-Anderson model when values of k range from 0.4 to 0.5, as shown in Figure 2-13.

Gallaer (1983) used tests obtained from three different precipitators tested at different conditions of SCA in order to compare the results of the Deutsch-Anderson and Matts-Ohnfeldt models. He began by testing each precipitator at a high SCA and determining the actual efficiency. He then set the value of k in the Matts-Ohnfeldt model to 0.5, and used the measured efficiency of each test to determine the corresponding value of ω_k. He then used this value of ω_k to predict the efficiency of the precipitator at a smaller SCA, and compared the results of the measured efficiency to the predicted efficiencies from the Deutsch-Anderson and the Matts-Ohnfeldt models. His results are summarized in Table 2-2.

Table 2-2. Comparison of measured efficiency and predicted efficiency using the Deutsch-Anderson and Matts-Ohnfeldt models.

Unit	Test Data		New Conditions		Predicted Efficiency (error) at new conditions, %	
Test	SCA	Eff	SCA	Eff	Deutsch-Anderson	Matts-Ohnfeldt
Neal #3	745	99.7	550	98.97	98.63 (-0.34)	99.32 (+0.35)
San Juan	385	99.74	270	99.61	98.46 (-1.15)	99.32 (-0.29)
Mt. Storm	287	96.3	217	95.3	91.75 (-3.55)	94.31 (-0.99)

Source: Gallaer, C. A. *Electrostatic Precipitation Reference Manual.* Electric Power Research Institute, Palo Alto, CA, (1983).

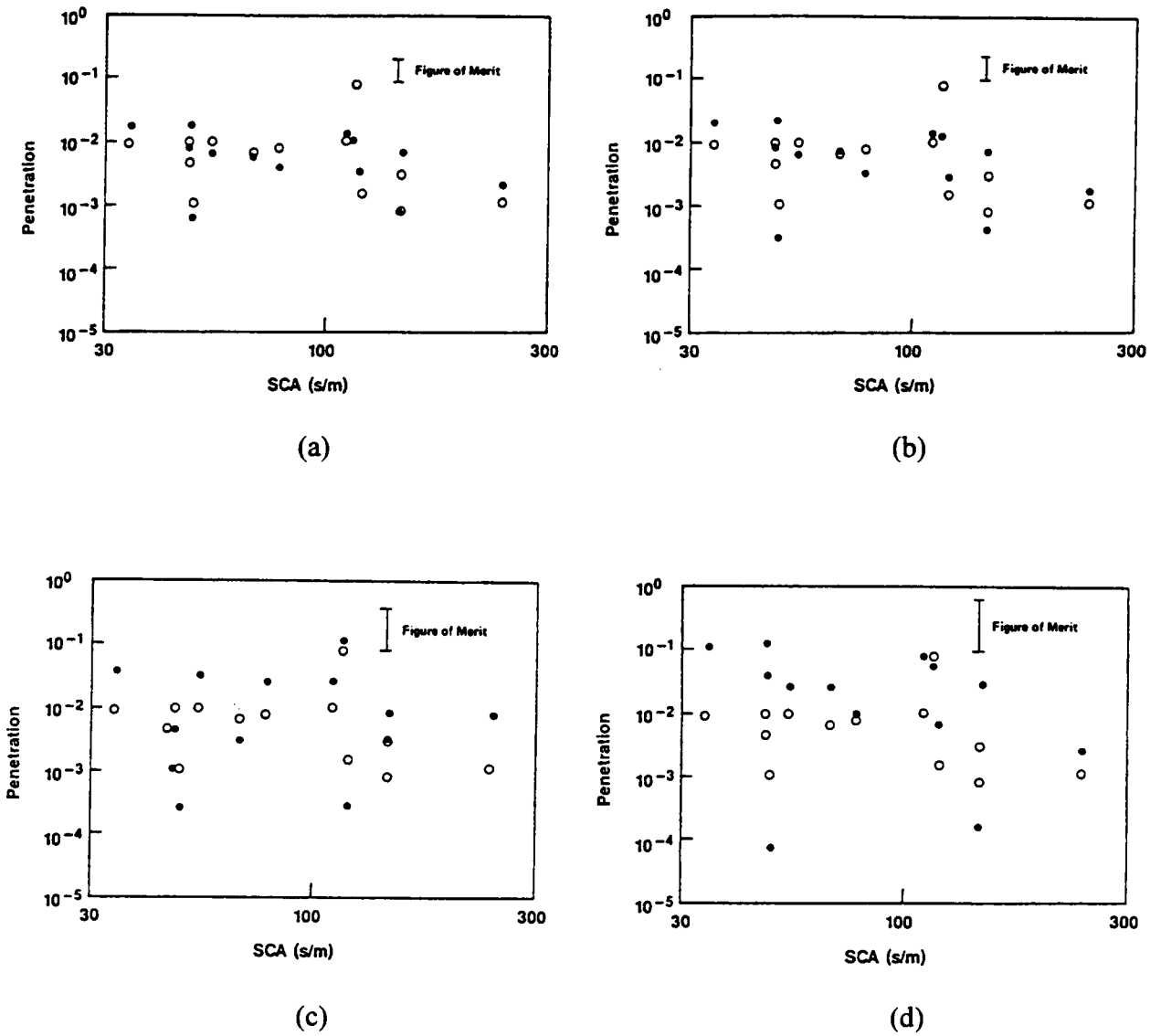

Figure 2-13. Comparison of predictive electrostatic models: (a) Matts-Ohnfeldt model results (•) compared with measured penetrations (k=0.4) (b) Matts-Ohnfeldt model results (•) compared with measured penetrations (k=0.5) (c) Cooperman model (•) compared with measured penetrations (d) Deutsch-Anderson model (•) compared with measured penetrations.

Source: Lawless, Phil A., and Leslie E. Sparks. "A Review of Mathematical Models for ESPs and Comparison of Their Successes." *Proceedings: Second International Conference on Electrostatic Precipitation.* Ed. Senichi Masuda. Pittsburgh: Air Pollution Control Association, 1985. 513-22.

These results also indicate that for the collection of flyash the Matts-Ohnfeldt model yields more accurate results at predicting the overall efficiency than the Deutsch-Anderson model, when a value of 0.5 is used for *k*.

2.4 IMAGE FORCE ATTRACTION

One of the five cases which describe the electrostatic relationships which exist between particles and collectors, as described by Nielsen and Hill (1976), is the electrical image force between a charged particle and a neutral collector. This mechanism of particle collection is known as image force attraction. The *Ceilcote* Ionizing Wet Scrubber (IWS) reportedly uses the principle of image force attraction in the collection of sub-micron particles. The IWS consists of two main components - an ionizing section, and a packed bed scrubber. A schematic of a typical system is shown in Figure 2-14.

The ionizing section of the IWS consists of a series of parallel plates with wires suspended equidistant between adjacent plates. The plates are continually flushed with water from an overflow weir located at the top of the plates. The water flow prevents particles from building up a resistive dust layer on the plates, and also serves to absorb acid gas from the gas stream in scrubbers where the scrubbing liquor contains an alkali such as sodium hydroxide. A series of smooth wires are centered between the plates. A negative D.C. voltage is applied between the wires and plates which creates an intense corona and causes particles in the gas stream to become electrostatically charged.

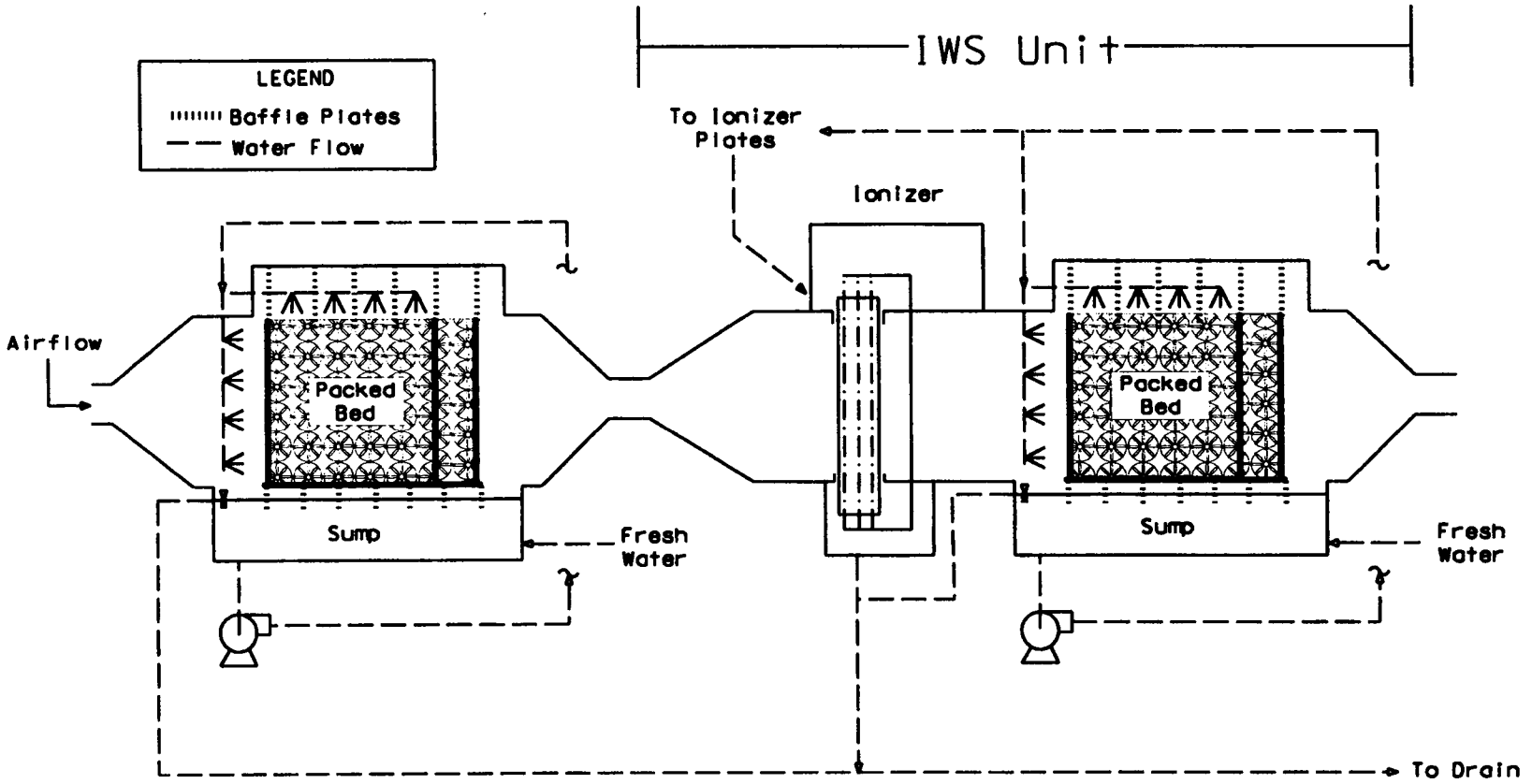

Figure 2-14. Schematic of typical IWS system.

The packed bed scrubber section of the IWS consists of a cross-flow scrubber which is packed with Tellerettes®. The gas stream travels horizontally through the packed bed, while the scrubbing liquor, which is supplied by a spray header and series of low pressure spray nozzles at the top of the packed bed, travels vertically downward through the bed. A header and series of spray nozzles located at the front of the bed continually flushes the Tellerette® packing in order to reduce particle build-up and plugging of the front face of the packing.

Although the mechanism of particle charging in the IWS is exactly the same as that for an ESP, the packed bed immediately downstream of the ionizing section employs an additional mechanism for collection known as image force attraction in order to collect sub-micron particles. Sheppard (1993) reports that image force attraction occurs when an electrostatically charged particle moves within the boundary layer of a neutral surface. The charged particle induces a charge of opposite polarity on the neutral surface. The force of attraction is equal to the force that would exist between the charged particle and an imaginary particle of opposite polarity located at an equal distance behind the surface. This is shown schematically in Figure 2-15.

The image force attraction occurs between the charged particles which exit the ionizing section of the IWS and the neutral Tellerette® packings and water droplets in the packed bed section of the IWS. As discussed by Sheppard (1993), the rose-like filaments of the Tellerette® packing in the packed bed provide a tortuous path through which the particles must travel. The distance that a particle must travel in order to reach a

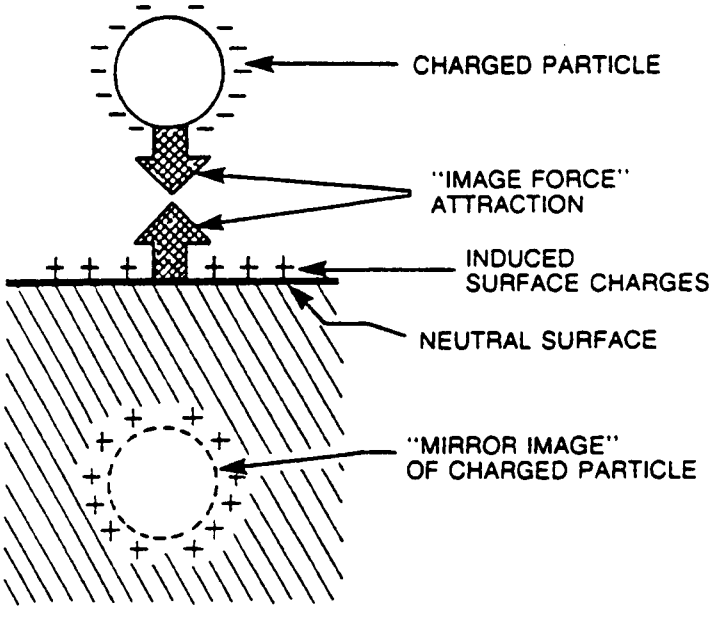

Figure 2-15. Image force attraction.

Source: Sheppard, Stanton V. "Fine Particle Removal for Hazwaste Incinerators with the Ionizing Wet Scrubber." Proceedings: 86th Annual Meeting of the Air and Waste Management Association (1993).

collecting surface is therefore, small compared to the distance particles in an ESP must travel in order to reach a collecting surface. This increases the probability the probability that a particle will come close enough to the surface of the packing to be collected by image force attraction. Upon collection, the particles are flushed from the surface of the packings by the scrubbing liquor. This reduces reentrainment of particles, and plugging of the packings.

2.5 THE IONIZING WET SCRUBBER

The Ionizing Wet Scrubber (IWS) was developed by Ceilcote Air Pollution Control in 1970 to remove fine solid and liquid particulate down to 0.05 microns with high efficiency and low energy consumption, as well as control acidic off-gases that contain compounds such as HCl, HF, and SO_2. The IWS reportedly combines the mechanisms of inertial impaction, interception, electrostatics, particle agglomeration, particle growth, and image force attraction in order to achieve high particle collection efficiencies.

As discussed in the previous section, the IWS consists of an ionizing section followed by a packed bed scrubber. The term IWS describes an ionizing section and packed bed as a single unit. In most applications, a pre-scrubber is placed upstream of the IWS. This pre-scrubber is generally dimensionally and functionally equivalent to the packed bed scrubber downstream of the IWS. The purpose of the pre-scrubber is to remove acid gases and assure that the gas stream entering the IWS is saturated.

In many applications, two or more IWS units are placed in series in order to improve the particle collection efficiency. Ensor and Harmon (1980) evaluated such an IWS installed on a refractory brick kiln. The particulate control system consisted of a quench tower, followed by a pre-scrubber with a cooling tower, and two IWS units in series. The flowrate of flue gas to the quench unit was 60,000 acfm at a temperature of 300° F. The temperature of the flue gas was reduced to 140° F in the quench tower by evaporative cooling before entering the pre-scrubber. The cooling tower reduced the

temperature of the scrubbing liquor from 120° F to 85° F. The facial area of the pre-scrubber was 3 m x 3 m with a 6 foot deep bed of Tellerettes®. After exiting the pre-scrubber, the flue gas entered the first IWS. The first ionizer operated at 30 kV, with a current of 100 to 110 mA. A scrubber containing 4 feet of irrigated 2" Type-R Tellerettes®, and 1 foot of non-irrigated Tellerettes® used for entrainment separation, followed the first ionizer. The second ionizing section operated at 32.5 kV with a current of 210 to 225 mA. A scrubber identical to the first scrubber followed the second ionizer.

Ensor and Harmon (1980) used an MRI cascade impactor, in-stack filters, and a TSI electric aerosol size analyzer (EASA) to characterize the particulates in the gas stream, and determine collection efficiency of the system. The flue gas was sampled upstream of the quench tower and downstream of the second IWS. Table 2-3 provides a summary of the overall mass collection efficiency as determined by the cascade impactor and in-stack filter tests. Figure 2-16 shows the dependence of particle size on penetration for the cascade impactor and EASA results.

Ensor and Harmon (1980) noted that aerosols were generated in the quench and pre-scrubber sections due to condensation and evaporation. However, the particles which were generated in the 1 - 10 micron size range were collected in the IWS, and the penetration of the fine particles was unaffected by particle generation.

The average overall mass collection efficiency for 3 days of testing was 93 percent, as shown in Table 2-3. Table 2-3 also indicates that the penetration was greater

Table 2-3. Summary of overall mass collection efficiency

Date (1978)	Run	Inlet Conc. mg/m3 (a) (gr/ft3)	Run	Outlet Conc. mg/m3 (a) (gr/ft3)	Penetration (%)	Efficiency (%)	Opacity (b) (%)	Comments
11/10	25	259	16	756				
	26	256	17	471				IWS Power
(c)	4a	271	46	360				Shut Off
		262 (0.114)		529 (0.231)	201.9	-101.9	81	
11/18	27	349	18	16.9				
	28	318	19	34.8				
		333 (0.145)		25.9 (0.0123)	7.77	92.2	11	
11/20	29	186	36	6.84				
	30	185	37	15.1				
(c)	5a	226	5c	7.41				Phase II Tests
		199 (0.0831)		9.78 (0.00426)	4.91	95.1	3.7	After Completion of Repairs
11/21	32	198	38	19.7				
	33	218	39	21.1				
(c)	66	311	6a	9.38				
		242 (0.106)		16.7 (0.00728)	6.9	93.1	6.8	

Note: Both impactors and in-stack filters were heated to 250 F at the outlet.
(a) 21.1 C, 76 cm, dry
(b) 5.5 ft path length
(c) In-stack filter samples - the other mass concentration results were computed from the cascade impactor tests

Source: Ensor, David S., and Dale L. Harmon. "Evaluation of the Ceilcote Ionizing Wet Scrubber." *EPA 600/9-80-039C, Vol III,* Sept. 1980.

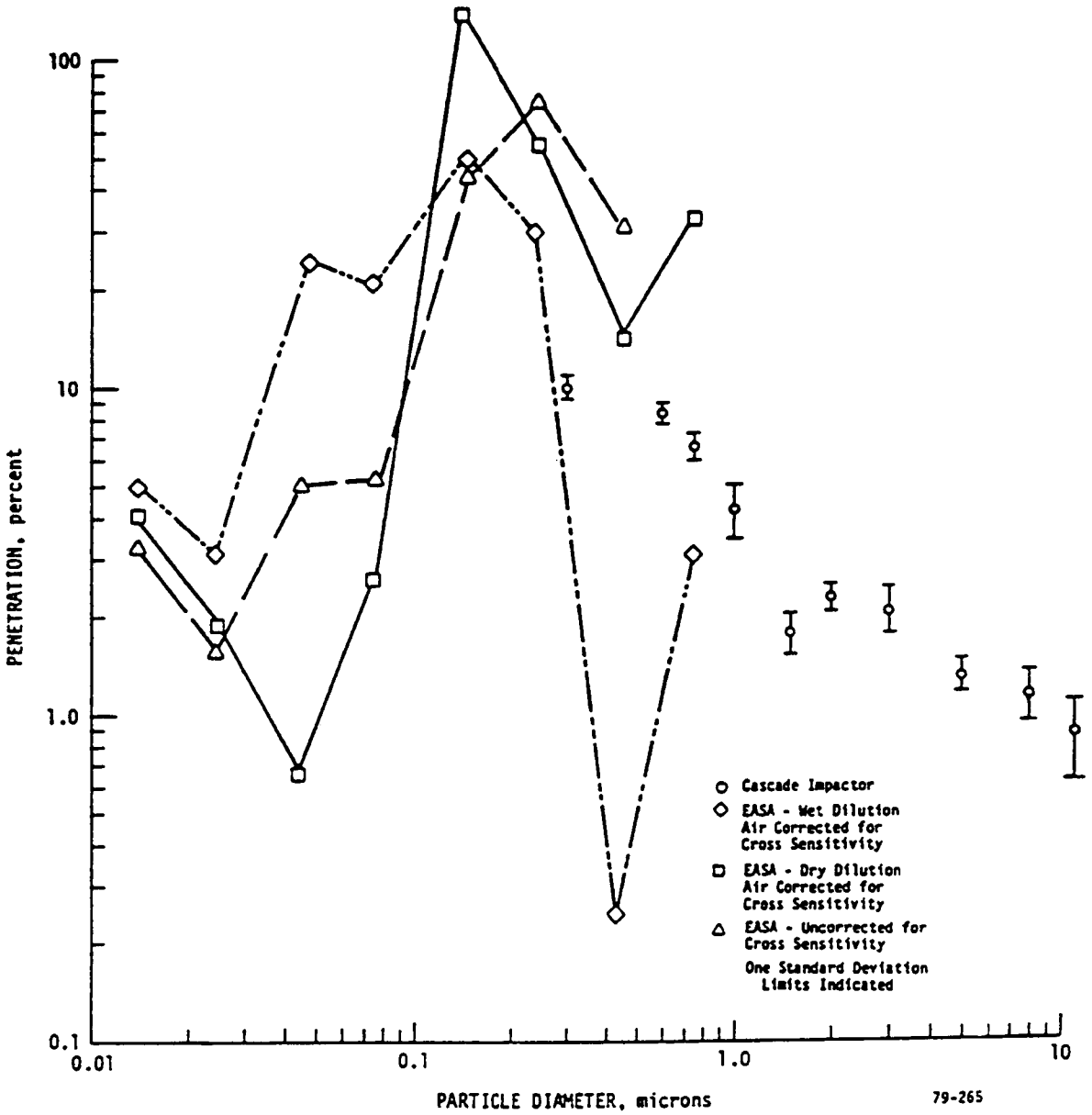

Figure 2-16. Particle size dependent penetration for cascade impactor and EASA results.

Source: Ensor, David S., and Dale L. Harmon. "Evaluation of the Ceilcote Ionizing Wet Scrubber."

than 100 percent when the ionizing section did not operate. This suggests that particle generation, particle growth, and droplet carryover affect the penetration.

Ensor and Harmon (1980) concluded that the cut diameter, the diameter of particles collected with 50% efficiency, of the system was 0.4 to 0.6 microns, and the average inlet concentration to the system was 0.0076 gr/dscf. They also noted that the power required to operate the system was considerably less than a high pressure-drop venturi scrubber, therefore the IWS was more practical for the removal of fine or sub-micron particles.

Troxler et al (1992) also evaluated a pilot scale Ionizing Wet Scrubber which used two IWS units in series to control emissions from a liquid hazardous waste incinerator. The pilot system consisted of a quench tower, a packed column pre-scrubber, and two IWS units in series. Samples were taken at the following four locations using the EPA Method V sampling procedure, with front half analysis, probe rinse, and filter:

- Port 1: upstream of the quench tower
- Port 2: between the pre-scrubber and IWS #1
- Port 3: between IWS #1 and IWS #2
- Port 4: downstream of IWS #2

Tests were conducted with four different process waste streams, and one remedial waste stream. The total particulate removal efficiencies ranged from 89.94 to 99.75% for all waste types, and the particulate emission concentration ranged from 0.00009 - 0.0319 gr/dscf. The average particulate removal efficiency was 95.84%, with an average particulate emission of 0.0094 gr/dscf corrected to 7% O_2.

Troxler et al. (1992) also determined that the average removal efficiency across the first IWS was 82%, while the average removal efficiency across the second IWS was 70%. They attribute this to the average particle size at the entrance of each IWS. The mass mean diameter (MMD) of the particles entering the first IWS was higher than the MMD of the particles entering the second IWS. Therefore, the gas entering the second IWS contained mostly small particles which were more difficult to remove.

It was determined that a relationship existed between the particle removal efficiency and the gas velocity through the IWS unit. With plate velocities in the second IWS of 2.0 to 4.5 feet per second, particulate emissions ranged from 0.005 - 0.02 gr/dscf. At velocities less than 3.75 feet per second, emissions were consistently below 0.01 gr/dscf corrected to 7% O_2.

3. PILOT PLANT SETUP, OPERATION, AND TESTING METHODS

3.1 PILOT PLANT SETUP

The pilot plant system used in this study consisted of a *Ceilcote* cross-flow packed bed pre-scrubber, an Ionizing Wet Scrubber (IWS), a dust-feed system, an induced draft fan, and a stack.. Figure 3-1 shows a picture of the pilot plant system as tested. Figure 3-2 shows a schematic of the pilot plant system tested. Tests were conducted at ambient conditions using air filtered with a HEPA filter. The use of the HEPA filter reduced the presence of particles from the ambient air and minimized the risk of particle concentration fluctuation due to external ambient conditions.

The particle feed system, which supplied a stable particle concentration, was located between the HEPA filter and the pre-scrubber. Flyash obtained from hoppers of out-of-service ESPs which had been converted to settling chambers at the Kingston Steam Plant, operated by TVA in Kingston, TN, was used to study particles with aerodynamic diameters ranging from 0.-to 5.0 microns. The flyash feed system consisted of a vibrating screw feeder with a heated hopper followed by a cyclone. The heated hopper reduced particle agglomeration and bridging of the flyash in the hopper. The screw feeder supplied flyash to the cyclone which removed the large particles from the feed. The flyash loading to the cyclone was adjustable from 5 lb/hr to 22 lb/hr, but was normally operated at 5.75 lb/hr. The particle size distribution of the flyash is included in Appendix A.

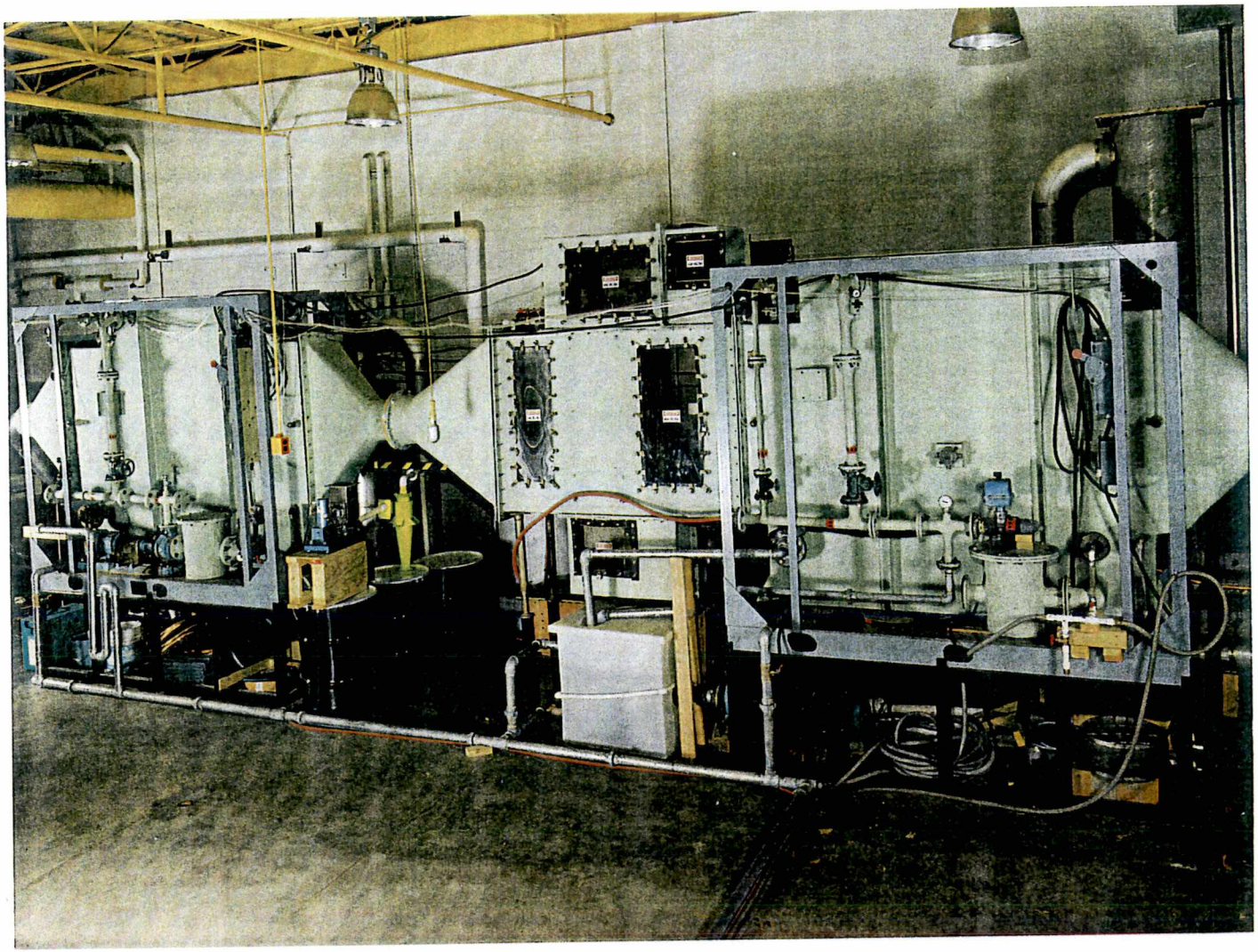

Figure 3-1. Pilot plant system. Gas flow is from left to right, pre-scrubber is on the left, followed by the ionizer in the middle, and the packed bed on the right.

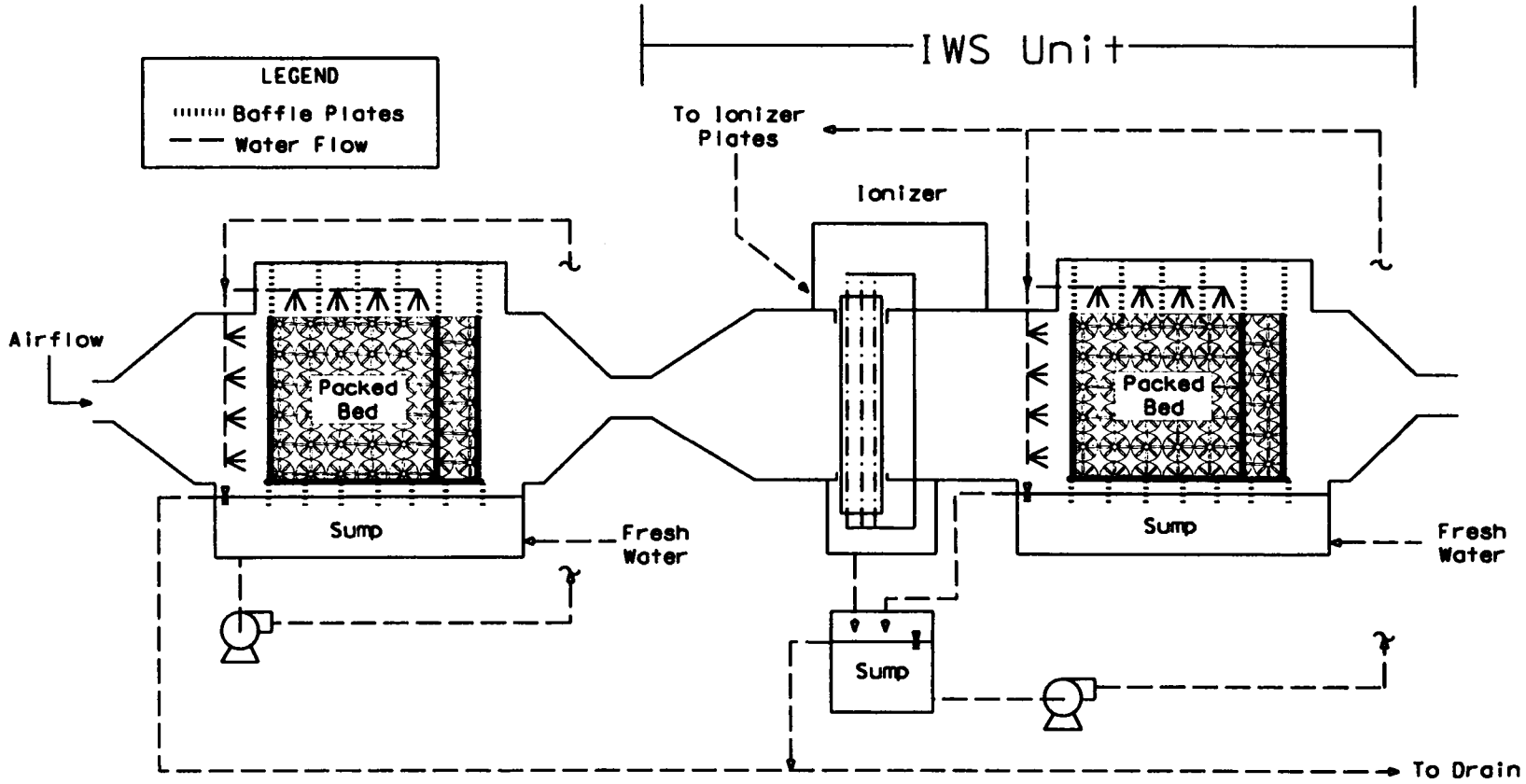

Figure 3-2. Schematic of pilot plant.

Because the MMD of the flyash was large, the concentration of sub-micron particles in the gas stream was low and non-detectable by the sampling equipment. Therefore, in the sub-micron particulate tests, a two-cycle gas powered weed eater was used to generate a combustion aerosol which was used to study the penetration at sub-micron diameters. After removing the flyash feed system, a portion of the exhaust gas from the weed eater was fed into the flue gas stream. Aerodynamic diameters ranging from 0.088 - 1.58 microns were studied using the combustion aerosol as the source of particles.

The particles were injected into the inlet gas stream which then passed through a cross-flow packed bed pre-scrubber. The pre-scrubber was constructed of fiberglass reinforced plastic (FRP), and utilized Tellerettes® as a packing media. Tests, to be described later, were conducted using 2" Type-R, 2" Type-K, and 1" Type-R Tellerettes®.

Figure 3-3 shows the packings that were tested. Physical characteristics of the packings are shown in Table 3-1.

Table 3-1. Physical characteristics of Tellerettes® packing media.

Nominal Packing Size	Maximum Dimension O.D.	Loop Height	Number Pieces/ft^3	Free Volume (%)	Surface ft^2/ft^3
1-inch Type-R	1.81"	0.75"	1000	87	55
2-inch Type-R	2.75"	1.00"	275	92	38
2-inch Type-K	3.25"	1.25"	165	95	28

Source: "Tellerette® Tower Packings." *Ceilcote Air Pollution Control Bulletin 12-20.*

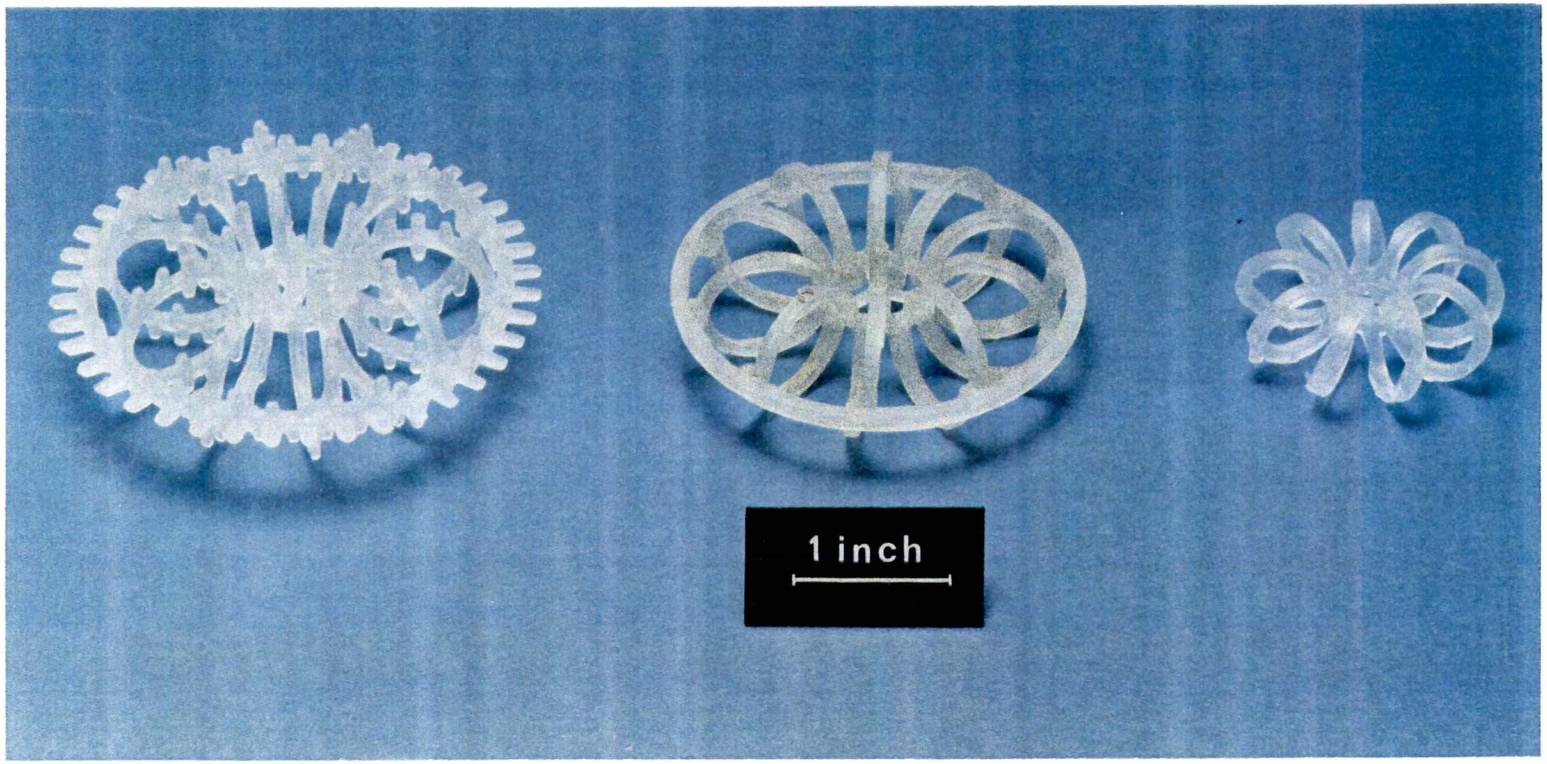

(a) (b) (c)

Figure 3-3. Types of Tellerettes® studied: (a) 2" Type-K ; (b) 2" Type-R ; (c) 1" Type-R

The pre-scrubber had an overall packing depth of 60 inches. The first 48 inches of the packing was irrigated by spray nozzles located at the top of the bed. The last 12 inches of the packing was unirrigated and aided in entrainment separation. The front face of the packing was continually flushed by a series of spray nozzles in order to reduce particle build-up and pluggage of the packing. The packing height was 55 inches and the width was 13.5 inches. An integral 12 inch deep sump was located below the packings. The scrubbing water flowed vertically downward through the packings and was collected in the sump. Fresh water was supplied to the sump, and blowdown from the sump was sent to a drain. This reduced the solids content of the recycle water in the sump. Water flowrates to the top and front spray nozzles were controlled by separate valves to the top and front headers. A calibration of flow rate versus the square root of pressure was performed in order to determine the required liquid flowrates. Data from the TSCA incinerator at Oak Ridge, TN was used to determine the gallons per minute of scrubber water per unit volume of flue gas. Using the baseline case of 900 acfm in the pilot system, the desired scrubber liquid flowrates were then calculated. The liquid flowrate to the nozzles at the front face of the packing was 3.4 gpm, while the liquid flowrate to the nozzles at the top of the packing was 31.1 gpm.

A single-stage IWS unit followed the pre-scrubber. The IWS consisted of an ionizing section followed by a second packed bed which was identical to the pre-scrubber. The ionizing section consisted of 5 parallel plates, with three $1/16$ inch diameter wires suspended between adjacent plates. The wires were $3\,3/8$ apart. The

plates were 47 inches high, 12 inches deep (in the direction of gas flow), $1\frac{3}{8}$ inches thick, and had a face-to-face spacing of $2\frac{7}{8}$ inches. Thus, the plate-to-wire spacing was $1\frac{7}{16}$ Overflow weirs were located at the top of each plate. A half-gallon of water per minute flowed over each weir and down the faces of each plate in order to reduce particle build-up on the plates. The voltage across the wires and plates was controlled by an automatic control system supplied with the IWS. The maximum D.C. voltage between the wires and plates was 35 kV, and dropped to 25 kV when spark-over occurred. The D.C. current was 100 mA when the voltage was 35 kV. After four hours of operation, the controls shut down the high voltage to the ionizer, at which time the plates and internal surfaces of the ionizer were flushed by a series of spray nozzles located inside of the unit. This removed residual particle build-up. This 2 minute backwash was followed by a drip-dry period of two minutes. Therefore, the ionizing portion of the system was non-operational for a period of 4 minutes every 4 hours. It should be noted that tests in this study were not conducted when the IWS was in the backwash mode.

Data from the TSCA incinerator was used as the guideline for setting the velocity of the flue gas between the ionizer plates under maximum flow conditions. This baseline velocity of 240 ft/min was used to determine a baseline gas flowrate in the pilot system of 900 acfm.

The IWS was followed by an induced draft fan which maintained a negative pressure in the system. The gas flowrate through the system was adjusted by a damper

located between the fan outlet and the stack. A calibration curve describing the gas flowrate as a function of the square root of the pitot tube ΔP was developed as outlined in 40 CFR 60.AppA. The calibration curve is shown in Appendix A. A standard pitot tube mounted at the point of average velocity in the duct downstream of the IWS, and connected to a magnehelic gage, was used to measure the gas flowrate. Gas flowrate could be adjusted from 500 to 1300 acfm, with a baseline of 900 acfm.

3.2 PILOT PLANT OPERATION

As discussed in the previous section, the baseline gas flowrate in the system was 900 acfm. However, tests were also conducted at 500, 700 and 1100 acfm in order to determine the effects of gas flowrate (i.e., velocity) on particle collection efficiency. In the tests conducted for this portion of the study, the liquid flowrate through the scrubbers was constant. The liquid flowrate to the nozzles at the front face of the packing was 3.4 gpm, while the liquid flowrate to the nozzles at the top of the packing was 31.1 gpm.

The operation of the ionizing section of the IWS was controlled by an automatic control system. The ionizer operated at a maximum D.C. voltage of 35 kV between the wires and the plates, while the D.C. current was 100 mA. The spark-rate was controlled by an automatic spark-rate controller. After four hours of operation, the ionizer entered the backwash mode as previously described. Tests were not performed during the backwash mode.

The baseline operating conditions of the system were at a gas flowrate of 900 acfm, liquid flowrates of 3.4 gpm to the front spray nozzles and 31.1 gpm to the top spray nozzles of the pre-scrubber and packed bed, and with the ionizer operating in the automatic mode with a liquid flowrate of 0.5 gpm to each of the plates. Under those operating conditions, the operating voltage of the ionizer varied from a minimum of 23 kV to a maximum of 35 kV. In order to determine the average operating voltage, the operating voltage was measured at intervals of 5 seconds for a period of 5 minutes. These voltages were then averaged to obtain an average operating voltage. The results of those measurements are shown in Table 3-2. Measurements of the operating voltage as a

Table 3-2. Operating voltage as a function of time under baseline operating conditions.

Time (sec)	Volt. (kV)	Time (sec)	Volt. (kV)	Time (sec)	Volt. (kV)	Time (sec)	Volt. (kV)	Time (sec)	Volt. (kV)
5	33	65	26	125	32	185	30	245	34
10	34	70	24	130	33	190	34	250	34
15	31	75	28	135	34	195	30	255	33
20	32	80	30	140	30	200	33	260	33
25	34	85	30	145	31	205	30	265	35
30	25	90	34	150	32	210	31	270	30
35	33	95	34	155	32	215	35	275	30
40	30	100	34	160	34	220	26	280	31
45	30	105	26	165	32	225	33	285	34
50	30	110	23	170	30	230	35	290	33
55	32	115	30	175	33	235	30	295	33
60	26	120	32	180	31	240	35	300	33

Average Operating Voltage = 31.1 kV

function of time were also made when the system operated at a gas flowrate of 900 acfm, with no scrubbing liquid flowing in the pre-scrubber or over the surface of the ionizing plates. The results of those measurements are shown in Table 3-3. Figure 3-4 shows the

relationship between the operating voltage and time for both of the operating conditions described.

Table 3-3. Operating voltage as a function of time under dry pre-scrubber and dry plate conditions.

Time (sec)	Volt. (kV)	Time (sec)	Volt. (kV)	Time (sec)	Volt. (kV)	Time (sec)	Volt. (kV)	Time (sec)	Volt. (kV)
5	28	65	25	125	29	185	26	245	31
10	30	70	26	130	30	190	28	250	24
15	31	75	29	135	23	195	29	255	26
20	24	80	27	140	26	200	29	260	27
25	24	85	28	145	24	205	31	265	28
30	26	90	30	150	27	210	31	270	29
35	26	95	30	155	28	215	24	275	30
40	27	100	24	160	29	220	24	280	31
45	28	105	24	165	30	225	26	285	26
50	29	110	25	170	31	230	28	290	24
55	29	115	26	175	24	235	30	295	25
60	23	120	28	180	32	240	30	300	27

Average Operating Voltage = 28.0 kV

The following calculations describe the operation of the ionizer at 900 acfm.

The conditions of the flue gas were as follows

Flue gas temperature	85 F

The parameters of the ESP were as follows

Wire to plate spacing	0.0365 m
Wire diameter	0.00159 m
Velocity of flue gas	1.2 m/s

Based on the theory presented by Turner et al (1992), the corona onset field can be estimated for a dry ESP. From equation 2-3, the relative gas density was found as:

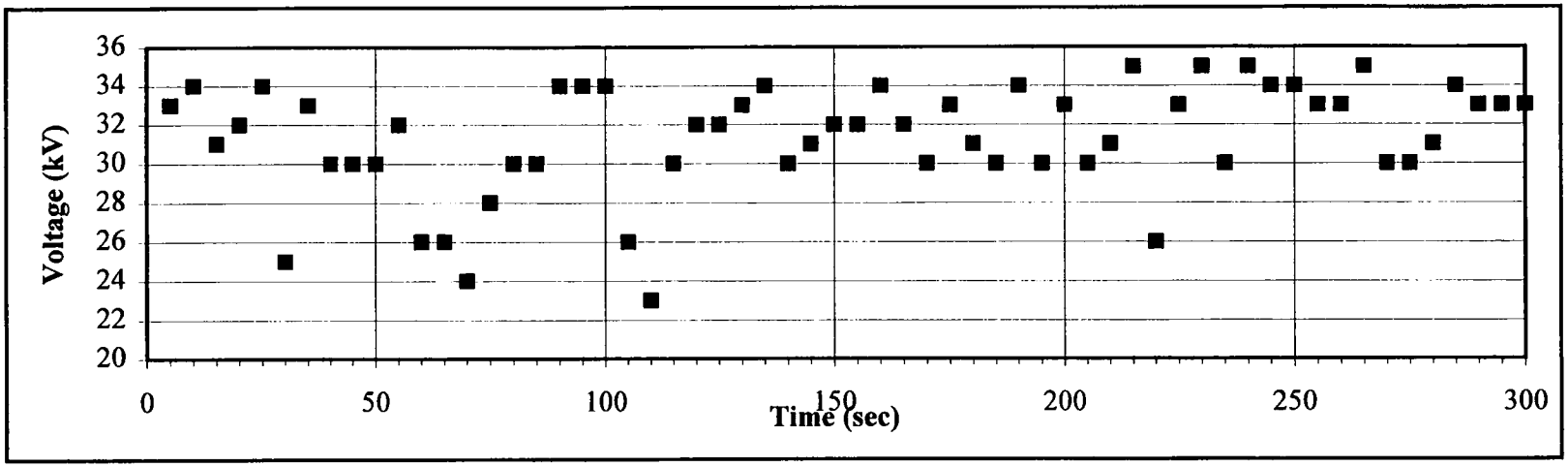

(a)

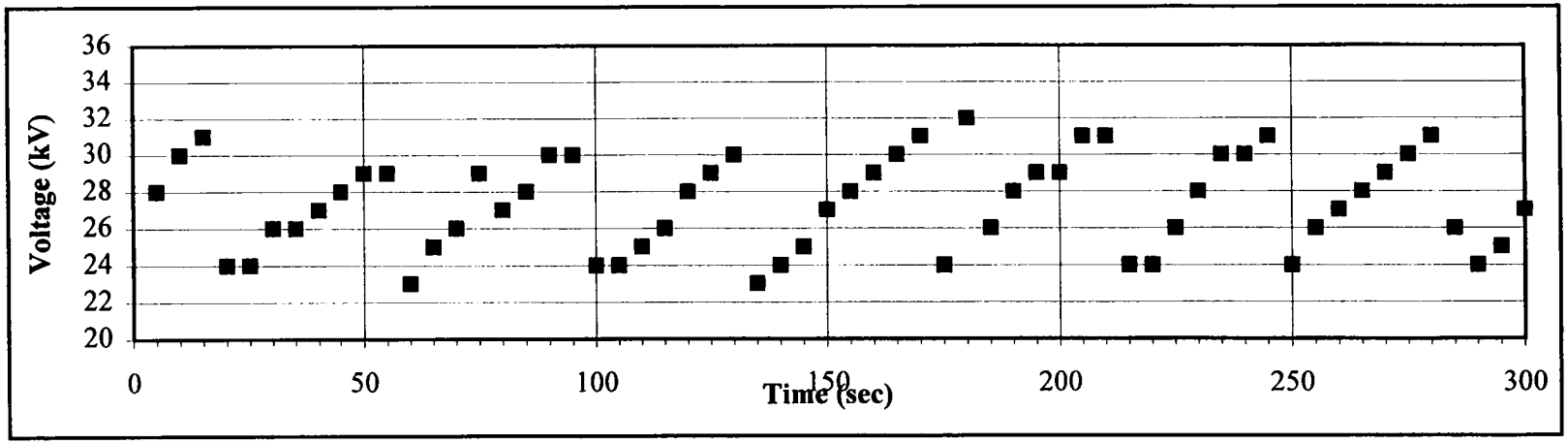

(b)

Figure 3-4. Voltage vs time for ionizer: (a) relationship for wetted plates (b) relationship for dry plates

$$d_r = \frac{T_o P}{T P_o} = \frac{293K(1atm)}{303.6K(1atm)} = 0.97$$

Equation 2-2 was used to calculate the corona onset field strength

$$E_c = 3.126 \times 10^6 \left[d_r + 0.0301 \left(\frac{d_r}{r_w} \right)^{0.5} \right] \text{f}$$

$$E_c = 3.126 \times 10^6 \left[0.97 + 0.0301 \left(\frac{0.97}{\left(\frac{0.00159m}{2} \right)} \right)^{0.5} \right] \times 0.6 = 3.8 \times 10^6 \text{ V/m}$$

The corona starting voltage was determined by equation 2-5 as follows

$$V_c = E_c r_w \ln\left(\frac{4L}{\pi r_w} \right) = \left(3.8 \times 10^6 V/m \right) \left(\frac{0.00159m}{2} \right) \ln\left(\frac{4(0.0365m)}{\pi \left(\frac{0.00159m}{2} \right)} \right) = 12 \text{ kV}$$

The sparking field strength was determined by equation 2-6

$$E_s = 6.3 \times 10^5 \left(\frac{273P}{T} \right)^{1.65} = 6.3 \times 10^5 \left(\frac{273K(0.98atm)}{303.6K} \right)^{1.65} = 5.1 \times 10^5 \text{ V/m}$$

The voltage at which spark-over occurs was determined by equation 2-7, by substituting the sparking field strength for E_{avg}

$$V_{avg} = E_{avg} L = \left(5.1 \times 10^5 V/m \right) (0.0365m) = 19 \text{ kV}$$

Thus, the empirical equations presented by Turner et al (1992) suggest that a dry ESP would operate at a voltage between 12 and 19 kV, whereas the IWS operated at a voltage between 23 and 32 kV when the plates were dry. Furthermore, the IWS operated at a

voltage between 23 and 32 kV when the plates were wetted. There is no apparent obvious reason as to why the IWS operated at higher voltages than a conventional ESP except that the wire-to-plate spacing was very uniform, possible giving rise to a higher operating voltage.

3.3 SAMPLING METHOD

Two primary sampling methods were employed during testing. An optical particle counter (OPC) was used to measure the number of particles with equivalent aerodynamic diameters ranging from 0.5 to 5.0 microns. An electric aerosol size analyzer (EASA) was used to measure the number of particles with aerodynamic diameters ranging from 0.088 to 1.58 microns. The measured penetrations of the system were based on the number of particles collected.

A *Climet* Model 208 optical particle counter was used to measure the number of particles in the aerodynamic size range of 0.5 to 5.0 microns. After particles entered the OPC, they passed through a focused light beam. The particles scattered the light beam, which was then reflected off of an elliptical mirror to a photomultiplier. The intensity of the reflected light was directly proportional to the diameter of the particle which reflected the light. The output from the photomultiplier was amplified to a voltage between 50 mV and 10 V, which corresponded to aerodynamic particle sizes of 0.5 and 10.0 microns, respectively. The signal was transferred to a personal computer containing a multi-

channel analyzer (MCA) which had a resolution of 1024 channels. Each of the channels represented an input voltage and therefore a specific particle size.

The OPC/MCA was calibrated in an ASTM 1215 Test Stand using a *TSI* single jet atomizer and monodisperse latex spheres with a density of 1 g/cm^3. Spheres with diameters of 0.624, 1.07, 2.06, and 2.92 microns were created by atomizing a solution of deionized/distilled water which contained the spheres. The atomized droplets were then dried with clean, dry dilution air to create an aerosol which contained the known diameter latex spheres. A sample was drawn from the test stand through the OPC, and a calibration curve of physical particle diameter versus channel number was developed. Since the flyash used during testing had a density of 2.5 g/cm^3, a curve describing the relationship between the aerodynamic particle size and channel number was developed and used to set regions of interest (ROI) on the MCA (i.e., the 1.0 micron physical diameter size was referred to as an aerodynamic particle size of $(1\mu)(2.5g/cm^3)^{0.5}$ = 1.58μ). Regions of interest were set on the MCA which summed the number of particles in a narrow range centered around aerodynamic particle sizes of 0.5, 1.0, 1.5, 2.0, 2.5, 3.0, 3.5, 4.0, 4.5, and 5.0 microns.

Since the particles in the flue gas sample downstream of the ionizer were charged, it was necessary to place charge neutralizers in the sampling line directly downstream of the sampling nozzle in order to assure that particle collection due to electrostatic forces did not occur in the sampling line. The charge neutralizers were from Static-Master® cartridges which are used in the photographic industry to neutralize charges on film

negatives. These cartridges contained two ^{85}krypton strips which were removed and placed inside of the sampling line. A total of four ^{85}krypton strips were placed in the sampling line. The sampling nozzle used with the OPC was constructed from $1/4$ inch diameter thin-walled stainless steel tubing and was connected to the OPC with Tygon tubing. During the 10 months of testing, no deposition or build-up of particles in the sampling line or sampling nozzle was observed.

A *TSI* Model 3030 electric aerosol size analyzer (EASA) was used to measure the number of particles in the aerodynamic size range of 0.088 - 1.58 microns. The main components of the EASA consisted of a vacuum pump, a charging section which was similar to a shell-and-tube electrostatic precipitator, an electrometer, and a control system. The vacuum pump pulled a continuous sample of flue gas through the EASA. After the flue gas sample entered the EASA, it passed through the charging section which consisted of a wire suspended in a tube. A pre-set voltage was automatically applied between the wire and the tube. This applied voltage charged the particles in the sample stream and caused some of the particles to be collected on the inside wall of the tube. The applied voltage corresponded to the collection of particles smaller than a given size. For example, Channel 4 on the output display corresponded to an applied voltage of 588 volts. At this applied voltage, particles with a diameter less than 0.0178 microns were collected on the inside wall of the tube. Channel 5 corresponded to an applied voltage of 1870 volts. At this applied voltage, particles with a diameter less than 0.0316 microns were collected on the inside wall of the tube. The charged particles which were not

collected on the tube passed through the charger and entered an absolute filter which was connected to an electrometer. The charges of the particles collected by the filter drained into the electrometer. The electrometer measured these charges and converted the signal to a current which was displayed on a digital readout on the control panel. The difference between the current outputs of two consecutive channels was directly proportional to the number of particles collected between the diameters which corresponded to those two channels.

The sampling nozzle used with the EASA was constructed of $\frac{1}{8}$ inch diameter glass. The tip of the nozzle was tapered in a manner similar to an EPA Method 5 sampling nozzle. The nozzle was connected to the EASA with Tygon tubing, and the charge neutralizers were placed in the sampling line directly downstream of the sampling nozzle. The flue gas sample downstream of the IWS unit was saturated with moisture. The saturated flue gas sample caused the EASA to become unstable and give erratic readings. Therefore, it was necessary to dilute the flue gas sample entering the EASA with clean dried dilution air. The dilution air was supplied by a compressed air line which passed through a pressure regulator, a drying bed which contained Drierite as a desiccant, a particle filter, and finally a flowmeter. Several different ratios of dilution air to sample air were tested, and a 4:1 ratio of dilution air to sample air was found to provide the most stable results. The dilution air was supplied to the flue gas sample directly downstream of the sampling nozzle and directly upstream of the charge neutralizers. The EASA operated at a flowrate of 8.2 L/min. Therefore, 6.56 L/min of

dilution air was supplied to the sampling line, while 1.64 L/min of flue gas sample was drawn from the duct. In order to maintain the same degree of non-isokinetic flow, the dilution system was used at all of the sampling ports during testing with the EASA, although isokinetic sampling of sub-micron particles is not as important as it is for particles with diameters greater than 1 micron.

The majority of data collected in this study was used to determine the penetrations of particles based on particle numbers. However, the overall mass collection efficiency of the system is an important parameter that must be known in order to properly design and predict outlet grain loading in the system. Therefore, tests were conducted in order to determine the overall mass collection efficiency of the system.

The results of the overall mass collection efficiency are included in Appendix C. Three independent methods were used to measure the overall collection efficiency, including a cascade impactor, an EPA Method V sampling train, and an optical particle counter. Results were not obtained with the cascade impactor because the grain loading was too low. However, tests which were conducted with an EPA Method V sampling train and the OPC were successful in regards to measuring the overall mass collection efficiency of the system. These tests are described in further detail in Appendix C.

3.4 SAMPLING LOCATIONS

Two sampling ports were located on the system. One of these ports, Port I, was located upstream of the pre-scrubber and downstream of the particle feed system.

Approximately 25 feet of ductwork separated the particle feed system and sampling port. This assured adequate mixing of the particles in the gas stream. The second port, Port O, was located downstream of the IWS and upstream of the I.D. fan. Adequate distance between the sampling ports and bends in the ductwork assured uniform distribution of dust in the gas stream and uniform distribution of the gas stream in the ducts.

Both of the sampling ports were located in 8-inch diameter ducts, therefore the velocity of flue gas at each sampling location was identical. Isokinetic sampling was not necessary since both the upstream and downstream samples were the same percent non-isokinetic. Errors due to non-isokinetic sampling were minimized since the efficiency was determined by a difference between the upstream and downstream values. Tests performed with nozzles of two different diameters showed minimal error in the results obtained due to non-isokinetic sampling.

3.5 SUMMARY OF TESTS CONDUCTED

Tests were conducted while the system operated both with and without power to the ionizing section, at gas flowrates of 500, 700, 900, and 1100 acfm. Tests were also conducted using different types of Tellerette® packing media. A summary of the tests conducted for this phase of the study is provided in Table 3-4. A complete summary of all tests conducted during all phases of the study is provided in Appendix B.

A "test" is defined as the collection and measurement of the number of particles in five flue gas samples taken consecutively from Port I, followed by the collection and

measurement of the number of particles in five flue gas samples taken consecutively from Port O. The number of particles collected in the five samples taken from Port I were averaged, as were the number of particles collected in the five samples taken from Port O. The average number of particles was then used to calculate the penetration of particles at each size range measured using the following equation:

$$\text{Fractional Penetration} = 1 - \text{Fractional Efficiency} = \frac{\text{Avg. No. of Counts at Outlet of IWS}}{\text{Avg. No. of Counts at Inlet of Prescrubber}} = \frac{\text{Avg. No. of Counts at Port O}}{\text{Avg. No. of Counts at Port I}} \quad (3\text{-}1)$$

Critical tests were repeated from three to five times in order to assure reproducibility of the results. Other less critical tests were only performed once.

Table 3-4. Summary of tests.

Gas Flowrate (acfm)	Operating * Conditions	Packing Media**	Particle Size Studied (microns)	Test Number+
500	p1w35p2w	2R	0.5 - 5.0	2R.05.O.T1
500	p1w35p2w	2R	0.5 - 5.0	2R.05.O.T2
500	p1w35p2w	2R	0.5 - 5.0	2R.05.O.T3
500	p1w35p2w	2R	0.5 - 5.0	2R.05.O.T4
500	p1w35p2w	2R	0.5 - 5.0	2R.05.O.T5
500	p1wp2w	1R	0.5 - 5.0	1R.05.O.G1
500	p1wp2w	1R	0.5 - 5.0	1R.05.O.G2
500	p1wp2w	1R	0.5 - 5.0	1R.05.O.G3
500	p1w35p2w	1R	0.5 - 5.0	1R.05.O.T1
500	p1w35p2w	1R	0.5 - 5.0	1R.05.O.T2
500	p1w35p2w	1R	0.5 - 5.0	1R.05.O.T3
500	p1wp2w	2R	<1.0	2R.05.E.BB1
500	p1w35p2w	2R	<1.0	2R.05.E.DD1
700	p1wp2w	2R	<1.0	2R.07.E.BB1
700	p1w35p2w	2R	<1.0	2R.07.E.DD1
900	p1w35p2w	2R	0.5 - 5.0	2R.09.O.T1

Table 3-4. Summary of tests (cont.).

Gas Flowrate (acfm)	Operating * Conditions	Packing Media**	Particle Size Studied (microns)	Test Number+
900	p1w35p2w	2R	0.5 - 5.0	2R.09.O.T2
900	p1w35p2w	2R	0.5 - 5.0	2R.09.O.T3
900	p1w35p2w	2R	0.5 - 5.0	2R.09.O.T4
900	p1w35p2w	2R	0.5 - 5.0	2R.09.O.T5
900	p1wp2w	2K	0.5 - 5.0	2K.09.O.G1
900	p1wp2w	2K	0.5 - 5.0	2K.09.O.G2
900	p1wp2w	2K	0.5 - 5.0	2K.09.O.G3
900	p1w35p2w	2K	0.5 - 5.0	2K.09.O.T1
900	p1w35p2w	2K	0.5 - 5.0	2K.09.O.T2
900	p1w35p2w	2K	0.5 - 5.0	2K.09.O.T3
900	p1wp2w	1R	0.5 - 5.0	1R.09.O.G1
900	p1wp2w	1R	0.5 - 5.0	1R.09.O.G2
900	p1wp2w	1R	0.5 - 5.0	1R.09.O.G3
900	p1w35p2w	1R	0.5 - 5.0	1R.09.O.T1
900	p1w35p2w	1R	0.5 - 5.0	1R.09.O.T2
900	p1w35p2w	1R	0.5 - 5.0	1R.09.O.T3
900	p1wp2w	2R	<1.0	2R.09.E.BB1
900	p1wp2w	2R	<1.0	2R.09.E.BB2
900	p1w35p2w	2R	<1.0	2R.09.E.DD1
900	p1w35p2w	2K	<1.0	2K.09.E.DD1
1100	p1w35p2w	2R	0.5 - 5.0	2R.11.O.T1
1100	p1w35p2w	2R	0.5 - 5.0	2R.11.O.T2
1100	p1w35p2w	2R	0.5 - 5.0	2R.11.O.T3
1100	p1w35p2w	2R	0.5 - 5.0	2R.11.O.T4
1100	p1w35p2w	2R	0.5 - 5.0	2R.11.O.T5
1100	p1wp2w	1R	0.5 - 5.0	1R.11.O.G1
1100	p1wp2w	1R	0.5 - 5.0	1R.11.O.G2
1100	p1wp2w	1R	0.5 - 5.0	1R.11.O.G3
1100	p1w35p2w	1R	0.5 - 5.0	1R.11.O.T1
1100	p1w35p2w	1R	0.5 - 5.0	1R.11.O.T2
1100	p1w35p2w	1R	0.5 - 5.0	1R.11.O.T3
1100	p1wp2w	2R	<1.0	2R.11.E.BB1
1100	p1w35p2w	2R	<1.0	2R.11.E.DD1

* This refers to the operating conditions of the system. The term p1wp2w describes the system when it operated with scrubbing liquid in the pre-scrubber and packed bed, however the ionizer was not operating. The term p1w35p2w describes the system when it operated with scrubbing liquid in the pre-scrubber and packed bed, and the ionizer operated in the automatic mode with a maximum voltage of 35 kV.

** Three types of packing media were studied. The term 2R describes the 2" Type-R Tellerettes®, the term 2K describes the 2" Type-K Tellerettes®, and the term 1R describes the 1" Type-R Tellerettes®.

+ Each test has been assigned a unique number. The results of all the tests performed are provided in Appendix B. This test number can be used to locate the results of the test.

4. RESULTS AND DISCUSSION

4.1 PARTICLE COLLECTION EFFICIENCY

Results of experiments conducted under the same operating conditions, but performed on different days, or at different times during the same day show some minor variations in particle collection efficiency. These variations may be the result of different ambient air temperatures, scrubbing liquid temperature, and other parameters beyond the control of these experiments. Therefore, the results of all tests performed under the same operating conditions were averaged during the data analysis.

The following nomenclature is used in this chapter:

p1wp2w - the pre-scrubber and packed bed each operated with liquid flowrates of 3.4 gpm to the front spray nozzles and 31.1 gpm to the top spray nozzles, and the ionizer did not operate.

p1w35p2w - the pre-scrubber and packed bed each operated with the same liquid flowrates as mentioned above, however, the ionizing section also operated in the automatic mode, with water flowing on the surface of the plates, at an average operating voltage of 31.1 kV.

Unless otherwise noted, the tests were performed with 2" Type-R Tellerette packing in the pre-scrubber and packed bed. It should be noted that electrostatic theory generally deals with the physical diameter of particles, while inertial impaction theory deals with the aerodynamic diameter. However, the physical and aerodynamic diameters are related as follows:

$$d_a = d_p \sqrt{\rho_p} \qquad (4\text{-}1)$$

where d_a is the aerodynamic diameter, d_p is the physical diameter of the particle, and ρ_p is the density of the particle in g/cm^3.

It should be noted that tests were conducted at gas flowrates of 500, 900 and 1100 acfm. Results of tests conducted on the system when operated at p1wp2w are reported in terms of the gas flowrate. However, in order to normalize the system, results of tests when operated at p1w35p2w are reported in terms of the specific collector area (SCA), as is common practice in the electrostatic precipitator industry. The SCA is defined as the plate area in ft^2 per 1,000 acfm of gas treated. Thus, based on an ionizer plate area of 31.3 ft^2, SCA's of 62.6, 34.8 and 28.5 correspond to gas flowrates of 500, 900 and 1100 acfm, respectively.

4.1.1 Effect of Particle Diameter on Penetration

Figure 4-1 shows the average results of five consecutive tests that were conducted while the system operated at p1w35p2w and a SCA of 34.8, for particles with aerodynamic diameters ranging from 0.118 - 5.0 microns. The data collected from 0.118 - 1.18 microns were obtained with the EASA, while the data collected from 2.5 - 5.0 microns were obtained with the OPC. Note that there is more scatter in the data collected with the EASA than in the data collected with the OPC. This scatter is a result of human error in reading the EASA, as well as error created by sampling with the EASA in a moisture saturated gas stream.

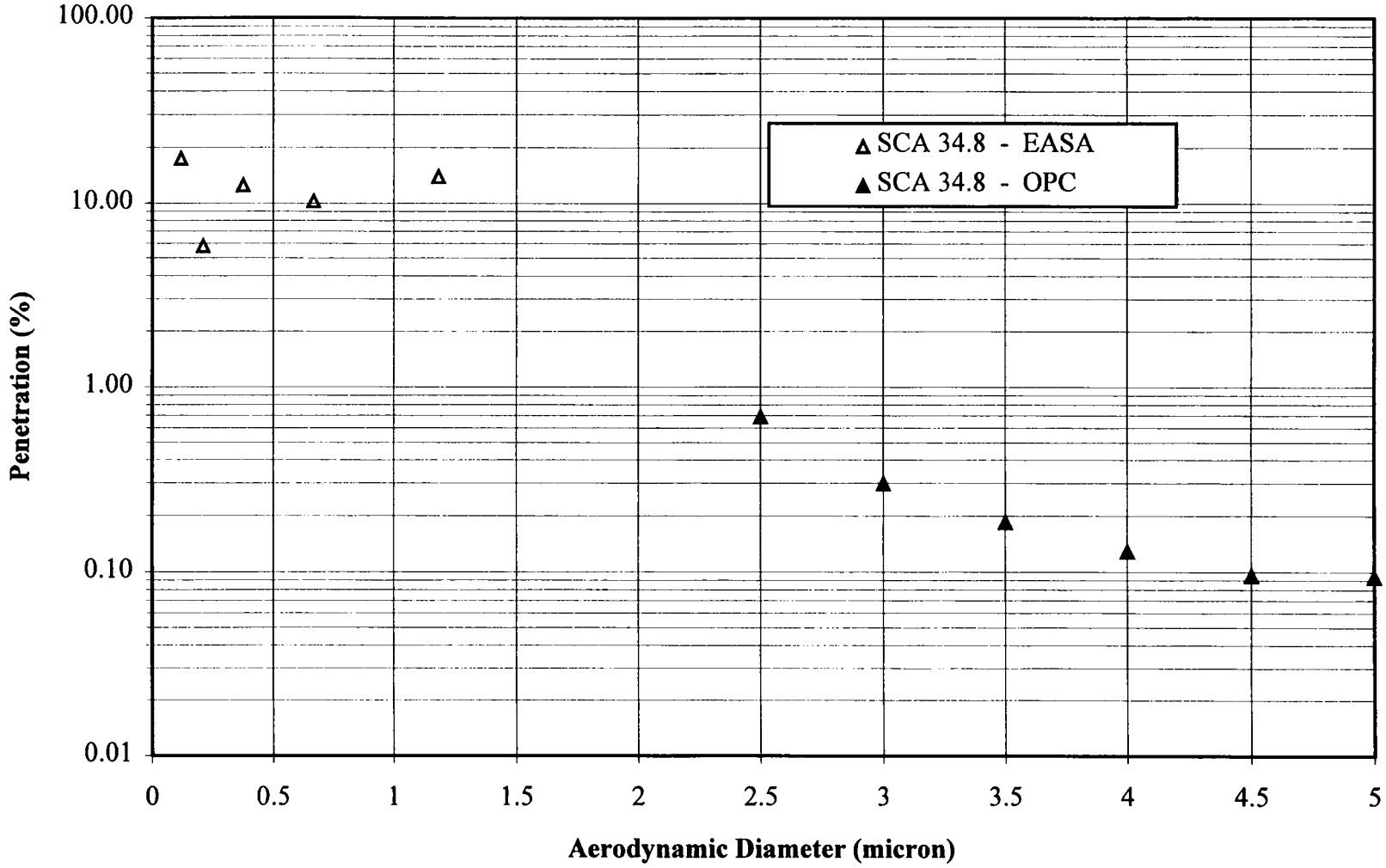

Figure 4-1. Measured penetrations at p1w35p2w for SCA of 34.8.

As indicated in the figure, there is a strong correlation between the penetration and aerodynamic diameter. In general, an increase in aerodynamic diameter results in decreased penetration. It is important to note that not only did inertial impaction occur, as studied by Abraham (1996), but electrostatic collection also occurred. Substantially lower penetrations (or higher efficiencies) were observed than those observed by Abraham, who studied the packed beds without the ionizer. These results generally agree with the theory which was cited in the literature review chapter which suggests that penetration decreases when particles are charged. Abraham showed that the penetration was a strong function of the aerodynamic diameter when the system operated at p1wp2w. Electrostatic theory also suggests that penetration is a strong function of physical diameter.

4.1.2 Effect of Gas Flowrate on Penetration

From the results of his studies with the system operating at p1wp2w, Abraham (1996) concluded that the efficiency of the system seemed to be fairly constant with an increase in the gas flowrate for particles with aerodynamic diameters from 2.0 - 5.0 microns. Further testing with the system operating at p1wp2w for various flowrates confirmed Abraham's conclusion.

Tests were also conducted in the present study while the system operated at p1w35p2w, at SCAs of 62.6, 34.8, and 28.5. Figure 4-2 shows the relationship between the penetration and aerodynamic diameter at those SCAs, for particles with aerodynamic

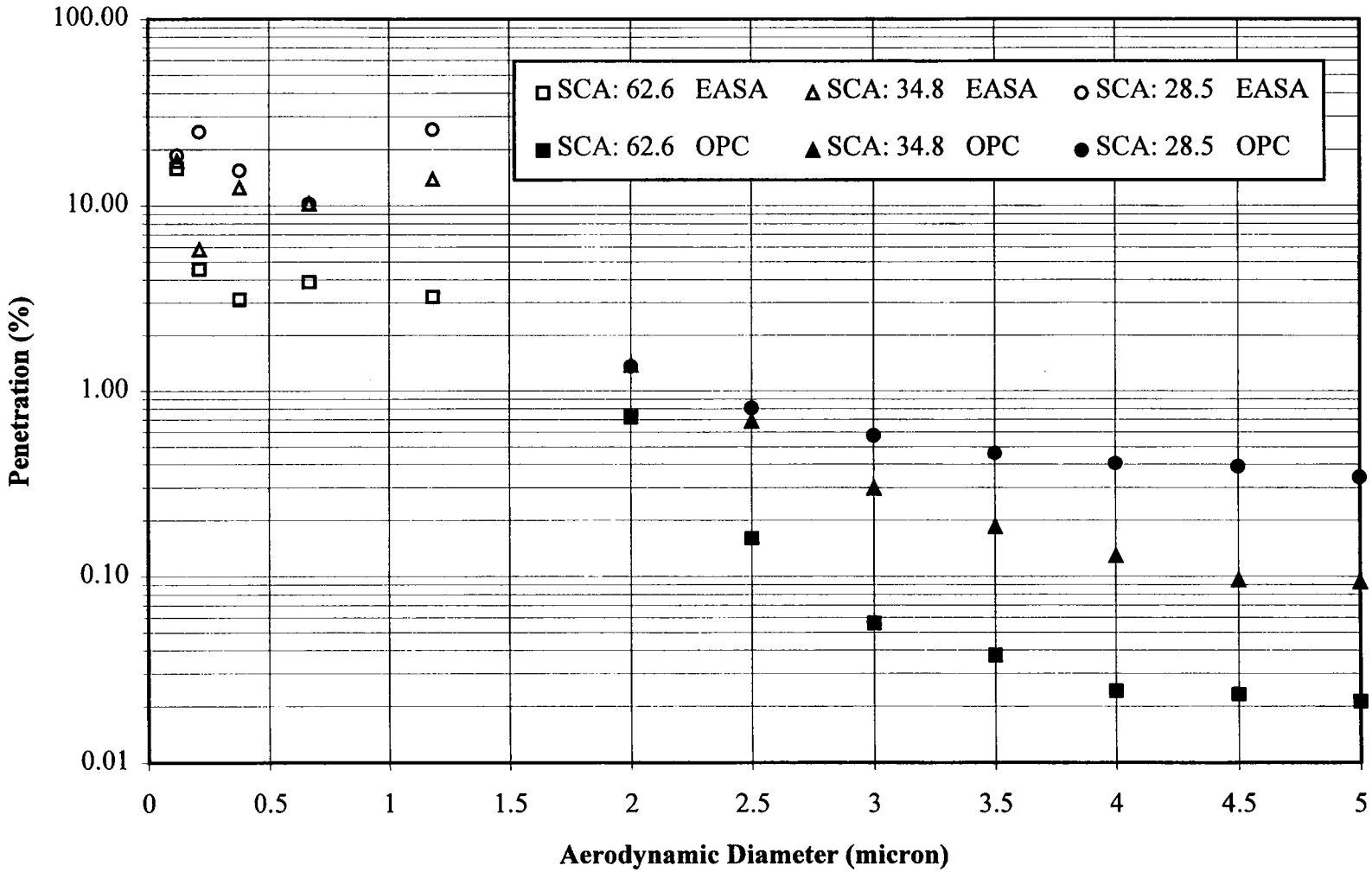

Figure 4-2. Measured penetrations at p1w35p2w for SCA of 62.6, 34.8 and 28.5.

diameters ranging from 0.118 - 5.0 microns. For particles with aerodynamic diameters larger than 2 microns, the penetration increased as the gas flowrate through the system increased. This tendency is in agreement with the theory of electrostatics. As shown in the literature review, he Deutsch-Anderson Model equation takes on the following form:

$$Pt = \exp\left(-w \times \frac{A}{Q}\right) \qquad (2\text{-}13)$$

where Pt is the fractional penetration, w is the migration velocity of the particles (proportional to d_p in theory) in ft/min, A is the area of plates in ft^2, and Q is the gas flowrate in acfm. Therefore, as the gas flowrate increases, the value of A/Q decreases, which causes the penetration to increase. As shown in the figure, for particles larger than 2 microns, the same effect occurs; the penetration increases as the gas flowrate increases.

At aerodynamic diameters from 0.118 - 1.18 microns, there is also a general trend of increased penetration at higher flowrates. This may be explained in terms of the residence time of the charged particles in the systems. In simple terms, as the gas flowrate increases, the gas velocity in the system increases, and the residence time decreases. As discussed in the literature review, diffusion is the major collection mechanism at sub-micron particle sizes. The amount of diffusion which occurs is directly proportional to the residence time of the particles in the system. Thus, at higher flowrates, fewer particles diffuse to the internal surfaces in the system, resulting in increased penetration.

4.1.3 Effect of Packing Media on Penetration

Tests were also conducted using 2" Type-K Tellerettes packing, and 1" Type-R Tellerettes packing. Figure 4-3 shows the relationship between the penetration and aerodynamic diameters for the three types of packing studied, when the system operated at p1wp2w with a gas flowrate of 900 acfm. As indicated in the figure, the penetration was higher when the system operated with the 2" Type-R packing, especially at the smaller aerodynamic diameters. The performance of the 2" Type-K and the 1" Type-R packing was nearly identical. The total pressure drop across the system was approximately equal, regardless of the type of packing used.

Figure 4-4 shows the relationship between the penetration and aerodynamic diameter for the three types of packing when the system operated at p1w35p2w and a SCA of 34.8. For particles with aerodynamic diameters larger than 2 microns, the type of packing does not have much of an effect on the penetration. However, at aerodynamic diameters less than 2 microns, the 2" Type-R packing yielded far better performance than the other two types of packing.

4.2 PREDICTIVE MODEL FOR PARTICLE COLLECTION EFFICIENCY

An empirical model was developed which can be used to predict the overall collection efficiency of an ionizing wet scrubber which uses 2" Type-R Tellerettes as the packing media, and operates with scrubbing liquid flowrates of 3.4 gpm and 31.1 gpm to the front and top spray nozzles, respectively.

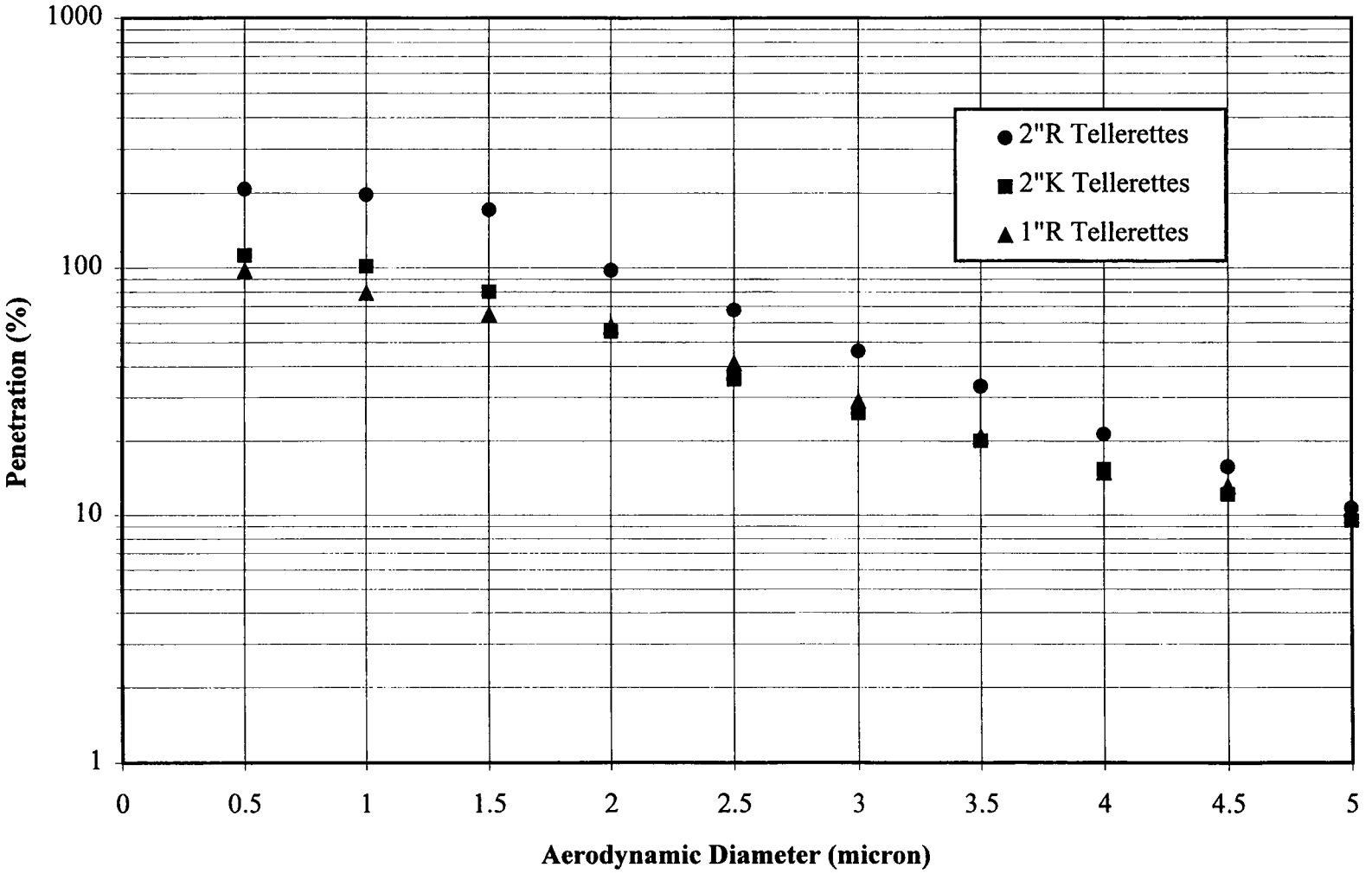

Figure 4-3. Penetration vs particle diameter for several packing at p1wp2w for 900 acfm.

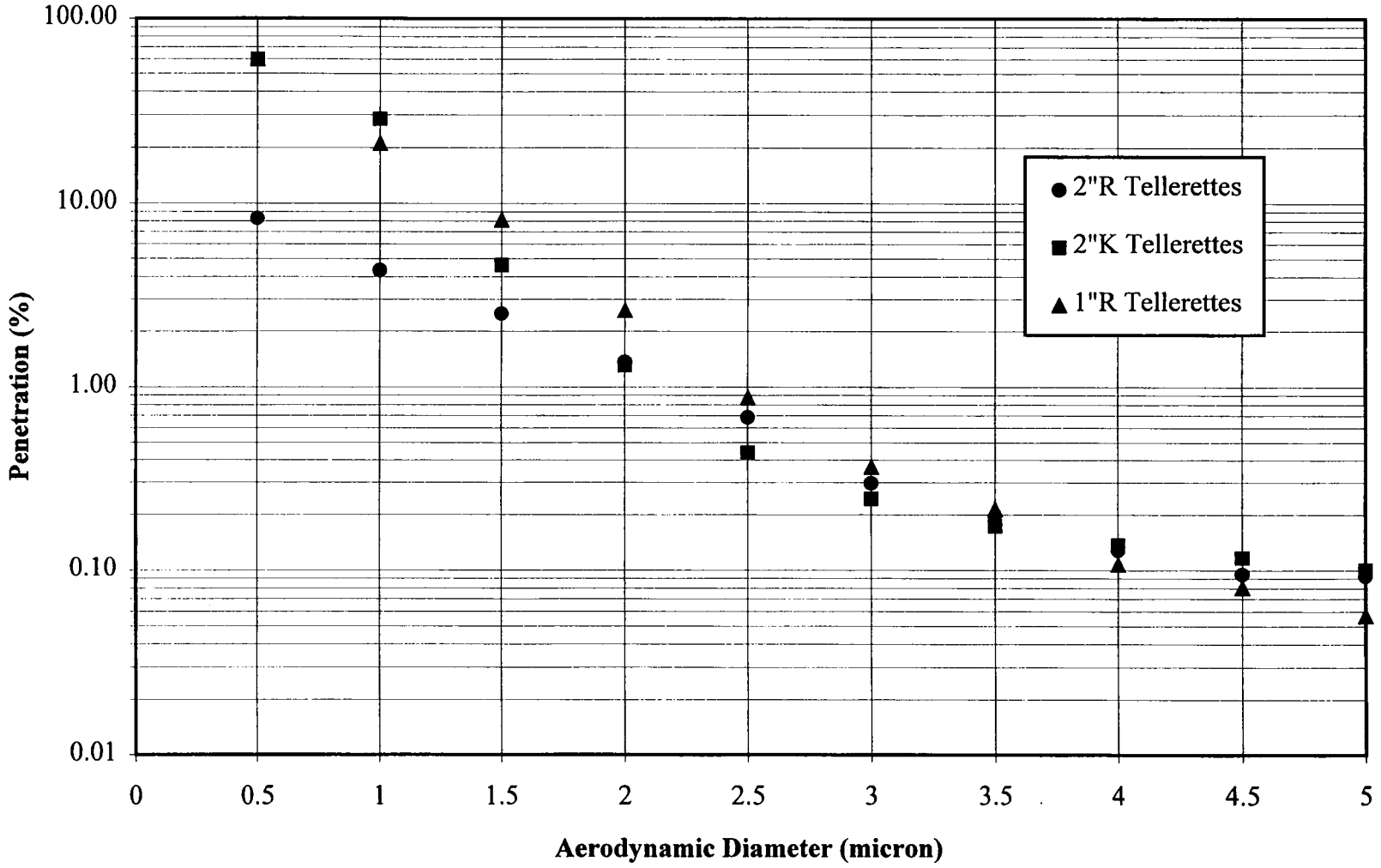

Figure 4-4. Penetration vs particle diameter for several packing at p1w35p2w for SCA of 34.8.

When more than one particle collection device is in series, the overall collection efficiency can be written as

$$\eta_o = 1 - (1 - \eta_1)(1 - \eta_2).....(1 - \eta_N) \qquad (4\text{-}2)$$

where η_o is the overall fractional collection efficiency of the system, $\eta_{i,...}$ represents each collector in the series, and N is the total number of collectors in series. The overall fractional penetration is defined as

$$Pt_o = 1 - \eta_o \qquad (4\text{-}3)$$

where Pt_o is the overall fractional penetration. Equation 4-2 may then be written as:

$$Pt_o = 1 - \eta_o = (Pt_1)(Pt_2).... (Pt_N) \qquad (4\text{-}4)$$

The pilot system that was tested was considered to be three separate particle collection devices in series. The first device in the series was the pre-scrubber, the second device was the ionizer, and the third device was the packed bed. Therefore, the pilot plant was modeled as follows

$$Pt_o = (Pt_{p1w})(Pt_{ioniz})(Pt_{p2w}) \qquad (4\text{-}5)$$

where Pt_o was the overall fractional penetration of the system, Pt_{p1w} was the penetration of the pre-scrubber, Pt_{ioniz} was the penetration of the ionizer, and Pt_{p2w} was the penetration of the packed bed downstream of the ionizer. Here, Pt_{ioniz} refers to the enhancement when the ionizing section is operating. It is noted that the mechanisms of collection may be a combination of removal on the plates of the ionizer, as well as any enhancement in removal as contributed by electrostatic forces (such as image force attraction) in the packed bed downstream of the ionizer. The overall penetration of the

system was measured during this study at SCAs of 62.6, 34.8, and 28.5 . The penetration of the pre-scrubber and packed bed in series was measured previously by Abraham, although additional tests were conducted in order to confirm his work The penetration of the ionizer, Pt_{ioniz}, may be calculated by rearranging equation 4-5 as follows:

$$Pt_{ioniz} = \frac{Pt_o}{\left(Pt_{p1w}\right)\left(Pt_{p2w}\right)} \qquad (4\text{-}5a)$$

Therefore, a model was developed which describes the penetration of the pre-scrubber and packed bed, and another model was developed which describes the penetration of the ionizing section as determined by calculations using equation 4-5a. These two models were then combined to develop a single model that predicts the overall penetration of the system.

4.2.1 Development of Pre-scrubber and Packed Bed Model

Abraham (1996) previously developed a model to describe the penetration of the pre-scrubber and packed bed at 900 acfm as a function of aerodynamic diameter and scrubbing liquid flowrates through the scrubbers. Although that model accurately predicted the penetration of the pre-scrubber and packed bed under a given set of operating conditions, further efforts were made to characterize the behavior of the packed beds. Additional tests were conducted operating at p1wp2w for flowrates of 500, 900 and 1100 acfm. Data from 0.5 - 5.0 microns were collected with the OPC, while data from 0.118 - 1.18 microns were collected with the EASA. The results of the tests are shown in Figure 4-5.

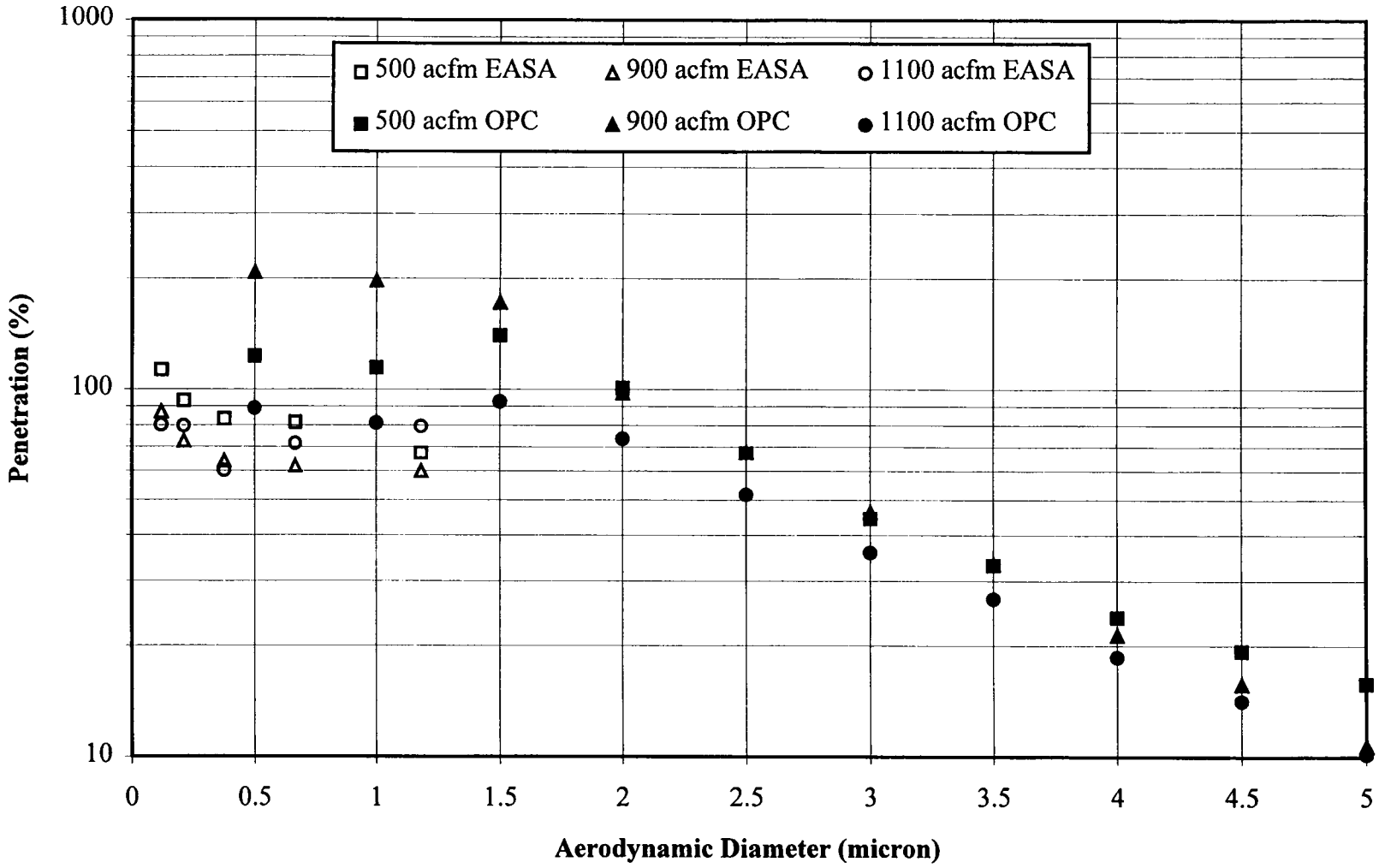

Figure 4-5. Measured penetrations vs particle diameter at p1wp2w for 500, 900 and 1100 acfm.

As shown in Figure 4-5, and as reported by Abraham (1996), the penetration generally exceeded 100% at aerodynamic diameters less than 2.5 microns, particularly for the data collected with the OPC. Other tests verify that this effect is from droplet carryover in the system. Droplets exited the packed bed with the gas stream, and were counted as particles when sampled with the OPC. The data collected with the EASA was not affected by droplet carryover because a drying/dilution system was incorporated into the EASA sampling method. The drying system caused the droplets to dry before reaching the EASA. Since the droplets were dried before entering the EASA, they were not measured as particles, thus the error associated with droplet carryover during measurements made with the EASA was negligible.

Studies were performed to determine the extent of droplet carryover using the OPC. These results indicate that data collected with the OPC at aerodynamic diameters of 0.5 - 2.0 microns were significantly impacted by droplet carryover when operating at p1wp2w. Quantifying the amount of droplet carryover and correcting the data to account for the effect of droplet carryover was not possible due to the many different parameters that affected the amount of droplet carryover on a day-to-day basis (i.e., indoor temperature, outdoor temperature, gas flowrate, etc.). Therefore, it was determined that the best method of handling droplet carryover was to exclude all data which had been affected by droplet carryover from the data analysis. Thus, data collected with the OPC at aerodynamic diameters of 0.5 - 2.0 microns when operating at p1wp2w were excluded

from analysis, as were data at aerodynamic diameters of 0.5 - 1.5 microns when operating at p1w35p2w.

As discussed by Abraham, the penetration for the packed bed scrubbers can be expressed as

$$Pt = \exp(-Kd_a^2) \tag{4-6}$$

where K is a constant, and d_a is the aerodynamic particle diameter. However, as indicated in Figure 4-5, a subtle relationship may exist between the penetration and gas flowrate. Therefore, equation 4-6 was modified to the following form:

$$Pt = \exp(-Kd_a^x Q^y) \tag{4-7}$$

where Q is the gas flowrate through the system, and all other terms are as previously defined. Equation 4-7 may be transformed into a linear form as follows:

$$\ln(Pt) = -Kd_a^x Q^y \tag{4-7a}$$

$$\ln(-\ln(Pt)) = \ln(K) + x\ln(d_a) + y\ln(Q) \tag{4-7b}$$

Using multiple linear regression techniques on data that had been collected at flowrates of 500, 900, and 1100 acfm when the system operated at p1wp2w with 2" Type-R Tellerette packing media, and a total wetted packing depth of 8 feet (4 feet in the pre-scrubber, and 4 feet in the packed bed), the following results were obtained:

$\ln(K) = -4.34$ i.e., $K = 1.30E\text{-}2$
$x = 0.66$
$y = 0.54$
$R^2 = 0.80$
$MSE = 0.43$

Using the values obtained from the regression, the model takes on the form of

$$Pt_{PB} = \exp[(-1.30E\text{-}2)Q^{0.54}d_a^{0.66}] \tag{4-8}$$

where Pt_{PB} is the fractional penetration through the packed beds, Q is the gas flowrate through the system in acfm , and d_a is the aerodynamic particle diameter in microns. It should be noted that data collected with the OPC at aerodynamic diameters less than 2.0 microns was excluded from the analysis and regression due to the adverse effects of droplet carryover.

The depth of the packing in the packed bed may also be incorporated into the model. Based on an overall wetted packing depth in the direction of gas flow of 8 ft in the pilot plant, the equation may be modified to the following form:

$$Pt_{PB} = \exp [(-1.6E\text{-}3)LQ^{0.54}d_a^{0.66}] \qquad (4\text{-}8a)$$

where Pt_{PB} is the fractional penetration through the packed beds, L is the total depth of wetted packing in the direction of gas flow in feet, Q is the gas flowrate through the system in acfm , and d_a is the aerodynamic particle diameter in microns.

According to Miller (1984), a biasing factor must be applied to the logarithmic transformation of the variables in order to reduce the effects of bias. Based on the linear regression, the variance (σ^2) was 0.43. The biasing factor is equal to $\exp(0.5\sigma^2)$. Thus, the biasing factor for the above model was $e^{0.215} = 1.24$. The model takes the final form of:

$$Pt_{PB} = \exp [(-1.6E\text{-}3)LQ^{0.54}d_a^{0.66}](1.24) \qquad (4\text{-}9)$$

Figure 4-6 shows the measured and predicted efficiencies, as determined by the model, at flowrates of 500, 900 and 1100 acfm as a function of aerodynamic diameter. As indicated, the model does a very poor job of predicting the penetration for a given

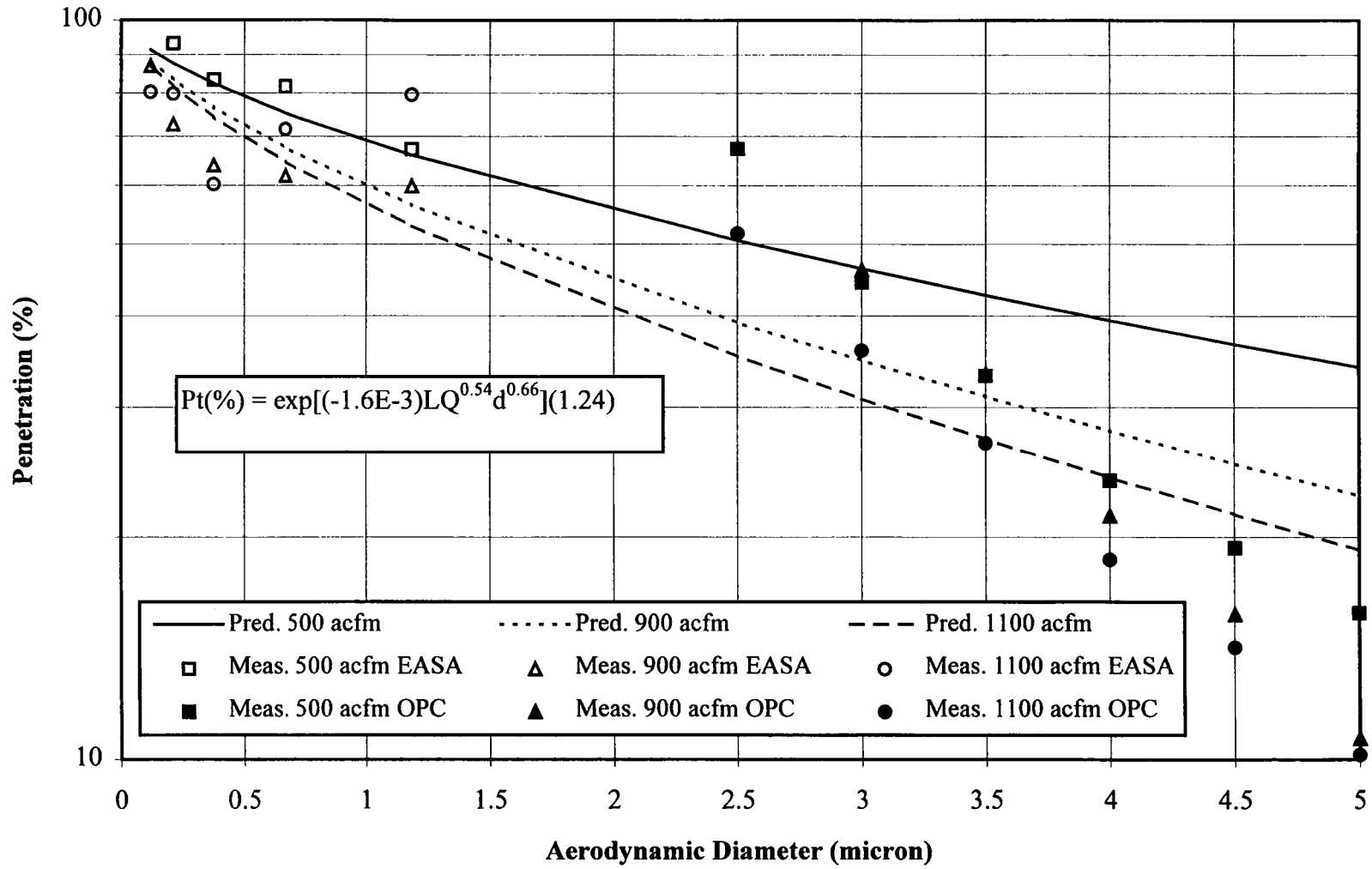

Figure 4-6. Measured and predicted penetrations (based on a form of Abraham's model) at p1wp2w.

flowrate. Efforts were made to develop a better predictive model, based on theory, that described the penetration of the packed beds at particle sizes from 0.188 - 5.0 microns. However, it was not possible to develop an accurate model based on theory. Therefore, it was decided to use a best-fit polynomial curve for each flowrate to describe the penetration as a function of aerodynamic diameter. The results of these efforts are shown in Figure 4-7. Upon examination of Figure 4-7, it became obvious that the penetration is not a strong function of the gas flowrate, as indicated by the overlapping nature of the three curves. Therefore, the data from the three sets of tests were combined, and a best-fit curve was applied to all of the data, which resulted in a third-order polynomial equation. The measured penetrations and predictive model are shown in Figure 4-8. As indicated, the model does a reasonable job of predicting the penetration as a function of aerodynamic diameter. Although the model does not have a theoretical basis, it is still very useful in predicting the penetration in the packed bed system. The final form of the packed bed model is

$$Pt_{PB} = [0.006199\, d_a^3 - 0.060103\, d_a^2 + 0.011302\, d_a + 0.77037]^{(L/8)} \qquad (4\text{-}10)$$

where Pt_{PB} is the fractional penetration of the cross-flow packed bed containing 2" Type-R Tellerette packing, and d_a is the aerodynamic diameter in microns. Using equation 4-4 as a basis, the term (L/8) was developed to allow the model to be used for wetted packing depths other than 8 feet, where L is the depth of wetted packings in the direction of gas flow in feet, and the value of 8 results from the fact that the total depth of wetted packing in the pilot plant was 8 feet. The model is valid for: d_a = 0.12 - 5.0 microns.

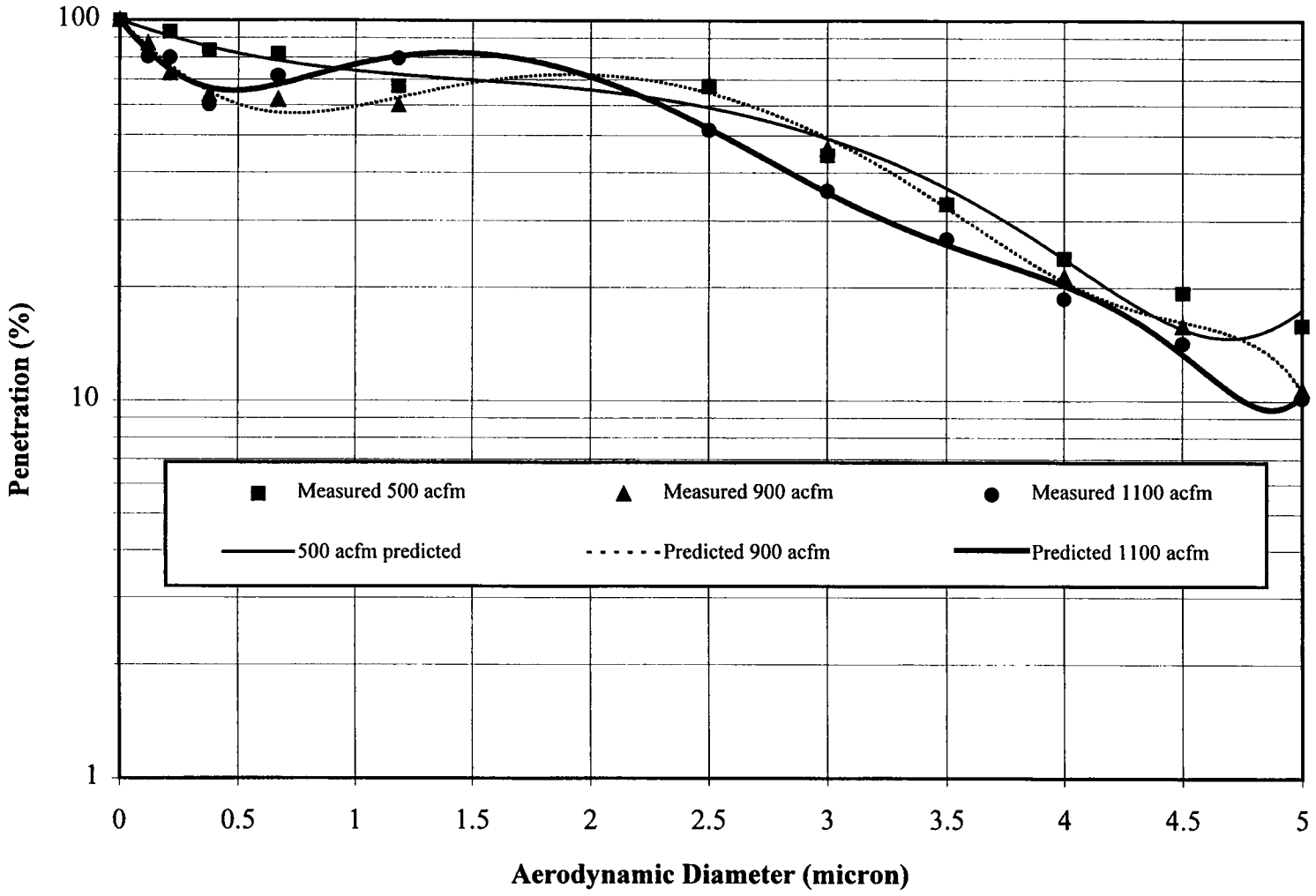

Figure 4-7. Measured and predicted penetrations for p1wp2w at particle diameters from 0.118 - 5.0 microns. "Best-fit" polynomial.

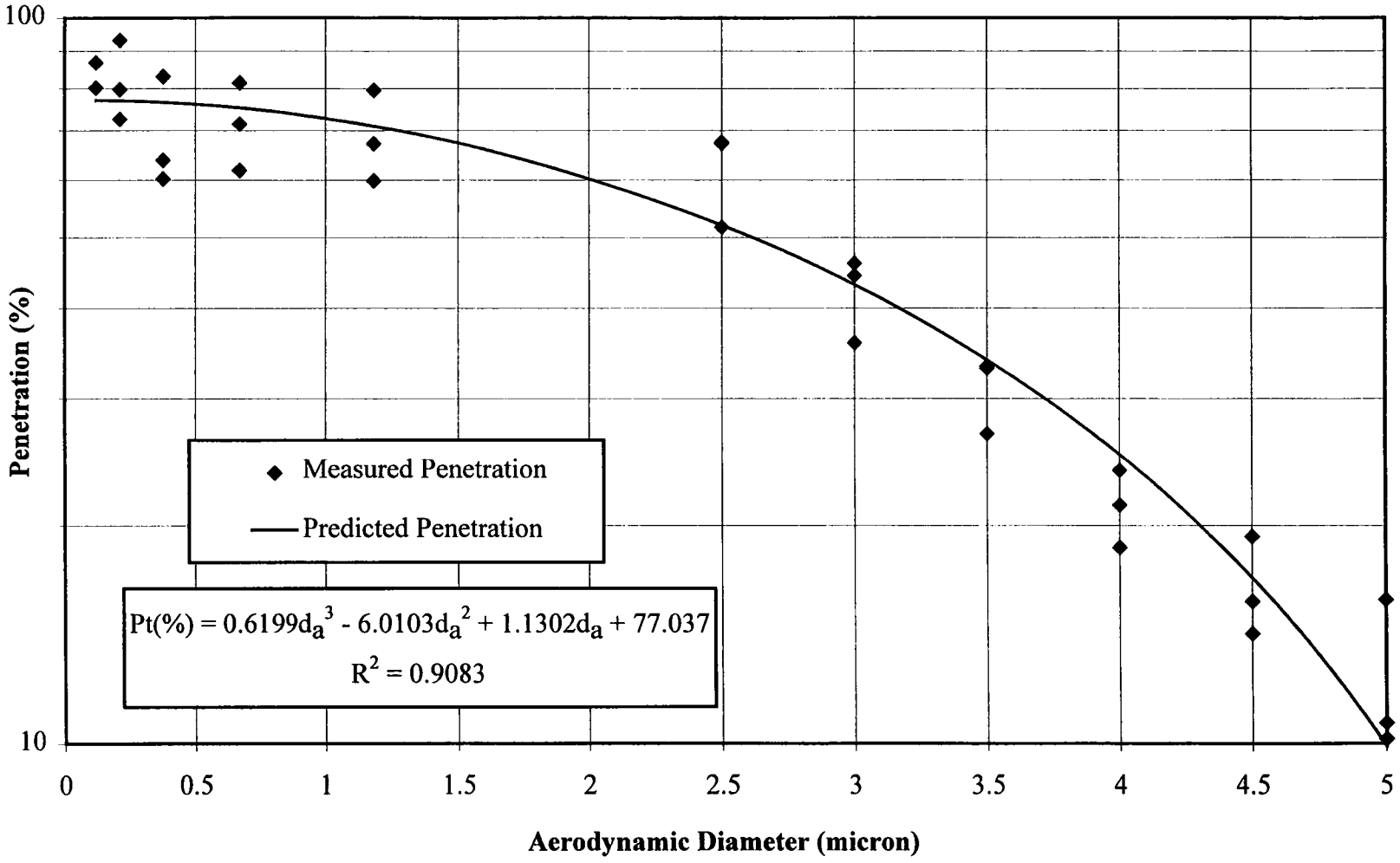

Figure 4-8. Measured and predicted penetrations (based on polynomial model) for p1wp2w at particle diameters from 0.118 - 5.0 microns.

4.2.2 Overall Penetration Studies

The overall penetration of the system was determined by measuring the concentration of particles upstream and downstream of the system when operating at p1w35p2w. In order to assure reproducibility of the results, multiple tests were conducted under those conditions, and the results were averaged. The results of those tests are shown in Figure 4-9 for SCAs of 62.6, 34.8, and 28.5, when the system operated at p1w35p2w. As discussed previously, data collected with the OPC at aerodynamic diameters less than 2.0 microns were adversely affected by droplet carryover, and therefore were not analyzed. Figure 4-10 shows the same results of the overall penetration, however, the data affected by droplet carryover are excluded.

4.2.3 Development of an Electrostatic Model

4.2.3.1 Determination of effective migration velocity

As discussed in the previous section, the penetration of the overall system was measured at SCAs of 62.6, 34.8 and 28.5, while the system operated at p1w35p2w. Those measurements describe the overall penetration of the system as a function of the particle size at each of the SCAs studied. The penetration of the system was also measured at the same flowrates while the system operated at p1wp2w. Based on the results of those two sets of tests, the penetration of the ionizing section of the system was calculated by modifying equation 4-5a as follows:

$$Pt_{ioniz} = \frac{Pt_o}{\left(Pt_{p1w}\right)\left(Pt_{p2w}\right)} = \frac{Pt_o}{\left(Pt_{PB}\right)} \qquad (4\text{-}5b)$$

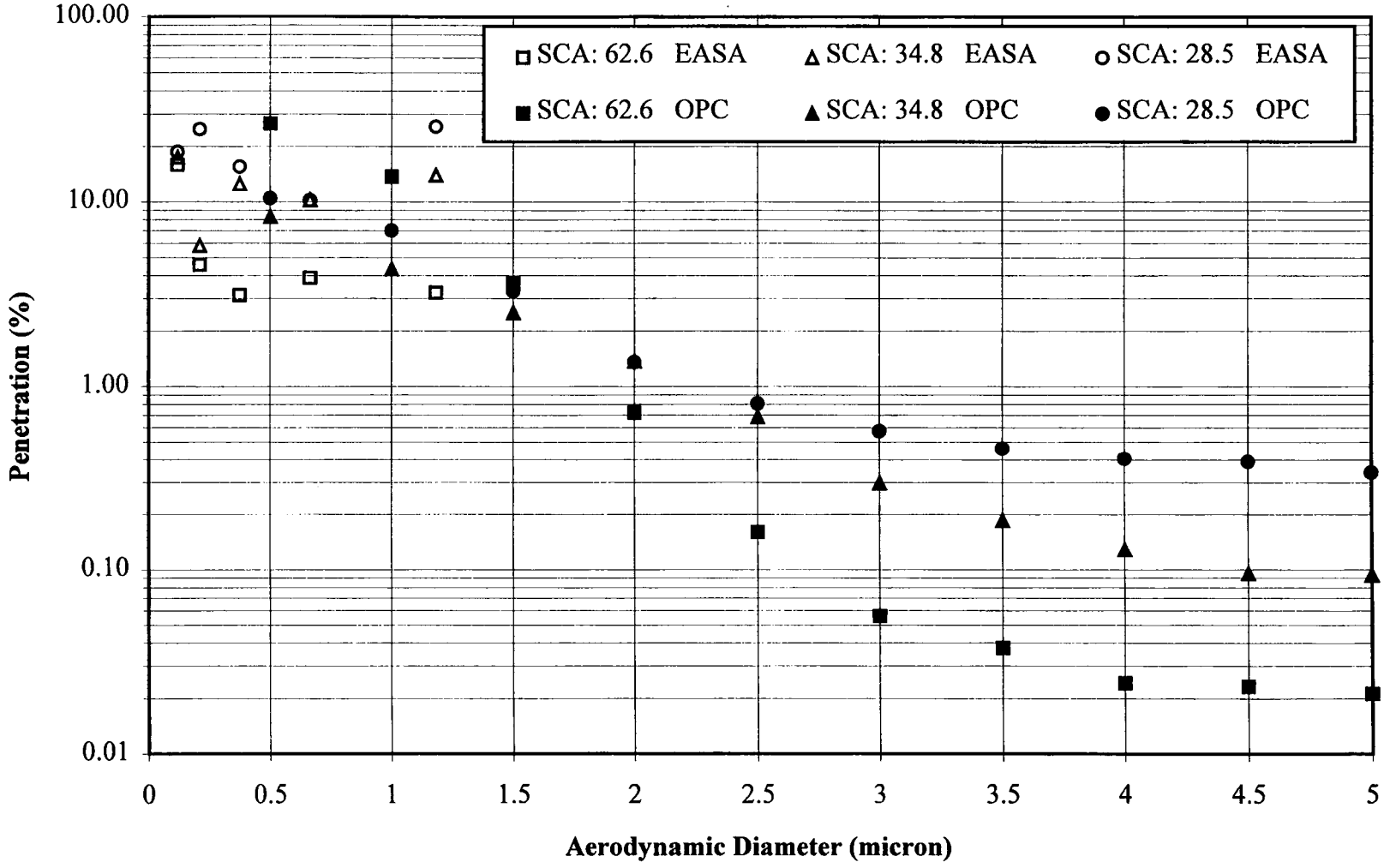

Figure 4-9. Measured penetrations for p1w35p2w at SCA of 62.6, 34.8 and 28.5.

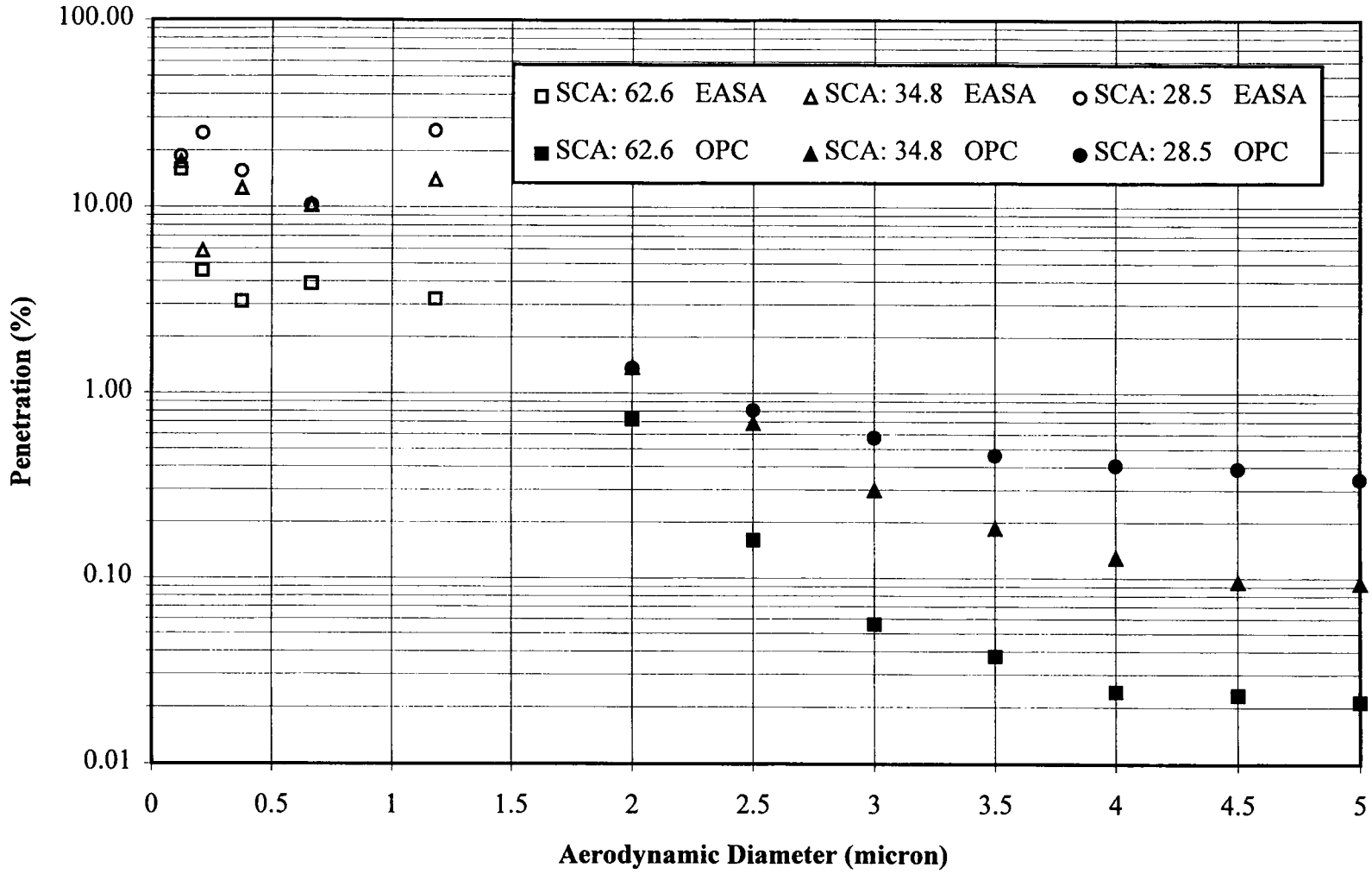

Figure 4-10. Measured penetrations for p1w35p2w at SCA of 62.6, 34.8 and 28.5. Data affected by droplet carryover excluded.

where Pt_o is the *measured* overall penetration of the system (i.e., penetration when system operated at p1w35p2w), and Pt_{PB} is the *measured* penetration of the system when the ionizer did not operate (i.e., penetration when system operated at p1wp2w).

A sample calculation of the ionizer penetration for a SCA of 34.8 is provided below for sub-micron particle sizes. It is important to note that the ionizer penetration was calculated by dividing the average value of the *measured* overall penetration at p1w35p2w (as determined from a series of tests) at a given particle size, by the average value of the *measured* penetration of the system which operated at p1wp2w at the same given particle size. These calculations were performed for each individual particle size.

Aerodynamic Diameter (microns)	**Measured Fractional Penetration** $Pt_o = Pt_{p1w35p2w}$	**Measured Fractional Penetration** $Pt_{PB} = Pt_{p1wp2w}$	**Calculated Fractional Penetration** $Pt_{ioniz} = (Pt_o / Pt_{PB})$
0.118	0.1735	0.8687	0.1997
0.210	0.0580	0.7258	0.0799
0.375	0.1247	0.6384	0.1954
0.669	0.1022	0.6182	0.1652

The results of these calculations are shown in Figure 4-11, where the particle size has been reported as the physical particle size since the data represent the electrostatic collection mechanisms. Note that at 2.0 microns, data from the OPC were excluded when the system operated at p1wp2w. However, the 2.0 micron data were not excluded from the p1w35p2w data set. Therefore, it was possible to predict, with reasonable accuracy, the penetrations at 2 microns based on the data from the p1w35p2w data set, and the estimated penetration from the p1wp2w model that was previously developed. This is, in fact, an alternative method of calculating the fractional penetration. One could divide

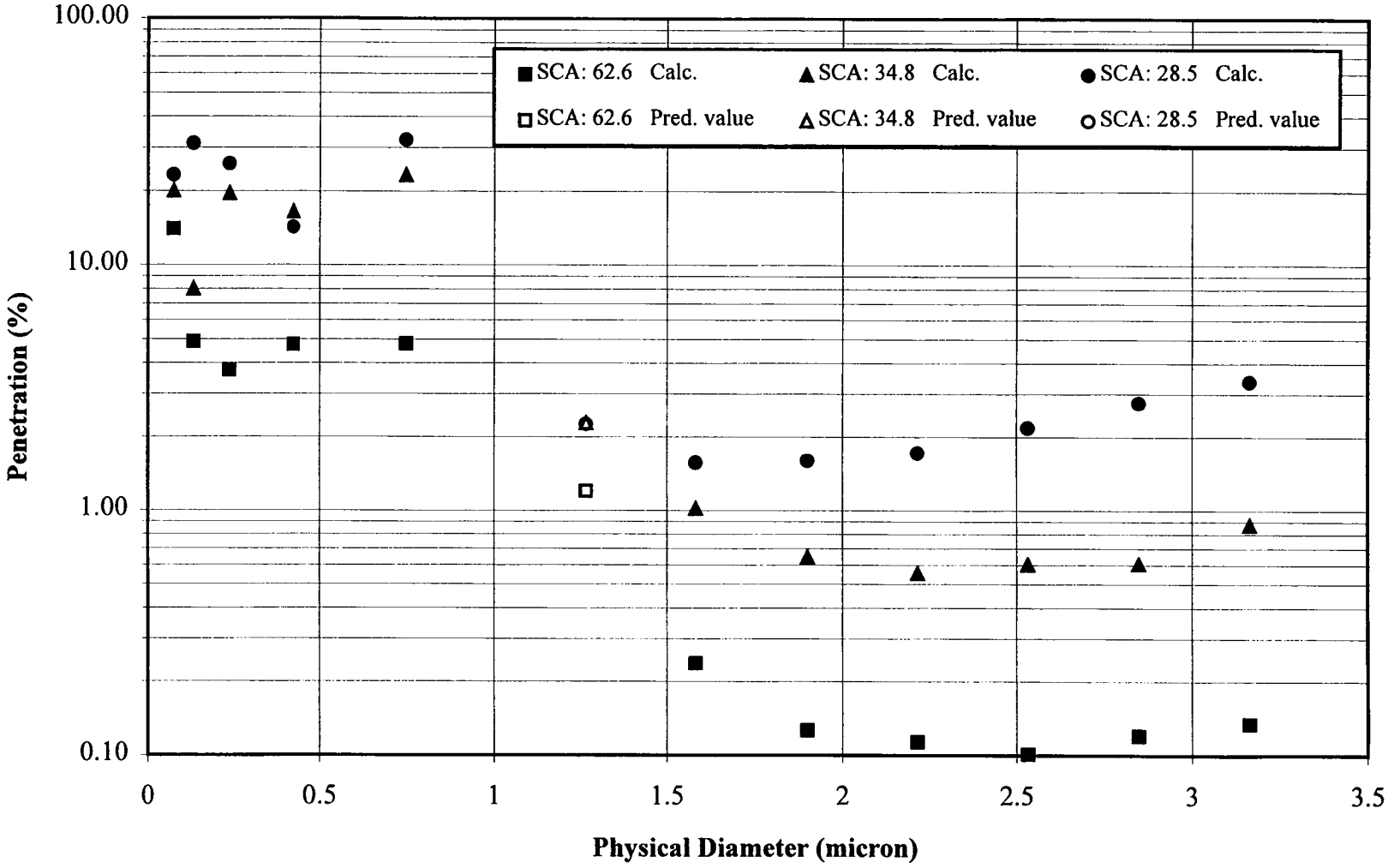

Figure 4-11. Calculated penetrations ionizer at SCA of 62.6, 34.8 and 28.5.

the average measured overall penetration at a given particle size by the calculated value of p1wp2w using the predictive model which was previously developed for the same particle size, and obtain an ionizer penetration at that particle size. However, this method tends to smooth the data and eliminate some of the sensitivity. Therefore, this method was not used to calculate the ionizer penetration.

4.2.3.2 Development of initial MO model based on linear regression

As shown in Figure 4-11, the penetration of the ionizer was calculated for SCAs of 62.6, 34.8 and 28.5. Based on the form of the Matts-Ohnfeldt model which is used to describe the penetration of particles through an electrostatic precipitator, efforts were made to develop an empirical model which describes the penetration of particles through the ionizing section as a function of the particle's physical diameter and A/Q. The Matts-Ohnfeldt model has the following form:

$$Pt = \exp\left[-\left(\omega_k \times \frac{A}{Q}\right)^k\right] \qquad (2\text{-}15)$$

where ω_k is the effective MO migration velocity, and k is an exponential factor which is commonly 0.5 for fly ash, but varies for different particles. The following equation describes the relationship between SCA and A/Q:

$$\frac{A}{Q} = 1000(SCA) \qquad (2\text{-}14)$$

Therefore, SCA is defined as the square feet of plates per 1000 acfm of gas treated when A/Q is expressed in ft^2/acfm . It was shown previously that the theoretical migration velocity is

$$\omega = \frac{p\varepsilon_o E_c E_p d_p K_c}{3\mu_g} \tag{2-12}$$

Therefore, by combining equations 2-12 and 2-15, the Matts-Ohnfeldt equation may be modified to the following form:

$$Pt = \exp\left[-\left(xd_p \frac{A}{Q}\right)^k\right] \tag{4-11}$$

where Pt is the fractional penetration, d_p is the physical diameter of the particle in microns, A is the area of the plates in ft^2 (which was 31.3 for the pilot plant), Q is the gas flowrate in acfm, and x accounts for all other terms. Equation 4-11 may be transformed into a linear form as follows:

$$\ln(Pt) = -\left(xd_p \frac{A}{Q}\right)^k \tag{4-12}$$

$$-\ln(Pt) = \left(xd_p \frac{A}{Q}\right)^k \tag{4-13}$$

$$-\ln(Pt) = x^k\left(d_p \frac{A}{Q}\right)^k \tag{4-14}$$

$$\ln[-\ln(Pt)] = k[\ln(x)] + k\left[\ln\left(d_p \frac{A}{Q}\right)\right] \tag{4-15}$$

Linear regression was employed to determine the relationship between the ionizer penetration and physical diameter at a gas flowrate of 900 acfm. The results of the analysis are as follows:

$k = 0.34$
$k[\ln(x)] = 2.36$ i.e. x = 1034
$R^2 = 0.68$
MSE = 0.31

As discussed previously, a bias factor must be applied after the logarithmic transformation. Recall that the bias factor is defined as $\exp(0.5\sigma^2)$. Therefore, the biasing factor for the above regression is $e^{0.16} = 1.17$.

Hence, the equation for the fractional penetration of the ionizer section as a function of the physical diameter and gas flowrate based on the MO equation is

$$Pt_{ioniz} = \exp\left[-\left(0.60 d_p \frac{A}{Q}\right)^{0.34}\right](1.17) \qquad (4\text{-}16)$$

where Pt_{ioniz} is the fractional penetration of the ionizer, d_p is the physical diameter of the particle in microns, A is the area of the plates in ft^2, and Q is the gas flowrate in acfm.

A similar linear regression was performed in order to develop a Deutsch-Anderson type model. The two models, along with the calculated values of the ionizer penetration, as determined by equation 4-5b, are shown in Figure 4-12 for a SCA of 34.8. As shown in the figure, neither model predicts the penetration with reasonable accuracy, which is not surprising considering the unique curvature that the calculated penetrations follow. The penetration tends to decrease with aerodynamic diameter up to 3.5 microns, at which time the penetration increases with increasing aerodynamic diameter. This

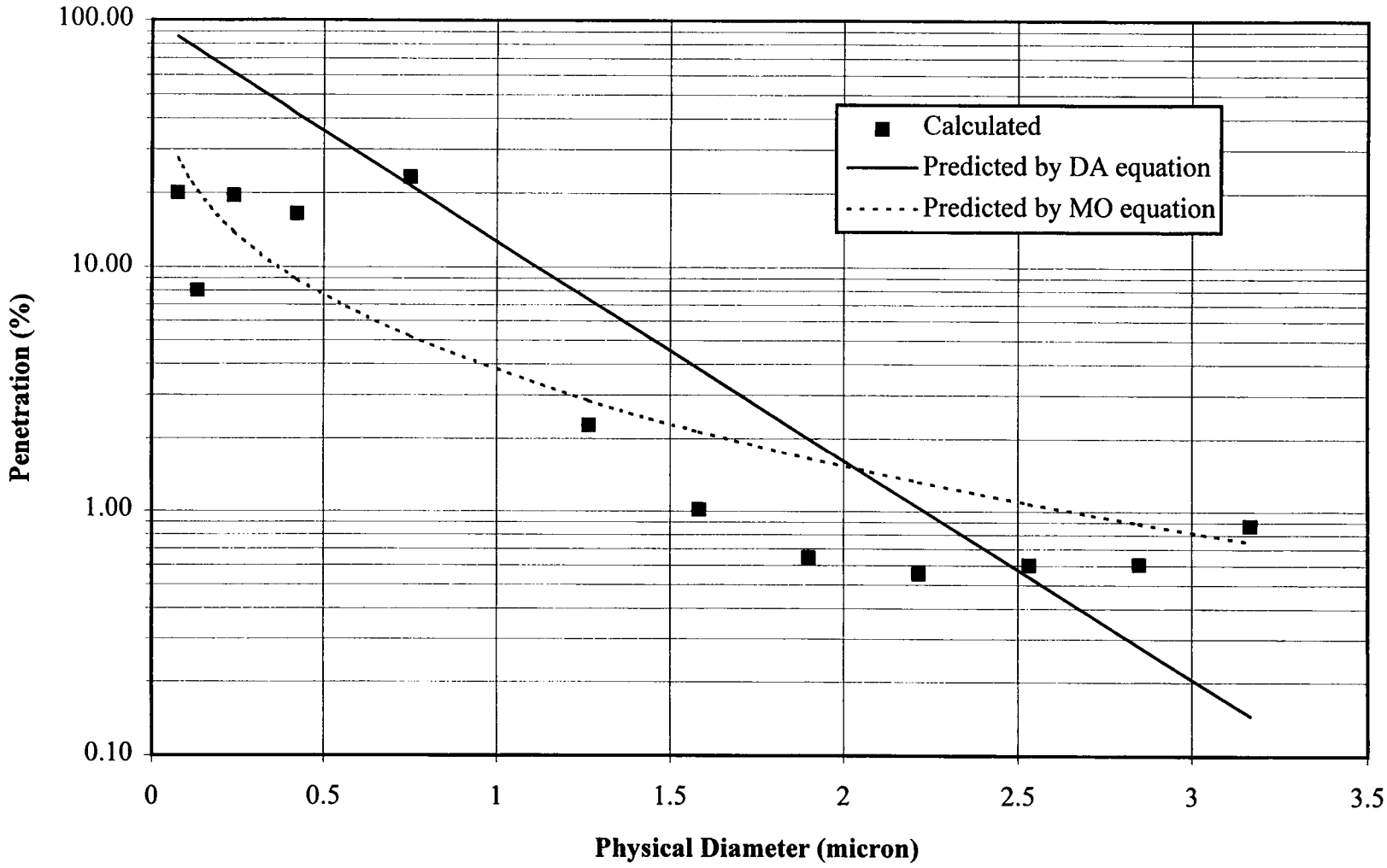

Figure 4-12. Comparison of Deutsch-Anderson (DA) type and Matts-Ohnfeldt (MO) type models to calculated penetrations for ionizer at SCA of 34.8.

phenomena is also observed at SCAs of 62.6 and 28.5, as shown in Figure 4-11. The upward curvature is contrary to the electrostatic theory which suggests that penetration decreases as particle size increases. Once again, recall from the literature review that

$$Pt = \exp\left[-\left(\omega_k \times \frac{A}{Q}\right)^k\right] \qquad (2\text{-}15)$$

where ω_k is the effective MO migration velocity, and k is an exponential factor which is commonly 0.5 for fly ash, but varies for different particles. Also recall that

$$SCA = \frac{A}{Q}(1000) \qquad (2\text{-}14)$$

where A is the area of the collecting electrode, and Q is the gas flow rate. Assuming that equation 2-15 correctly describes the mechanism of electrostatic particle collection, it becomes obvious that at a given gas flowrate, penetration will only increase if the effective migration velocity decreases. As discussed in the literature review, the migration velocity is defined as

$$\omega = \frac{p\varepsilon_o E_c E_p d_p K_c}{3\mu_g} \qquad (2\text{-}12)$$

where ε_o is the free-space permitivity, E_C is the strength of the charging field, E_p is the strength of the collecting field, d_p is the physical particle diameter, K_C is the Cunningham correction factor, μ_g is the viscosity of the gas, and p is defined as:

$$p = \frac{3D}{D+2} \qquad (2\text{-}9)$$

where D is the dielectric constant. As indicated in equation 2-12, as the physical diameter increases, the migration velocity increases, which implies that the penetration should decrease with increasing particle size. The fact that the penetration increases with increased particle size for aerodynamic diameters larger that 3.5 microns suggests that another mechanism may be competing with the electrostatic collection mechanism and causing increased penetration (i.e., particle bounce). However one problem with the theory is that it assumes that the migration velocity is only a function of the physical diameter of the particle, and that all of the other parameters in equation 2-12 are constant for all particle sizes at any given instance in time. However, if the dielectric constant was not the same for all particle sizes, then the migration velocity would vary as a function of the product of p and d_p. Thus, depending on the dielectric constant of the individual particles, the migration velocity could decrease with increased particle size, which would lead to increased penetration. Through visual observation, it was obvious that the flyash used during testing was composed of many types of particles, including coal, and most likely inorganics, metals, and silica. It's conceivable that the different components in the flyash have different dielectric constants, and therefore behave differently in regards to electrostatic collection, and possibly cause deviations in the electrostatic theory. It is interesting to note that Pilat (1975) reported similar results in his studies of an electrostatic spray scrubber as shown in previously in Figure 2-7.

In an effort to further understand the unique curvature in the figure of the penetration as a function of the particle size, the theoretical migration velocity was

determined for all of the particle sizes studied. However, in order to calculate the theoretical migration velocity, one must either know or estimate the dielectric constant of the particles. It was determined that the sub-micron particles present in the gas stream may have acted as condensation nuclei for the water vapor in the gas stream. Therefore, small particles may have been either partially or completely coated with a thin film of water. Water has a dielectric constant of approximately 88 under the conditions at which the system operated (*Handbook of Physics and Chemistry*), whereas the dielectric constant of the dry flyash, as determined by scientists at Oak Ridge National Laboratory in Oak Ridge, TN, has an average value of approximately 2. Thus, depending on whether or not the surface of the particles was coated with water, the dielectric constant could vary substantially. Therefore, an estimate of the maximum theoretical migration velocity at each particle size was made by using a dielectric constant of 88 in conjunction with equations 2-9 and 2-12. An estimate of the minimum theoretical migration velocity was made at each particle size by using a dielectric constant of 1. It should be noted that the dielectric constant in a vacuum is 1, and that this is the lowest dielectric constant an object may have. Therefore, the following values were used in conjunction with equations 2-9 and 2-12 to calculate the maximum and minimum theoretical migration velocities:

$D_{max} = 88$ $D_{min} = 1$
$V = 31{,}100$ volts
$L = 3.65$ cm $= 0.0365$ m
$\mu_g = 1.81E\text{-}5$ kg/m-s
$\varepsilon_o = 8.854E\text{-}12$ coul/V-m
d_p is the physical particle diameter in meters

The following results were obtained:

	$d_p = 2.0\ \mu$ K_c=1.083	$d_p = 2.0\ \mu$ K_c=1.083	$d_p = 3.0\ \mu$ K_c=1.056	$d_p = 3.0\ \mu$ K_c=1.056
ω_{max}	0.75 (m/s)	147 (fpm)	1.09 (m/s)	215 (fpm)
ω_{min}	0.25 (m/s)	50 (fpm)	0.37 (m/s)	73 (fpm)

Figure 4-13 shows the relationship between the physical diameter and the maximum and minimum theoretical migration velocities.

4.2.3.3 Development of a DA model based on the DA effective migration velocity

In order to compare the measured results with the theory, calculations were performed to determine the DA effective migration velocity, which is commonly done in the electrostatic precipitation industry with the use of the DA equation:

$$Pt = \exp\left[-\left(\omega_e \times \frac{A}{Q}\right)\right] \qquad (2\text{-}13)$$

where Pt is the *measured* fractional penetration at a given particle size for a given A/Q, ω_e is the effective migration velocity in ft/min of the given particle, and A/Q is the plate area in ft^2 per acfm of gas. Figure 4-13 shows the relationship between the individual calculated values of the DA migration velocity as a function of physical diameter, based on the above equation. In addition, a best-fit relationship between the DA calculated effective migration velocity and the physical diameter was obtained by fitting a polynomial equation to the individual data points. This is referred to as the general DA

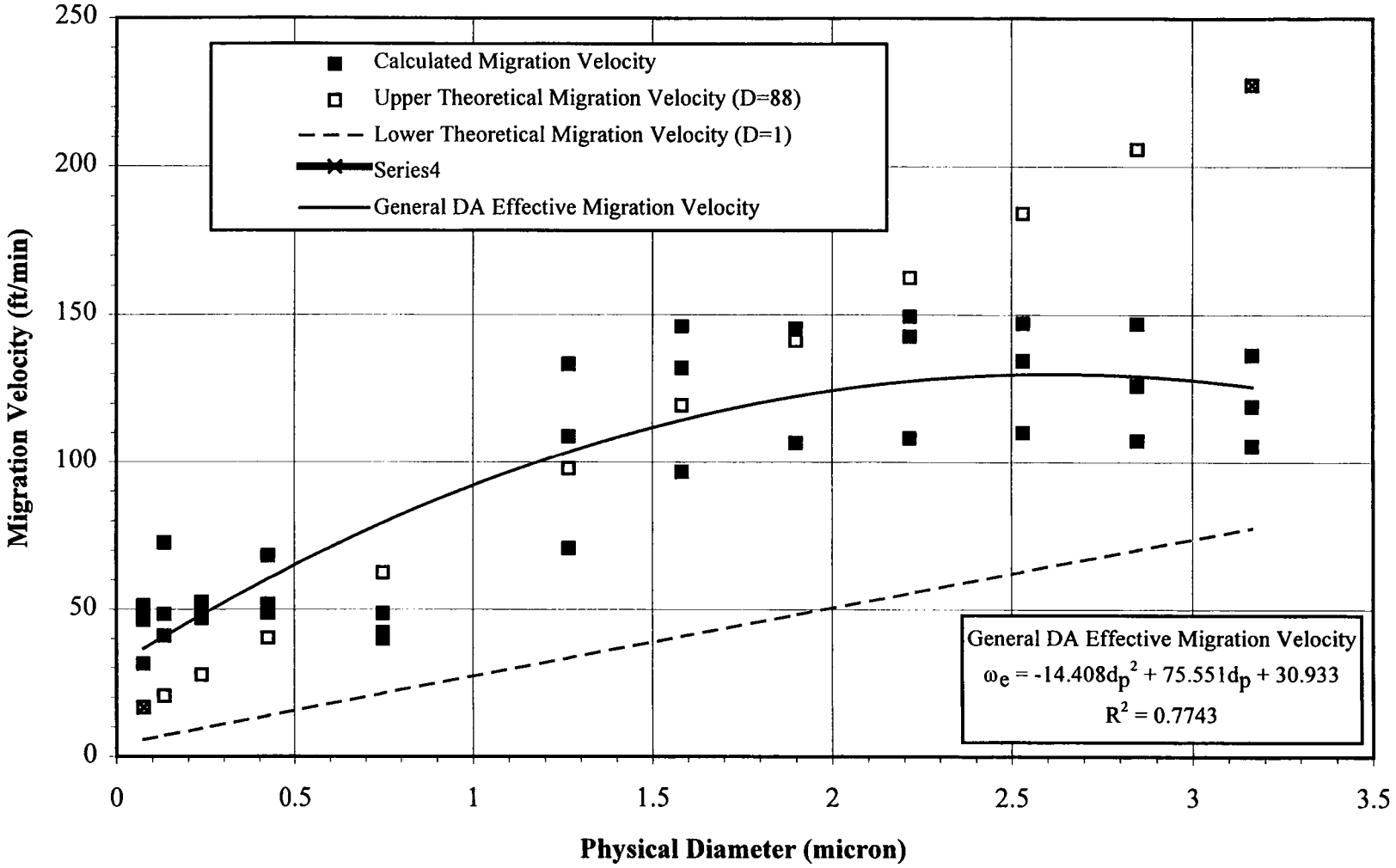

Figure 4-13. General DA effective, theoretical, and individual calculated migration velocities as a function of physical particle diameter.

effective migration velocity. As indicated in Figure 4-13, particles with physical diameter less than 2.0 microns tend to lie near the maximum theoretical migration velocity. This evidence supports the claim that the sub-micron particles are acting as condensation nuclei, and therefore have a dielectric constant essentially equal to that of water. Large particles promote less condensation, and therefore maintain a dielectric constant closer to that of the flyash.

In an effort to develop an empirical model in order to describe the penetration of the ionizer as a function of particle size and gas flowrate, the equation for the general DA effective migration velocity that was obtained from the data presented in Figure 4-13 by fitting a polynomial to the data was substituted into the Deutsch-Anderson equation to obtain the following relationship:

$$Pt = \exp\left[-\left(14.408 d_p^2 + 75.551 d_p + 30.933\right)\right] \qquad (4\text{-}17)$$

Figure 4-14 shows the relationship of the predicted penetrations, as determined by equation 4-17, and the calculated penetrations. As shown in the figure, the predictive equations do not accurately predict the penetrations. Therefore, another equation was developed using a similar approach.

By fitting the data set for each SCA with a different polynomial, an equation for effective migration velocity that was specific to each SCA was obtained. Each of those SCA-specific equations was substituted into the following form of the Deutsch-Anderson equation:

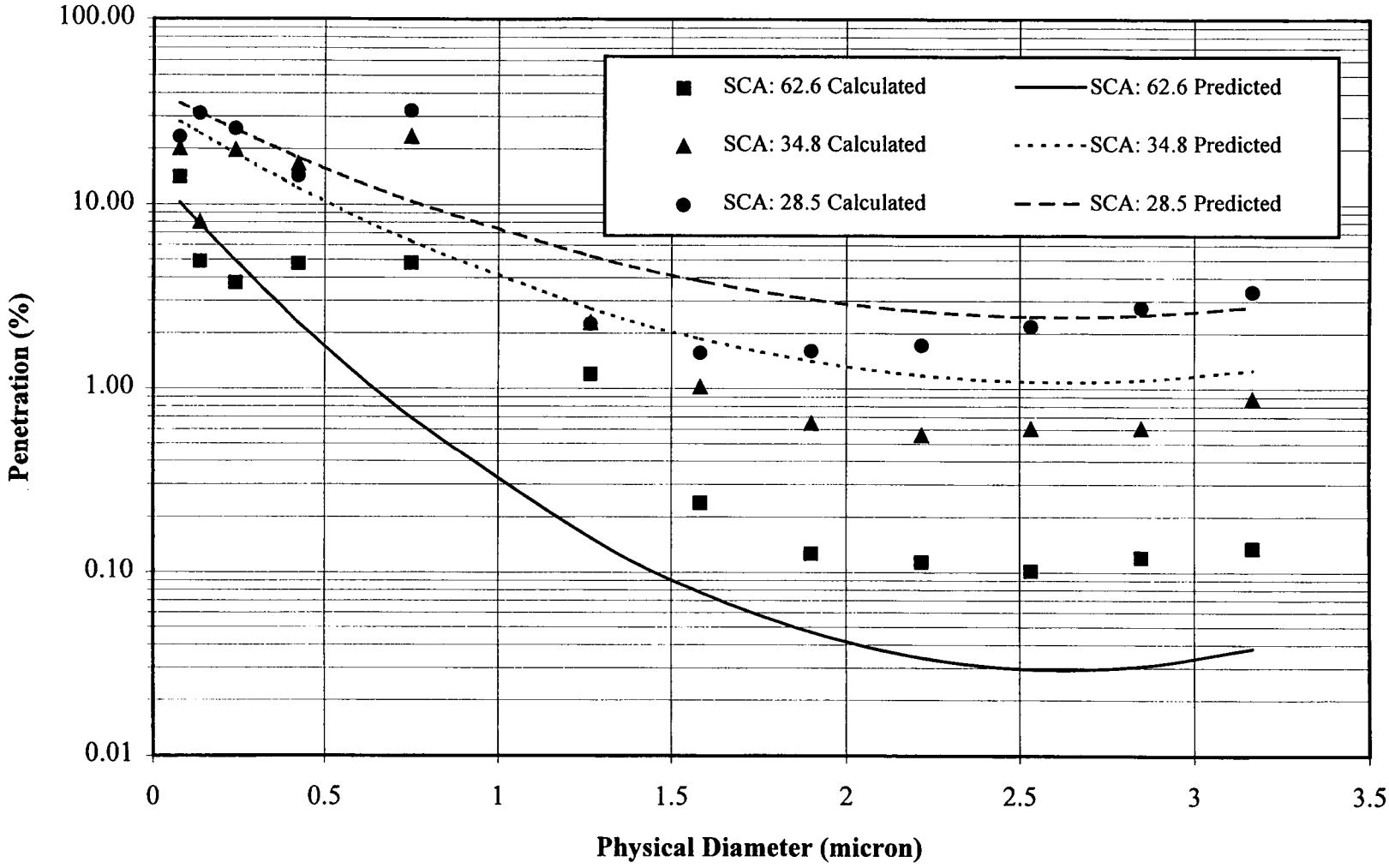

Figure 4-14. Predicted and calculated ionizer penetrations using the general DA effective migration velocity equation, at SCAs of 62.6, 34.8 and 28.5.

$$Pt = \exp\left[-\left(\omega_e \frac{A}{Q}\right)\right] \qquad (2\text{-}13)$$

where Pt is the fractional penetration, ω_ε is the effective migration velocity, A is the area of plates in ft^2, and Q is the gas flowrate in acfm. Using this procedure, three equations were successfully developed that describe the penetration as a function of physical diameter for each SCA. The term DA SCA-specific refers to equations which were developed using the DA equation that are only valid at the SCA for which each was developed.

Figures 4-15, 4-16, and 4-17 show the DA SCA-specific effective, theoretical, and individual calculated migration velocities for SCA's of 62.6, 34.8 and 28.5. respectively. The following three equations were developed on this basis for SCAs of 62.6, 34.8, and 28.5, respectively :

DA SCA-Specific Ionizer: 62.6 SCA (For d_p= 0.075 - 3.2μ)

$$Pt_{(62.6)ioniz} = \exp\left[-(-0.48\, d_p^2 + 3.07\, d_p + 2.02)\right] \qquad (4\text{-}18)$$

DA SCA-Specific Ionizer: 34.8 SCA (For d_p= 0.075 - 3.2μ)

$$Pt_{(34.8)ioniz} = \exp\left[-(-0.43\, d_p^2 + 2.60\, d_p + 1.20)\right] \qquad (4\text{-}19)$$

DA SCA-Specific Ionizer: 28.5 SCA (For d_p= 0.075 - 3.2μ)

$$Pt_{(28.5)ioniz} = \exp\left[-(-0.66\, d_p^2 + 2.93\, d_p + 0.74)\right] \qquad (4\text{-}20)$$

where Pt is the fractional penetration, and d_p is the physical diameter of the particle in microns. It is important to note that these equation are only valid at physical particle diameters from 0.075 - 3.2 microns. Figure 4-18 shows the relationship between the

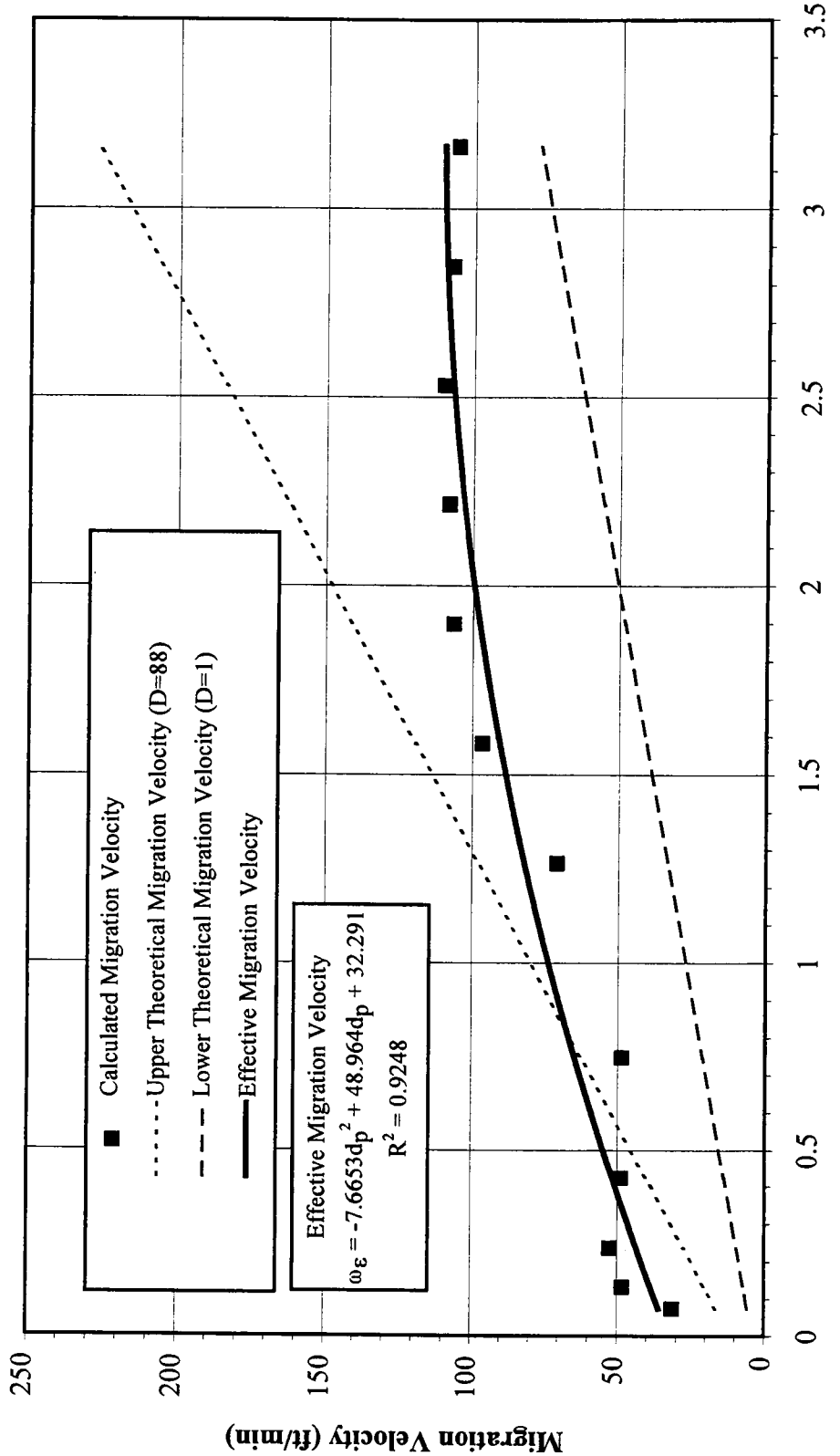

Figure 4-15. DA 62.6 SCA effective, individual calculated and theoretical migration velocities.

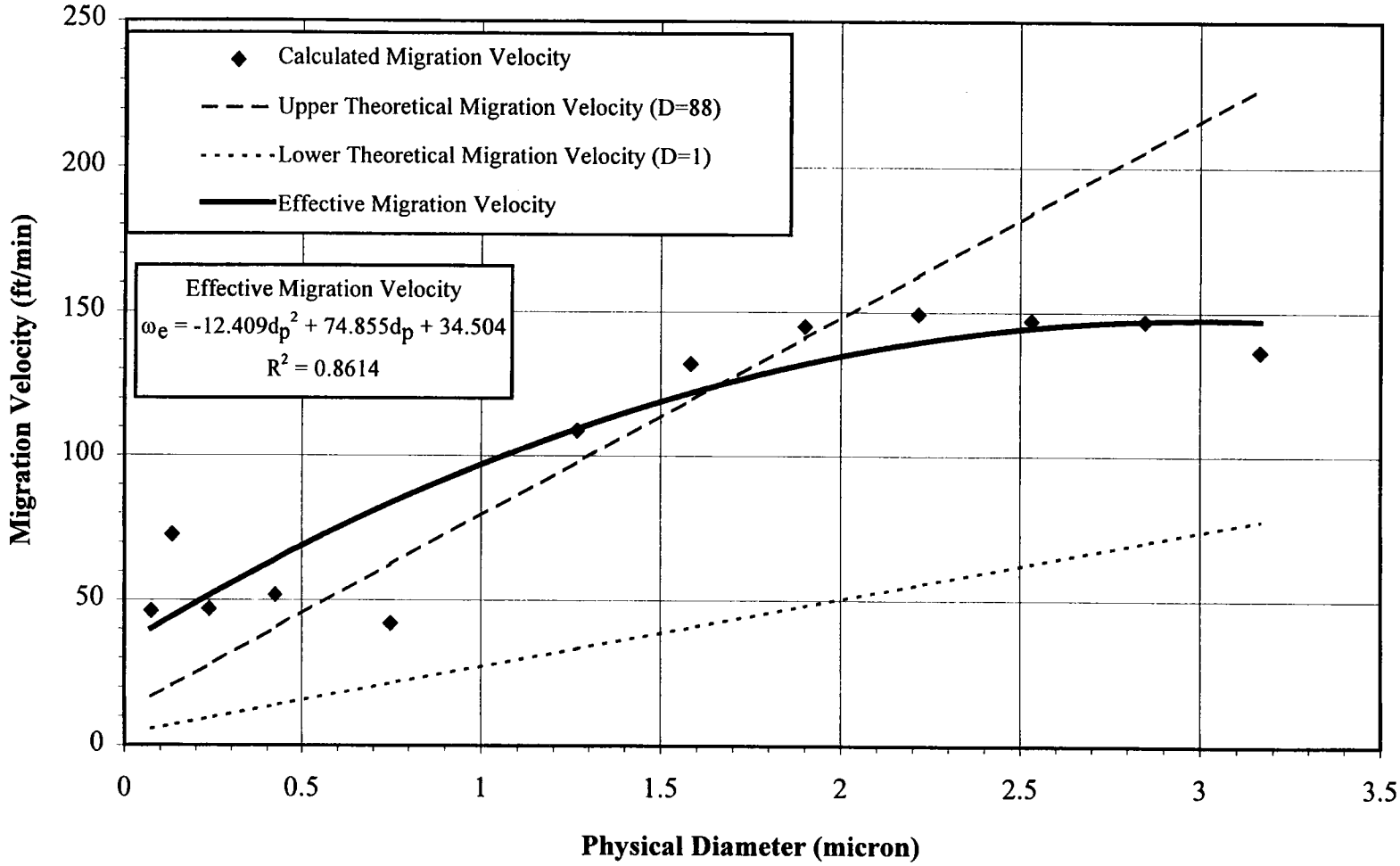

Figure 4-16. DA 34.8 SCA effective, individual calculated and theoretical migration velocities.

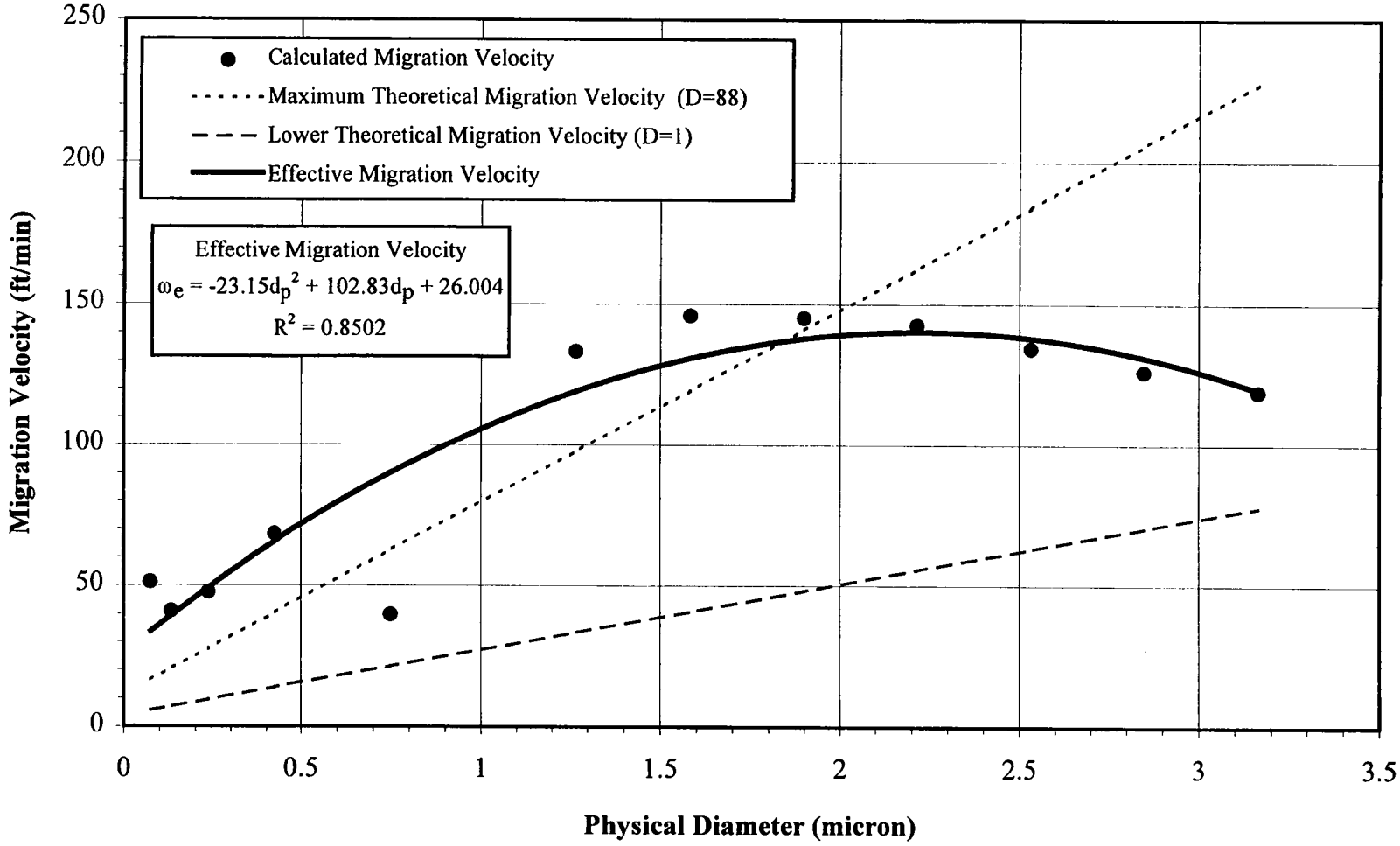

Figure 4-17. DA 28.5 SCA effective, individual calculated and theoretical migration velocities.

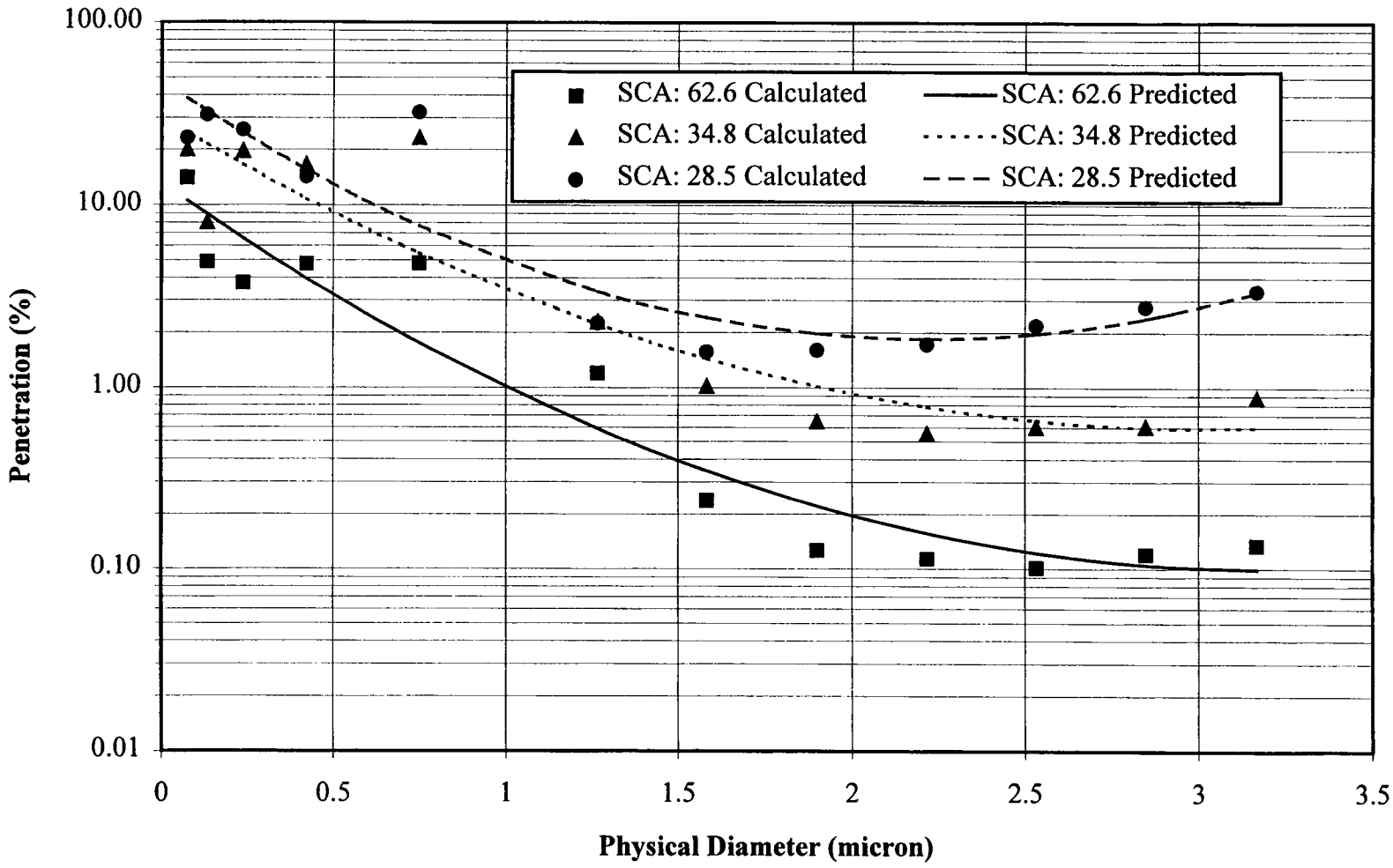

Figure 4-18. Predicted and calculated penetrations of ionizer using the DA SCA-specific effective migration velocity equations.

predicted penetration, using the DA SCA-specific equations, and the calculated penetration of the ionizer for each of the SCAs studied. As shown in the figure, the equations do a good job of predicting the penetration.

4.2.3.4 Development of a MO model based on the MO effective migration velocity

Although the three DA SCA-specific equations (4-18, 4-19 and 4-20) do a good job of predicting the penetration of the ionizer, further efforts were made to develop a single equation that would predict the penetration based on the particle size and gas flowrate. As discussed in the literature review, the Matts-Ohnfeldt (MO) equation has the following form:

$$Pt = \exp\left[-\left(\omega_k \frac{A}{Q}\right)^k\right] \qquad (2\text{-}15)$$

where Pt is the fractional penetration, ω_k is the MO effective migration velocity in ft/min, A is the area of plates in ft^2, Q is the gas flowrate in acfm, and k is an exponent that varies but is commonly 0.5 for flyash.

The MO equation generally predicts the penetration of an ESP more accurately than the DA equation. Therefore, the MO equation was used as the basis for further development of the predictive equations. Similar procedures to those used in developing the DA based equations were used to develop MO based equations.

The first stage of development was to determine the MO effective migration velocity. Recall that the penetration of the ionizer was calculated at all particle sizes for the three SCAs studied. The SCA and A/Q are related as follows:

$$SCA = \left(\frac{A}{Q}\right)(1000) \qquad (2\text{-}14)$$

Thus, given the calculated penetrations at known values of A/Q, ω_k can be calculated when k is known. However, the value of k could take on an infinite number of values, thus, a trial and error solution was used in order to solve for ω_k.

Therefore, a value was assigned to k, and ω_k was calculated for all particle diameters at all SCAs. The MO effective migration velocities at that value of k were then plotted versus the physical diameter, for all SCAs. A polynomial equation was then fit to that data. Thus, an equation was developed which described the MO effective migration velocity as a function of d_p and k, as was a coefficient of determination, R^2, which described how well the polynomial equation fit the calculated values of ω_k. Higher values of R^2 indicate a better correlation. The process was repeated after assigning a new value for k, and adjusting k to obtain the highest coefficient of determination. The results indicated that the highest correlation occurs when k has a value of 0.5. Figure 4-19 shows the relationship between the MO effective migration velocity, and calculated migration velocity using 0.5 for the value of k. Therefore, the polynomial equation that was developed at a k of 0.5 was used as the best estimate of the MO effective migration velocity. The polynomial was substituted back into equation 2-15 in order to obtain the following equation to predict the penetration as a function of d_p and SCA:

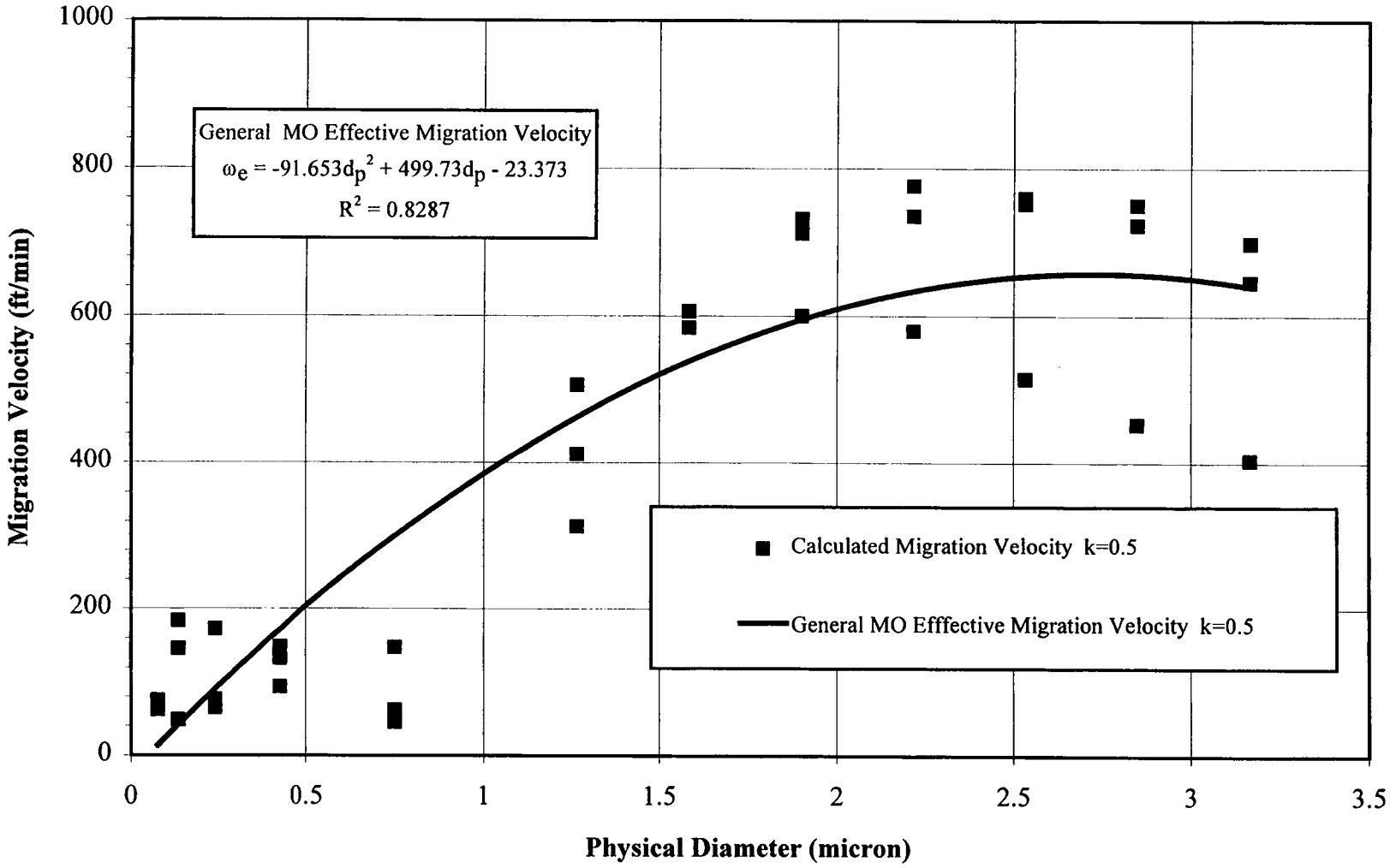

Figure 4-19. General MO effective and individual migration velocities as a function of physical particle diameter.

$$Pt = \exp\left[-\left((-91.653\, d_p^2 + 499.73\, d_p - 23.373)(A/Q)\right)^{0.5}\right] \qquad (4\text{-}21)$$

where Pt is the fractional penetration, d_p is the physical particle diameter in microns, A is the area of plates in ft^2, and Q is the gas flowrate in acfm. Figure 4-20 shows the predicted penetrations, as determined by equation 4-21, and the calculated penetrations for SCAs of 62.6, 34.8 and 28.5. As shown in the figure, the equation does a fair job of describing the penetration in terms of d_p and A/Q. Comparisons between Figure 4-14 and Figure 4-20 indicate that the equation developed using the MO approach (equation 4-21) predicts the penetration more accurately than the equation developed using the DA approach (equation 4-17). However, the MO approach was not as accurate as the DA SCA-specific approach, as indicated by comparison of Figure 4-18 and Figure 4-20.

As a final effort, the MO equation was used to develop three SCA-specific equations which predicted the penetration as a function of d_p for a given SCA. The procedure of varying k that was previously employed was used to determine the optimum value of k for each SCA. Table 4-1 shows the correlation coefficients for each SCA as k was varied.

Table 4.1. Correlation coefficients as a function of k and SCA.

k	SCA: 62.6	SCA: 34.8	SCA: 28.5
0.3	0.8884	0.8722	0.8469
0.4	0.904	0.8821	0.8566
0.5	0.9129	0.8818	0.8592
0.6	0.9182	0.8782	0.8591
0.7	0.9213	0.8738	0.8578
0.8	0.9232	0.8693	0.8561
0.9	0.9243	0.8652	0.8542
1.0	0.9248	0.8614	0.8524
1.1	0.9251	0.8581	0.8508
1.2	0.9252	0.8550	0.8492
1.3	0.9251	0.8523	0.8478

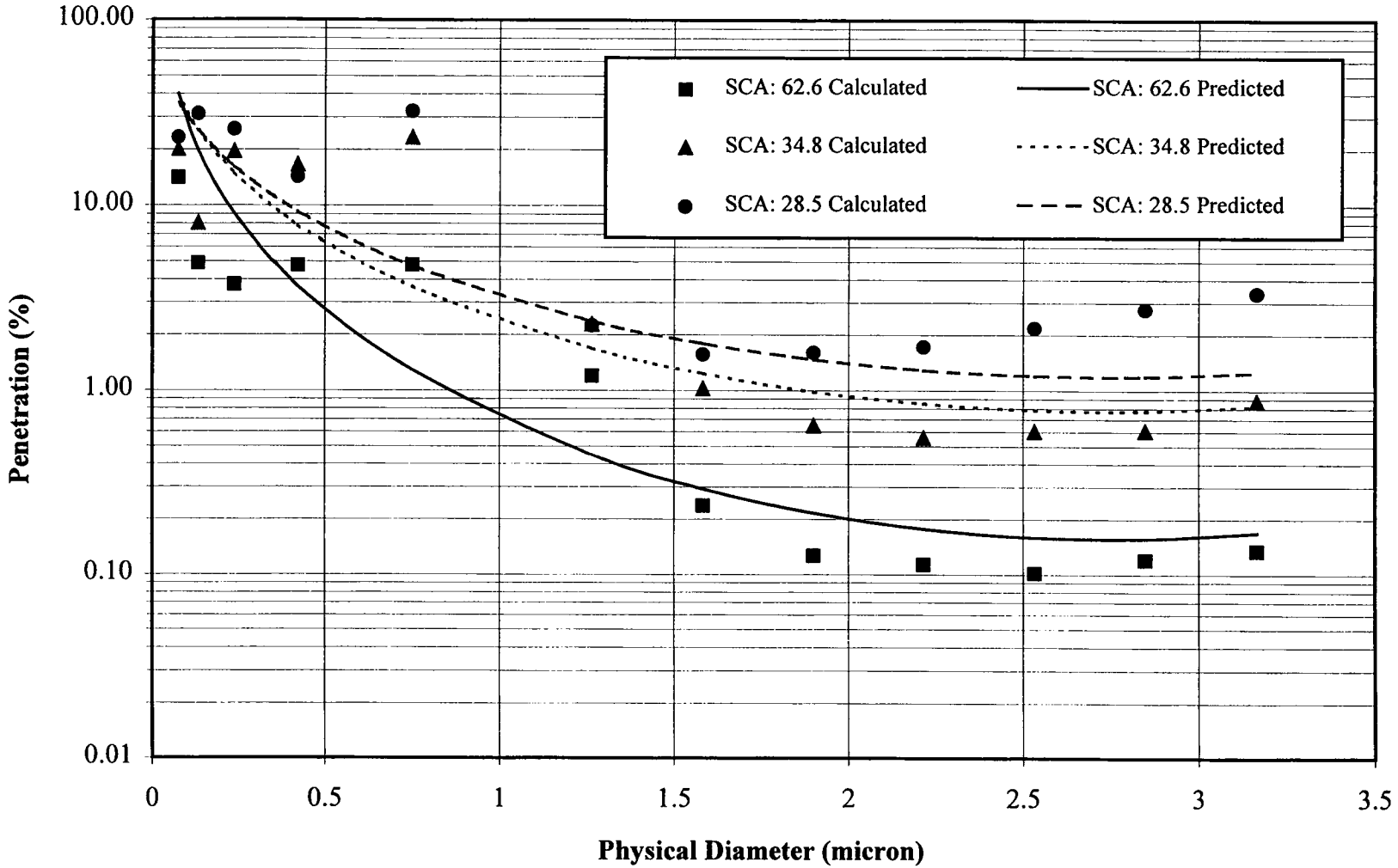

Figure 4-20. Predicted and calculated ionizer penetrations using the general MO effective migration velocity equation, at SCAs of 62.6, 34.8 and 28.5.

As indicated in the table, the highest correlation coefficients were obtained at k values of 1.2, 0.4 and 0.5 for SCAs of 62.6, 34.8 and 28.5, respectively. The MO effective migration velocities, based on those values of k, and the individual calculated migration velocities are shown in Figures 4-21, 4-22 and 4-23 for SCAs of 62.6, 34.8 and 28.5, respectively.

The MO migration velocities were then substituted into the MO equation to obtain the following MO SCA-specific predictive equations:

MO SCA-Specific Ionizer: 62.6 SCA (For d_p= 0.075 - 3.2μ)

$$Pt_{(62.6)ioniz} = \exp\left[-\left(-0.32\, d_p^{\,2} + 2.02\, d_p + 1.84\right)^{1.2}\right] \qquad (4\text{-}22)$$

MO SCA-Specific Ionizer: 34.8 SCA (For d_p= 0.075 - 3.2μ)

$$Pt_{(34.8)ioniz} = \exp\left[-\left(-6.49\, d_p^{\,2} + 40.67\, d_p - 5.64\right)^{0.4}\right] \qquad (4\text{-}23)$$

MO SCA-Specific Ionizer: 28.5 SCA (For d_p= 0.075 - 3.2μ)

$$Pt_{(28.5)ioniz} = \exp\left[-\left(-3.89\, d_p^{\,2} + 16.55\, d_p - 1.76\right)^{0.5}\right] \qquad (4\text{-}24)$$

where Pt is the fractional penetration of the ionizer and d_p is the physical particle diameter in microns. Figure 4-24 shows the predicted penetration, based on equations 4-22, 4-23 and 4-23, and the calculated penetration of the ionizer. As indicated in the figure, the MO SCA-specific equations do a good job of predicting the penetration.

Comparison of Figure 4-18 and Figure 4-24 indicates that the MO and DA SCA-specific equations predict the penetration with about the same level of accuracy. In order to quantify the level of accuracy, and determine which equations most accurately predicted the penetration, the predicted penetration was plotted against the calculated

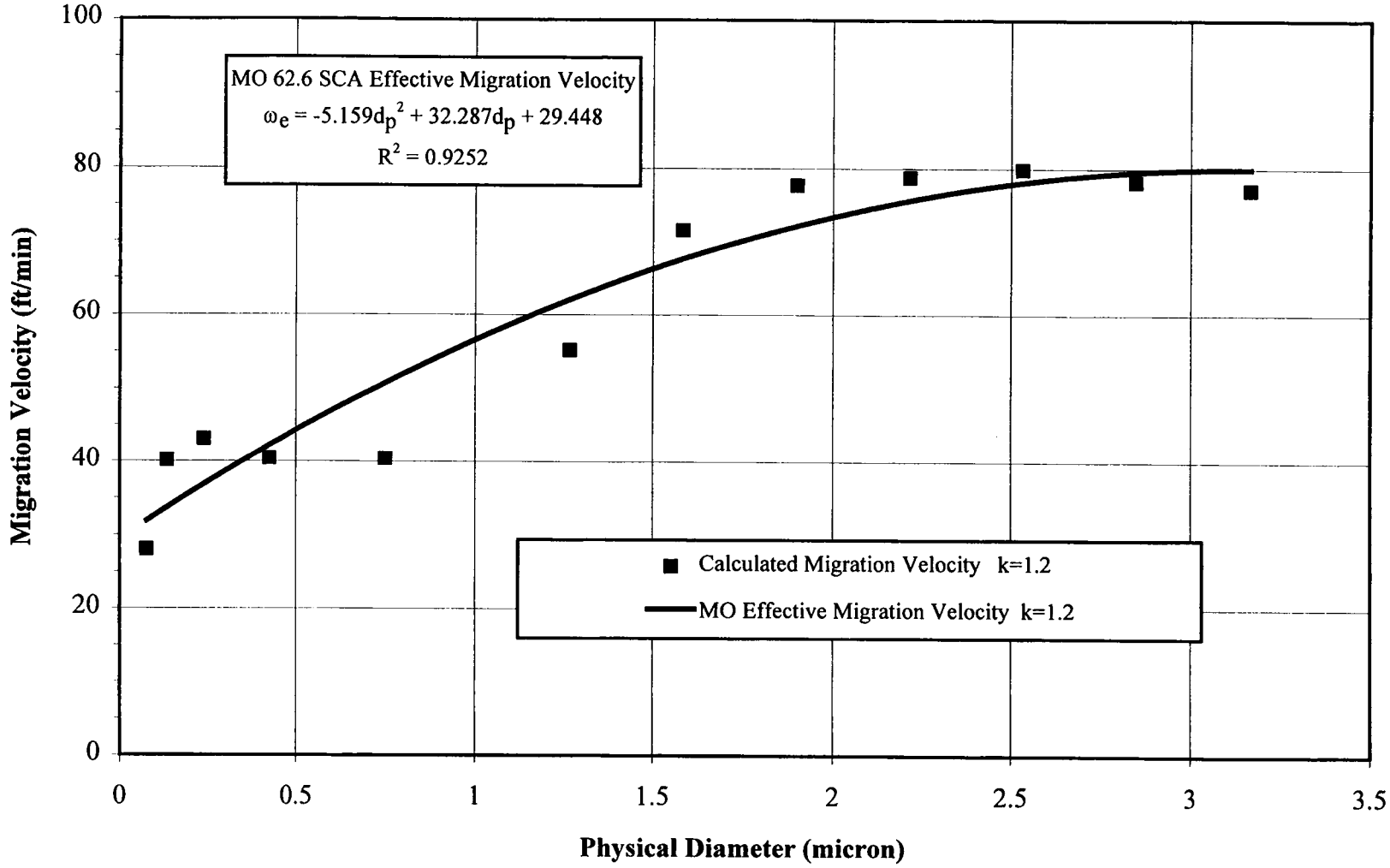

Figure 4-21. MO 62.6 SCA effective and individual calculated migration velocities.

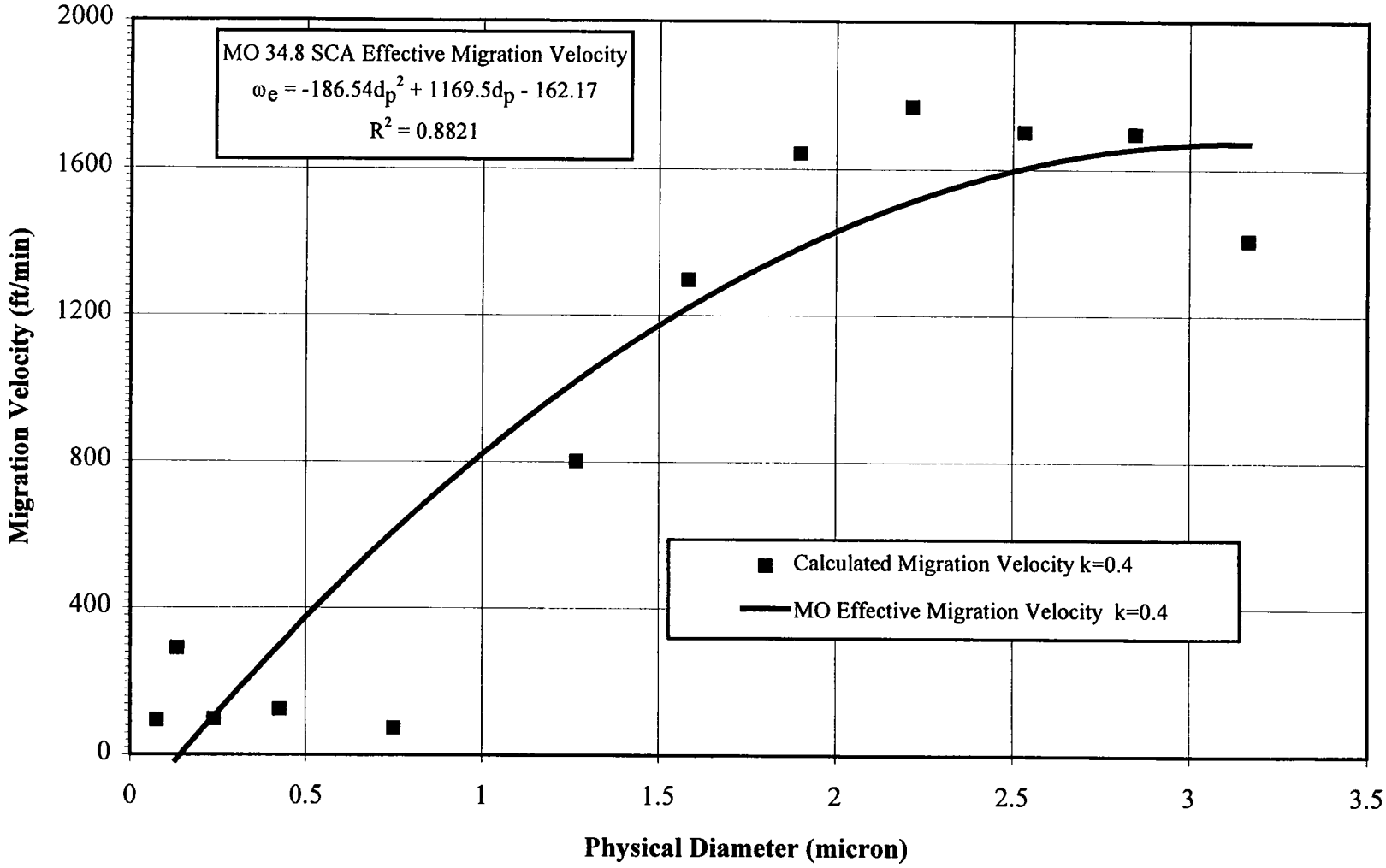

Figure 4-22. MO 34.8 SCA effective and individual calculated migration velocities.

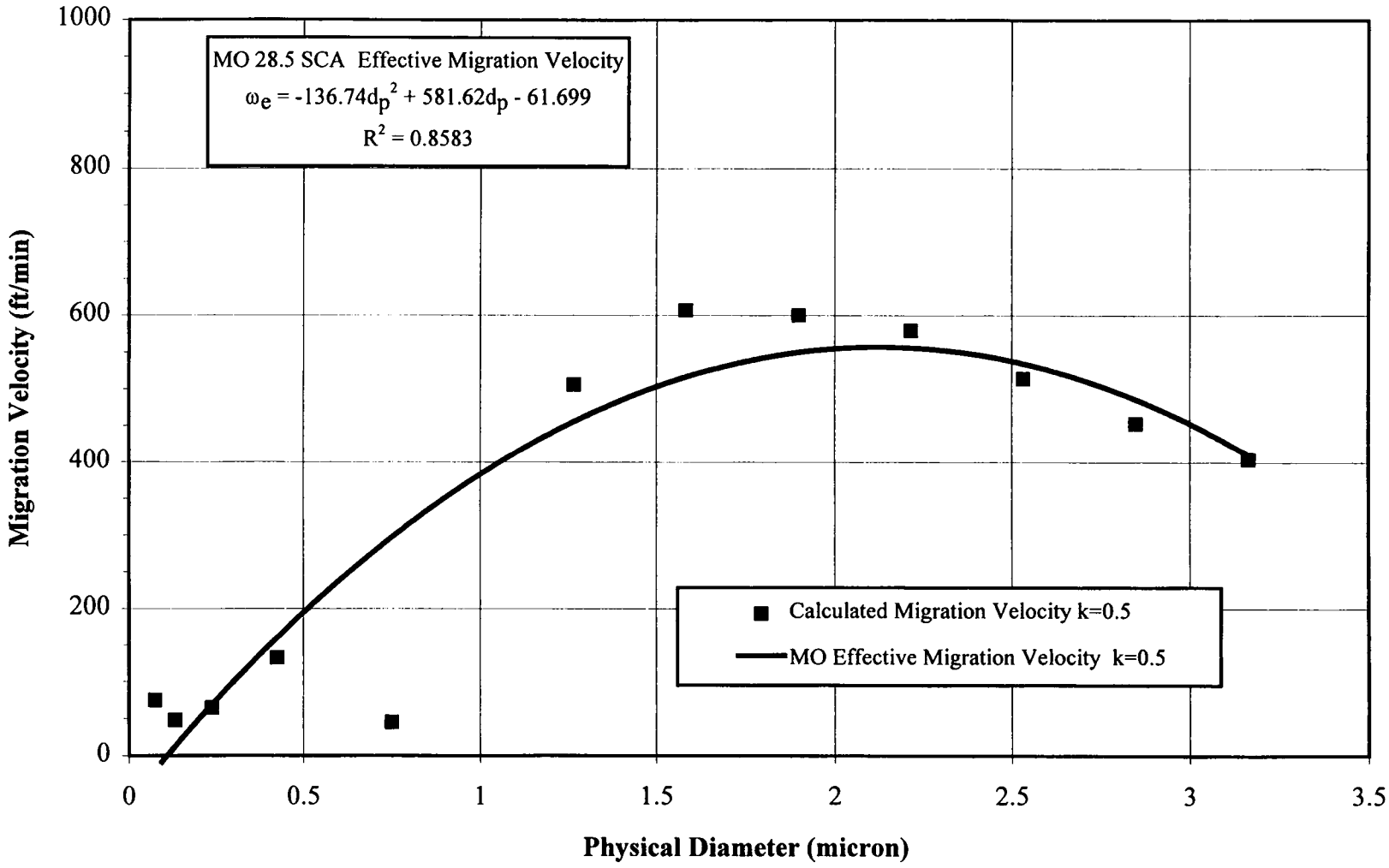

Figure 4-23. MO 28.5 SCA effective and individual calculated migration velocities.

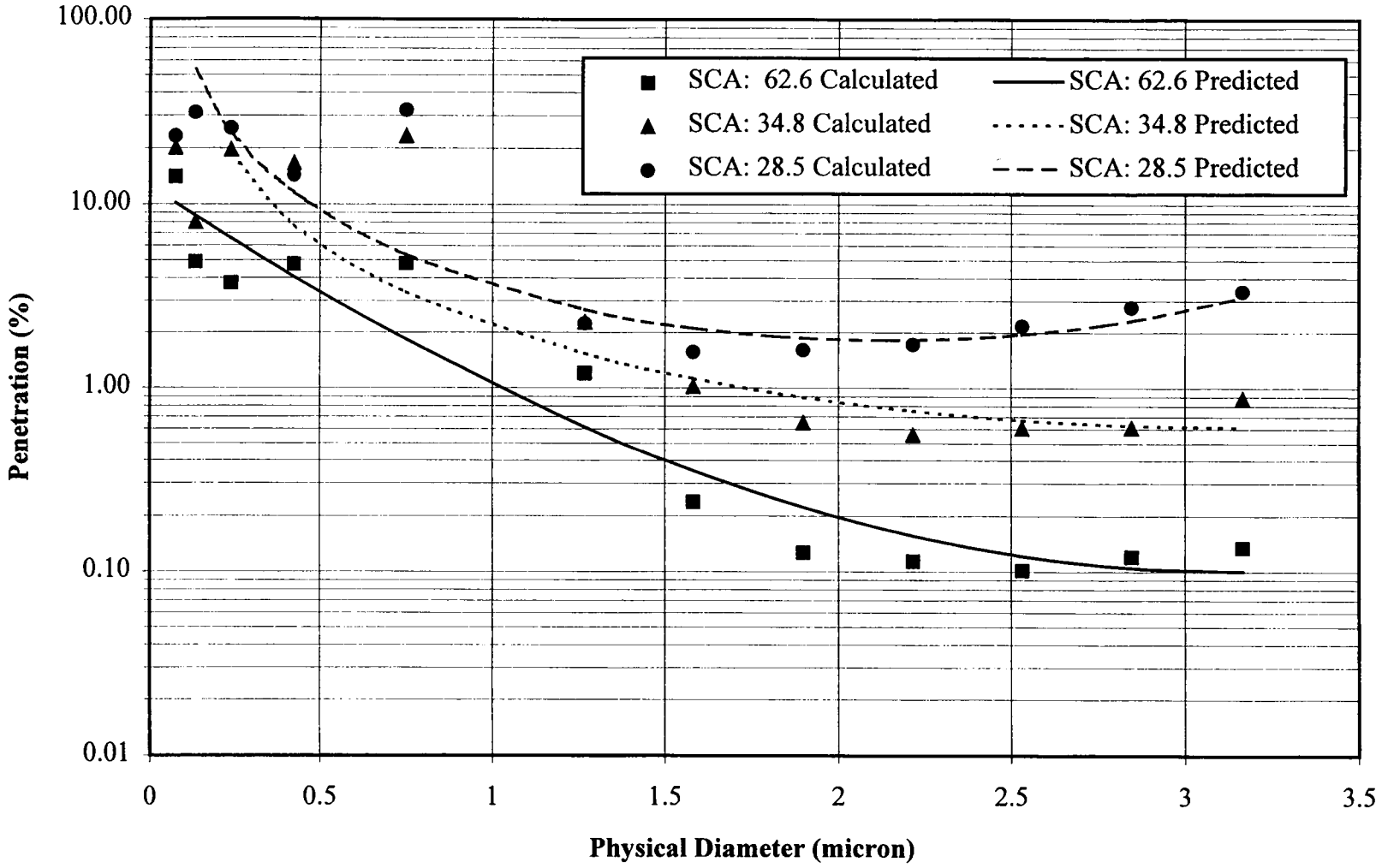

Figure 4-24. Predicted and calculated penetrations of the ionizer using the MO SCA-specific effective migration velocity equations.

penetration for all SCAs combined, and a correlation coefficient was determined. These results are shown in Figure 4-25 and Figure 4-26, for the DA and MO based equations, respectively. Comparison of Figure 4-25 and Figure 4-26 and the correlation coefficients indicates that the DA based equations more accurately predict the penetration than the MO based equations. Therefore, the predictive model that is developed in the remainder of this chapter is based on the DA SCA-specific equations which describe the ionizer penetration.

4.2.4 Development of an IWS Model

As discussed previously, the following relationship is valid if the pilot plant is considered to be three control devices in series:

$$Pt_o = (Pt_{p1w})(Pt_{ioniz})(Pt_{p2w}) \qquad (4\text{-}5)$$

where Pt_o is the overall fractional penetration of the system, Pt_{p1w} is the fractional penetration of the pre-scrubber, Pt_{ioniz} is the fractional penetration of the ionizer, and Pt_{p2w} is the fractional penetration of the packed bed downstream of the ionizer. The IWS consists of an ionizer and packed bed in series, thus

$$Pt_{IWS} = (Pt_{ioniz})(Pt_{p2w}) \qquad (4\text{-}25)$$

therefore, the overall model used to predict the penetration for the IWS was developed by combining the equation for the packed bed (equation 4-10) and the DA SCA-specific equations for the ionizer (equations 4-18, 4-19, 4-20) to yield the following:

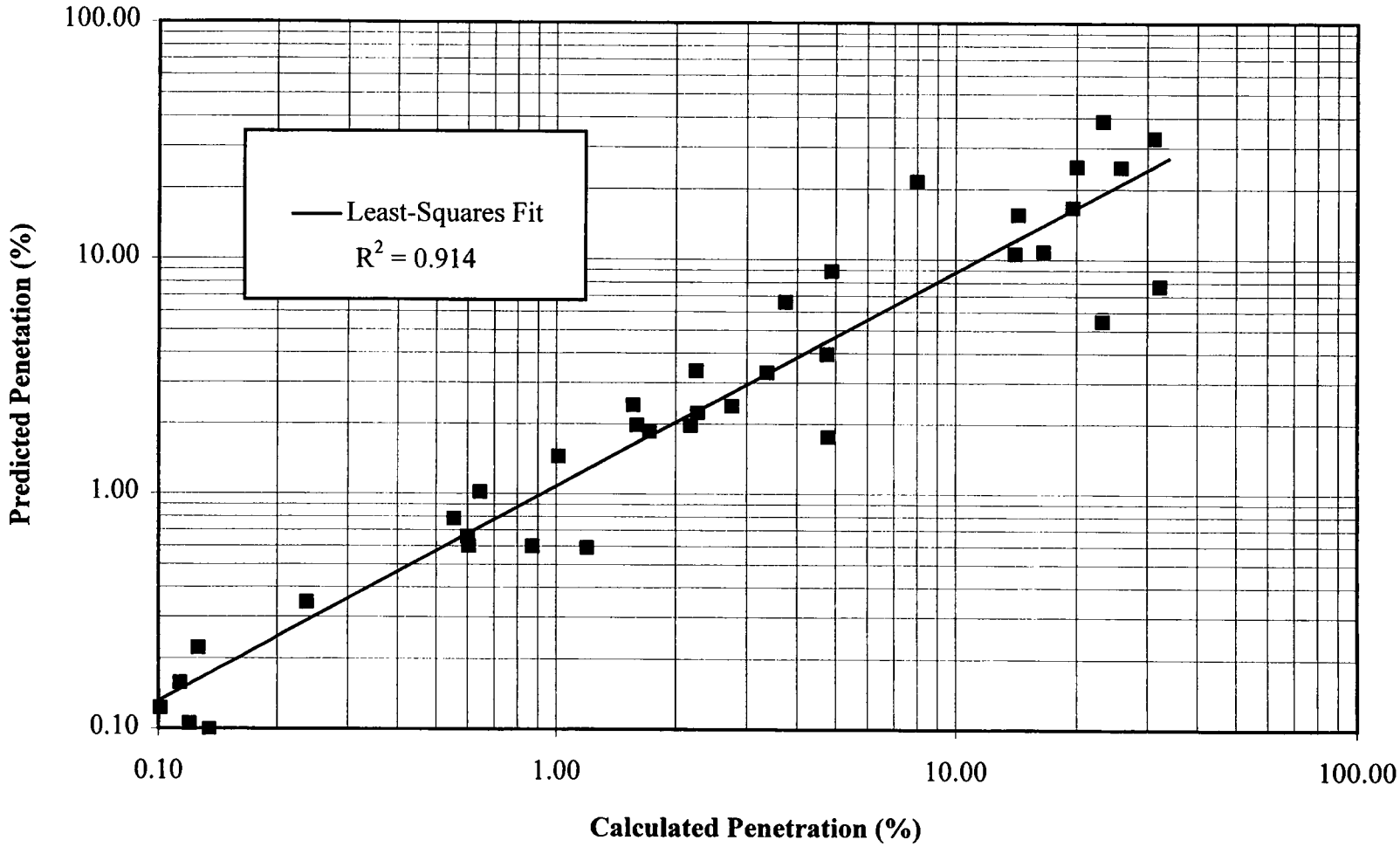

Figure 4-25. Predicted vs calculated penetrations for ionizer using DA SCA-specific effective migration velocity equations.

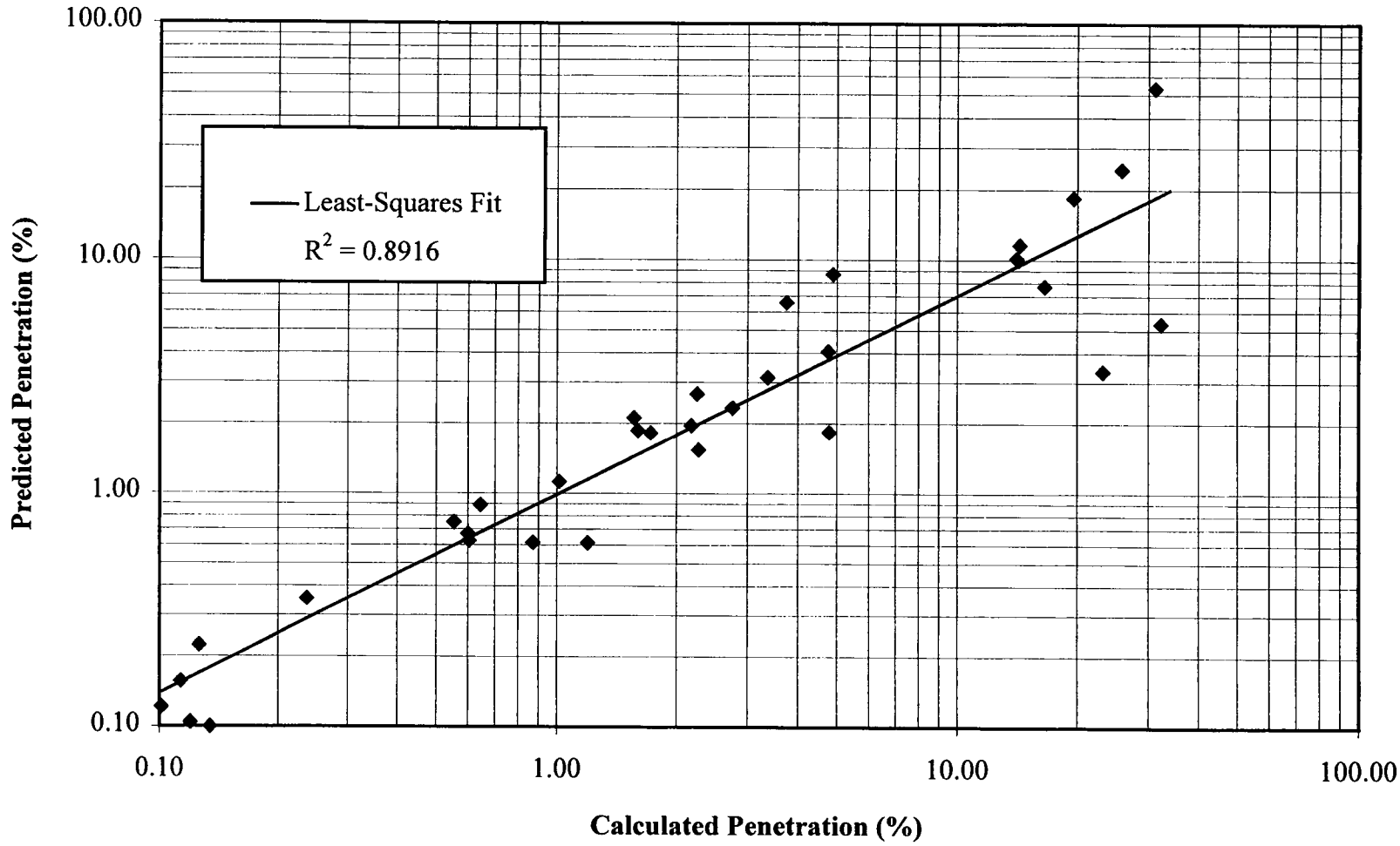

Figure 4-26. Predicted vs calculated penetrations for ionizer using MO SCA-specific effective migration velocity equations.

IWS Model: 62.6 SCA (For d_p= 0.075 - 3.2μ ; d_a=0.12 - 5.0μ)

$$Pt_{(62.6)IWS} = \exp [- (-0.48\ d_p^2 + 3.07\ d_p + 2.02)] \quad (4\text{-}26)$$

$$X\ [0.006199\ d_a^3 - 0.060103\ d_a^2 + 0.011302\ d_a + 0.77037]^{(L/8)}$$

IWS Model: 34.8 SCA (For d_p= 0.075 - 3.2μ ; d_a=0.12 - 5.0μ)

$$Pt_{(34.8)IWS} = \exp [- (-0.43\ d_p^2 + 2.60\ d_p + 1.20)] \quad (4\text{-}27)$$

$$X\ [0.006199\ d_a^3 - 0.060103\ d_a^2 + 0.011302\ d_a + 0.77037]^{(L/8)}$$

IWS Model: 28.5 SCA (For d_p= 0.075 - 3.2μ ; d_a=0.12 - 5.0μ)

$$Pt_{(28.5)IWS} = \exp [- (-0.66\ d_p^2 + 2.93\ d_p + 0.74)] \quad (4\text{-}28)$$

$$X\ [0.006199\ d_a^3 - 0.060103\ d_a^2 + 0.011302\ d_a + 0.77037]^{(L/8)}$$

where Pt is the fractional penetration, d_p is the physical diameter of the particle in microns, d_a is the aerodynamic diameter of the particle in microns, and L is the depth of wetted packing in the direction of gas flow in feet. Note that it may be more convenient to replace the aerodynamic diameter, d_a, by an equivalent physical diameter. The aerodynamic and physical diameters are related as follows:

$$d_a = d_p \sqrt{\rho_p} \quad (4\text{-}1)$$

where d_a is the aerodynamic diameter in microns, d_p is the physical diameter of the particle in microns, and ρ_p is the density of the particle in g/cm^3. Thus, d_a in equation 4-10 may be replaced by the term $d_p \sqrt{\rho_p}$.

4.2.4 Overall Model for Predicting Penetration Using the Deutsch-Anderson Approach

The general model which is used to predict the overall penetration in the pilot plant is the same model used to predict the penetration through the IWS. The only difference between the IWS and the overall system is the depth of wetted packing; the overall system had a total wetted packing depth of 8 feet, while the IWS had a wetted packing depth of 4 feet. Therefore, by using the appropriate value of wetted packing depth, the IWS model may be used to model other systems which have a single ionizer with a single packed bed or multiple packed beds in series.

4.2.5 Limitations of the Models

Limitations exist on the model that was developed in this section. Most importantly, the model is specifically designed for the SCAs indicated. However, a reasonable estimate of penetration may be obtained by interpolating between the values in two of the equations to obtain estimates of penetrations at other SCAs. However, it is not recommended that extrapolation of the model be used to predict penetrations at SCAs outside of the range of those used in this study.

Another important limitation of the models is that it was developed to predict the penetration of particles with physical diameters of 0.075 - 3.2 microns. The models should not be used to predicted the pentetration of particles with diameters outside of that size range.

5. CONCLUSIONS

As indicated in the results, the penetration through the system, whether operated at p1wp2w or p1w35p2w, is a strong function of the particle diameter for aerodynamic diameters ranging from 0.118 - 5.0 microns. When operating at p1w35p2w and a SCA of 34.8, the penetration is approximately 8.5% for 0.5 micron particles, and steadily decrease to 0.09% for 5.0 micron particles.

The penetration is also a strong function of the gas flowrate in the system. When operated at p1w35p2w, the penetration increases as the gas flowrate through the system increases. This is attributed to the decrease in residence time through the ionizer as the gas flowrate increases.

The type of packing in the scrubbers also effects the penetration. When operated at p1wp2w, the 2" Type-K and 1" Type-R Tellerettes performed equally well, and yielded penetrations lower than those with the 2" Type-R Tellerettes. However, when operated at p1w35p2w, the 2" Type-R yielded penetrations lower than those with the 2" Type-K or 1" Type-R.

A model was developed to describe the penetration when operated at p1wp2w with 2" Type-R Tellerettes, as a function of the aerodynamic particle diameter. The model is valid for aerodynamic particle diameters from 0.5 - 5.0 microns. The model has the following form:

$$Pt_{PB} = [0.006199\, d_a^{3} - 0.060103\, d_a^{2} + 0.011302\, d_a + 0.77037]^{(L/8)}$$

where Pt_{PB} is the fractional penetration, L is the total depth of wetted packing in feet, and d_a is the aerodynamic particle diameter in microns. It may be more convenient to replace the term d_a by an equivalent physical diameter. The aerodynamic and physical diameters are related as follow:

$$d_a = d_p\sqrt{\rho_p}$$

where d_a is the aerodynamic diameter in microns, d_p is the physical diameter of the particle in microns, and ρ_p is the density of the particle in g/cc.

Three equations were developed to describe the penetration of particles through the ionizer with the following forms:

Ionizer: 62.6 SCA (For d_p= 0.075 - 3.2μ ; d_a=0.12 - 5.0μ)

$$Pt_{(62.6)ioniz} = \exp\left[-\left(-0.48\, d_p^2 + 3.07\, d_p + 2.02\right)\right]$$

Ionizer: 34.8 SCA (For d_p= 0.075 - 3.2μ ; d_a=0.12 - 5.0μ)

$$Pt_{(34.8)ioniz} = \exp\left[-\left(-0.43\, d_p^2 + 2.60\, d_p + 1.20\right)\right]$$

Ionizer: 28.5 SCA (For d_p= 0.075 - 3.2μ ; d_a=0.12 - 5.0μ)

$$Pt_{(28.5)ioniz} = \exp\left[-\left(-0.66\, d_p^2 + 2.93\, d_p + 0.74\right)\right]$$

where Pt_{ioniz} is the fractional penetration of the ionizer, d_a is the aerodynamic particle diameter in microns, d_p is the physical particle diameter in microns. These equations are valid at physical particle diameters from 0.075 - 3.2 microns.

Three equations were developed to describe the behavior of the IWS, which consists of an ionizer and a packed bed in series. The equations have the following forms:

IWS Model: 62.6 SCA (For d_p= 0.075 - 3.2μ ; d_a=0.12 - 5.0μ)

$$Pt_{(62.6)IWS} = \exp [- (-0.48\ d_p^2 + 3.07\ d_p + 2.02)]$$

$$X\ [0.006199\ d_a^3 - 0.060103\ d_a^2 + 0.011302\ d_a + 0.77037]^{(L/8)}$$

IWS Model: 34. 8SCA (For d_p= 0.075 - 3.2μ ; d_a=0.12 - 5.0μ)

$$Pt_{(34.8)WS} = \exp [- (-0.43\ d_p^2 + 2.60\ d_p + 1.20)]$$

$$X\ [0.006199\ d_a^3 - 0.060103\ d_a^2 + 0.011302\ d_a + 0.77037]^{(L/8)}$$

IWS Model: 28.5 SCA (For d_p= 0.075 - 3.2μ ; d_a=0.12 - 5.0μ)

$$Pt_{(28.5)IWS} = \exp [- (-0.66\ d_p^2 + 2.93\ d_p + 0.74)]$$

$$X\ [0.006199\ d_a^3 - 0.060103\ d_a^2 + 0.011302\ d_a + 0.77037]^{(L/16)}$$

where Pt is the fractional penetration, d_p is the physical diameter of the particlein microns, d_a is the aerodynamic diameter of the particle in microns, and L is the depth of wetted packing in the direction of gas flow in feet. This overall model, which consists of these three equations is valid at physical particle diameters of 0.12 - 3.2 microns (aerodynamic diameters of 0.118 - 5.0 microns).

The ionizing wet scrubber (IWS) is an efficient particulate control device which has been demonstrated to achieve overall mass collection efficiencies as high as 99.7%. The major mechanisms of particulate collection in the IWS are inertial impaction and electrostatic forces. Studies are under way to further quantify and describe the effects of electrostatics on the collection efficiency of the system. Additional studies may be warranted using higher grain loadings and different types of particulates.

BIBLIOGRAPHY

Abraham, Sunil. M.S. Thesis, University of Tennessee, Tennessee (1996).

Calvert, Seymour, and Shui-Chow Yung. "Advanced Developments in Novel Particulate Control Technology." Proceedings: 72nd Annual Meeting of the Air Pollution Control Association (1979).

Cooper, C. David, and F. C. Alley. *Air Pollution Control: A Design Approach.* Second Edition. Waveland Press, Inc., Prospect Heights, IL, (1994).

Ensor, David S., and Dale L. Harmon. "Evaluation of the Ceilcote Ionizing Wet Scrubber." *EPA 600/9-80-039C, Vol III*, Sept. 1980.

Gallaer, C. A. *Electrostatic Precipitation Reference Manual.* Electric Power Research Institute, Palo Alto, CA, (1983).

Goyer, Guy G., et al. "Filtration of Monodisperse Electrically Charged Aerosols." *Journal of Physics and Chemistry* 58 (1954): 137-142.

Hesketh, Howard E., *Air Pollution Contol: Traditional and Hazardous Pollutants*, Technomic Publishing Company, Lancaster, PA, (1991).

Johnstone, J. F., and M. H. Roberts. "Depostion of Aerosol Particles from Moving Gas Streams." *Industrial Engineering Chemistry* 41 (1949): 2417.

Klugman, W., and S.V. Sheppard. "The Ionizing Wet Scrubber." *Air Pollution Control and Design Handbook Part 2.* Ed. P.N. Chevemisinoff and R.A. Young.

Kraemer, Herbert F., and H. F. Johnstone. "Collection of Aerosol Particles in Presence of Electrostatic Fields." *Industrial and Engineering Chemistry* 47, No. 12, (1955): 2426-2434.

Lawless, Phil A., and Leslie E. Sparks. "A Review of Mathematical Models for ESPs and Comparison of Their Successes." *Proceedings: Second International Conference on Electrostatic Precipitation.* Ed. Senichi Masuda. Pittsburgh: Air Pollution Control Association, 1985. 513-22.

Nielsen, Kenneth A., and James C. Hill. "Collection of Inertialess Particles on Spheres with Electrical Forces." *Industrial Engineering Chemistry Fundamentals* 15, No. 3. (1976): 149-156.

Oglesby, Jr., Sabert, and Grady B. Nichols. *Electrostatic Precipitation.* Marcel Dekker, Inc., New York, NY, (1978).

Pilat, Michael J., "Collection of Aerosol Particles by Electrostatic Droplet Spray Scrubbers." *Journal of the Air Pollution Control Association* 25, (1975): 176-178.

Sears, Francis W., et al. *University Physics.* Seventh Edition. Addison-Wesley Publishing Company, Reading, MA, (1987).

Sheppard, Stanton V. "Fine Particle Removal for Hazwaste Incinerators with the Ionizing Wet Scrubber." *Proceedings: 86th Annual Meeting of the Air and Waste Management Association* (1993).

Stern, Arthur C. Vol. IV of *Air Pollution.* Third Edition. Academic Press, New York, NY, (1977).

Sumiyoshitani, Satoru, et al. "Direct Observation of the Collection Process for Dust Particles from an Air Stream by a Charged Water Droplet." *IEEE Transactions on Industry Applications* IA-20, No. 2, (1984): 274-281.

Troxler, William L., et al. "Ionizing Wet Scrubber Pilot Test Results for Controlling Emissions from a Liquid Hazardous Waste Incinerator." *Proceedings: 85th Annual Meeting of the Air and Waste Management Association* (1992).

Turner, James H., et al. "Electrostatic Precipitators." *Air Pollution Control Engineering Manual.* Ed. Anthony J. Buonicore and Wayne T. Davis. Van Nostrand Reinhold, New York, NY, (1992).

Wark, Kenneth, and Cecil F.Warner. *Air Pollution: It's Origin and Control*, Second Edition. Harper Collins Publishers Inc., New York, NY, (1981).

APPENDIX A

CALIBRATION CURVES AND SIZE DISTRIBUTION OF FLYASH

APPENDIX A: GAS FLOW RATE CALIBRATION

METHODOLOGY:

a. Velocity traverses are performed for IWS static pressures of 4, 6, and 8 inches of water. For each of these traverses, an average ΔP is calculated, which is then used to determine the volumetric flowrate.
b. The flowrates of water through the growth chamber, venturi, packed bed, and IWS will remain constant for all gas flowrates through the system. These flowrates are adjusted at the beginning of the testing.
c. After starting the system, the damper on the induced draft fan is adjusted until the IWS static pressure is 4 inches of water.
d. After the system reaches steady-state, the barometric pressure, stack gage pressure, stack gas dry bulb temperature, and stack gas wet bulb temperature are recorded.
e. Velocity pressure is measured in the exhaust duct approximately 6 feet upstream for the induced draft fan. Twelve measurements are taken in the horizontal direction, and twelve measurements are taken in the vertical direction.
f. Based on the velocity pressure, stack temperature, stack absolute pressure, molecular weight of the flue gas, and cross sectional area of the duct, the volumetric flowrate is calcualted.
g. The procedure is repeated for IWS static pressures of 6 and 8 inches of water
h. A calibration curve is plotted, and linear regression is used to plot a "best fit" line.

RESULTS:

A. Location of Traverse Points

Inside diameter of stack: 8 inches
Cross sectional area of stack: 0.35 sq. ft.
Barometric pressure: 30.00 in Hg

Traverse Point Number	% of Stack Dia from Inside Wall to Traverse Point	Distance from Inside Wall to Traverse Point (inches)	Wall Thickness (inches)	Distance from Outside Wall to Traverse Point (inches)
1	2.1	0.168	0.125	0.29
2	6.7	0.536	0.125	0.66
3	11.8	0.944	0.125	1.07
4	17.7	1.416	0.125	1.54
5	25	2	0.125	2.13
6	35.5	2.84	0.125	2.97
7	64.5	5.16	0.125	5.29
8	75	6	0.125	6.13
9	78.3	6.264	0.125	6.39
10	88.2	7.056	0.125	7.18
11	93.3	7.464	0.125	7.59
12	97.9	7.832	0.125	7.96

B. Velocity Traverse 1 - Stack Gage Pressure = 4" water

Stack gage pressure: 4 in water = 0.29 in Hg
Stack absolute pressure: 29.71 in. Hg
Stack gas temperature: 45 °F = 505 R

	Horizontal	Traverse	Vertical	Traverse
Traverse Point	Δ P, (in water)	$\frac{\sqrt{\Delta P}}{24}$	Δ P, (in water)	$\frac{\sqrt{\Delta P}}{24}$
1	0.22	0.019	0.22	0.019
2	0.24	0.02	0.24	0.02
3	0.25	0.02	0.24	0.02
4	0.26	0.021	0.26	0.021
5	0.28	0.022	0.26	0.021
6	0.28	0.022	0.28	0.022
7	0.28	0.022	0.28	0.022
8	0.26	0.021	0.26	0.021
9	0.24	0.020	0.24	0.02
10	0.22	0.019	0.2	0.018
11	0.2	0.018	0.18	0.017
12	0.14	0.015	0.14	0.015

$$\sum \frac{\sqrt{\Delta P}}{24} = 0.4841$$

$$\Delta P_{avg} = \left[\sum \frac{\sqrt{\Delta P}}{24}\right]^2 = [0.4841]^2 = 0.2343 \text{ in. water}$$

$$V_s = 174(C_p)\sqrt{(\Delta P_{avg})(T_s)\left(\frac{29.92}{P_s}\right)\left(\frac{28.96}{M_s}\right)} = 174(0.99)\sqrt{(0.2343)(505)\left(\frac{29.92}{29.71}\right)\left(\frac{28.96}{28.96}\right)}$$

$$= 1880.8 \text{ ft/min}$$

$$Q = V(A) = \left(\frac{1880.8\,ft}{\text{min}}\right)(0.35\,ft^2) = 658.28\,acfm$$

C. Velocity Traverse 2 -Stack Gage Pressure = 6" water

Stack gage pressure: 6 in water = 0.44 in Hg
Stack absolute pressure: 29.56 in Hg
Stack gas temperature: 45 °F = 505 R

	Horizontal	Traverse	Vertical	Traverse
Traverse Point	Δ P, (in water)	$\frac{\sqrt{\Delta P}}{24}$	Δ P, (in water)	$\frac{\sqrt{\Delta P}}{24}$
1	0.28	0.022	0.31	0.0232
2	0.3	0.023	0.33	0.0239
3	0.34	0.024	0.36	0.025
4	0.34	0.024	0.36	0.025
5	0.36	0.025	0.38	0.0256
6	0.36	0.025	0.38	0.0256
7	0.36	0.025	0.38	0.0256
8	0.35	0.0246	0.36	0.025
9	0.32	0.0235	0.34	0.024
10	0.3	0.0228	0.28	0.022
11	0.26	0.0212	0.24	0.02
12	0.2	0.0186	0.2	0.0186

$$\sum \frac{\sqrt{\Delta P}}{24} = 0.5639$$

$$\Delta P_{avg} = \left[\sum \frac{\sqrt{\Delta P}}{24}\right]^2 = [0.5639]^2 = 0.318 \text{ in. water}$$

$$V_s = 174(C_p)\sqrt{(\Delta P_{avg})(T_s)\left(\frac{29.92}{P_s}\right)\left(\frac{28.96}{M_s}\right)} = 174(0.99)\sqrt{(0.318)(505)\left(\frac{29.92}{29.56}\right)\left(\frac{28.96}{28.96}\right)}$$

=2196.43 ft/min

$$Q=V(A)=\left(\frac{2196.43\,ft}{\text{min}}\right)(0.35\,ft^2) = 768.75\,acfm$$

D. Velocity Traverse 3 - Stack Gage Pressure = 8" water

Stack gage pressure: 8 in water = 0.59 in Hg
Stack absolute pressure: 29.41 in Hg
Stack gas temperature: 45 °F = 505 R

	Horizontal	Traverse	Vertical	Traverse
Traverse Point	Δ P, (in water)	$\frac{\sqrt{\Delta P}}{24}$	Δ P, (in water)	$\frac{\sqrt{\Delta P}}{24}$
1	0.48	0.0288	0.52	0.03
2	0.5	0.0294	0.56	0.0311
3	0.54	0.0306	0.58	0.0317
4	0.58	0.0317	0.58	0.0317
5	0.6	0.0322	0.6	0.0322
6	0.64	0.0333	0.62	0.0328
7	0.64	0.0333	0.62	0.0328
8	0.62	0.0328	0.6	0.0322
9	0.58	0.0317	0.54	0.0306
10	0.5	0.0294	0.46	0.0282
11	0.4	0.0263	0.4	0.0263
12	0.34	0.0243	0.32	0.0257

$$\sum \frac{\sqrt{\Delta P}}{24} = 0.7279$$

$$\Delta P_{avg} = \left[\sum \frac{\sqrt{\Delta P}}{24}\right]^2 = [0.7279]^2 = 0.5298 \text{ in. water}$$

$$V_s = 174(C_p)\sqrt{(\Delta P_{avg})(T_s)\left(\frac{29.92}{P_s}\right)\left(\frac{28.96}{M_s}\right)} = 174(0.99)\sqrt{(0.5298)(505)\left(\frac{29.92}{29.41}\right)\left(\frac{28.96}{28.96}\right)}$$

$$= 2842.1 \text{ ft/min}$$

$$Q = V(A) = \left(\frac{2842.1 ft}{\text{min}}\right)(0.35 ft^2) = 994.74 acfm$$

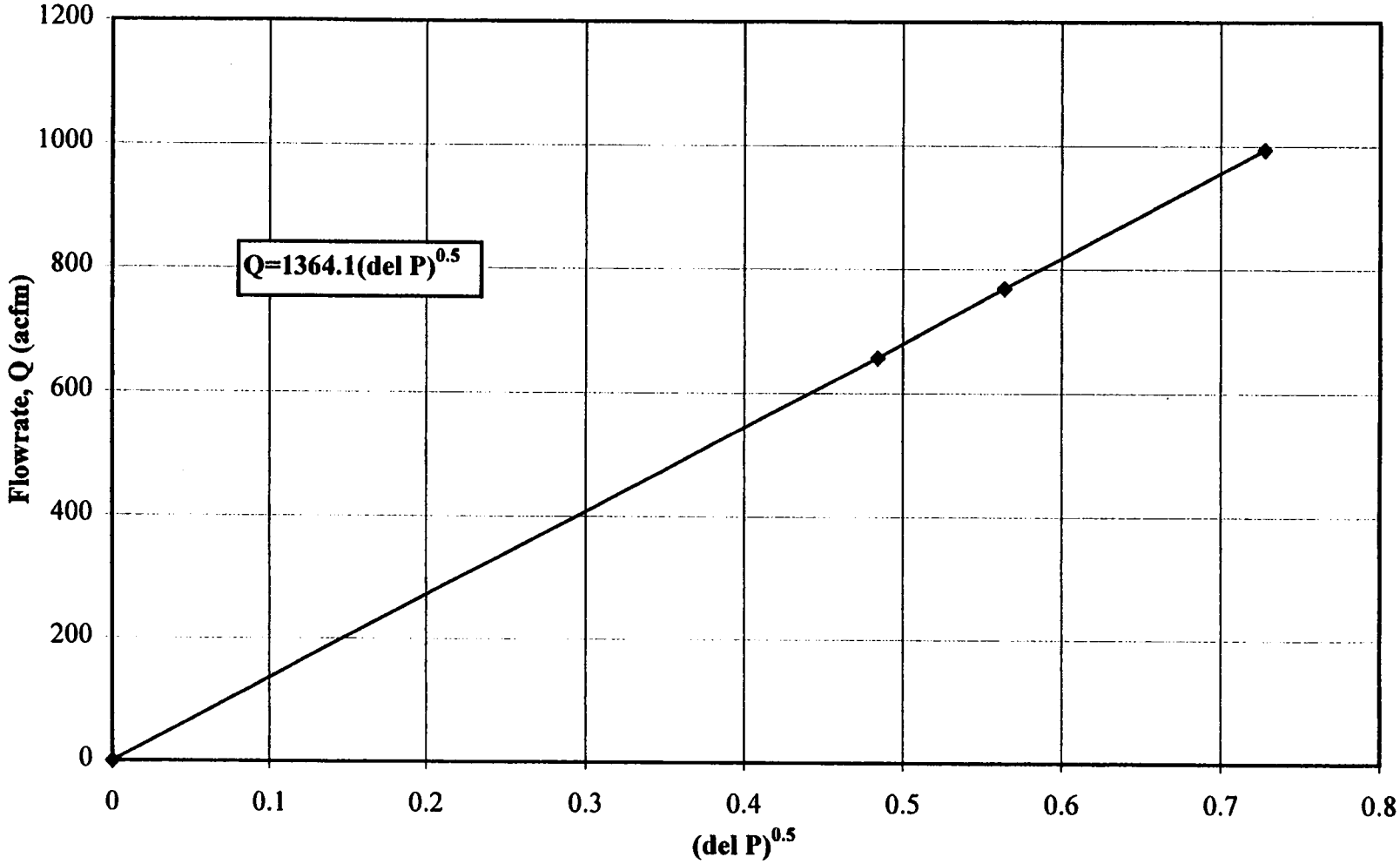

Figure A-1. Calibration Curve for Gas Flowrate in Pilot Plant.

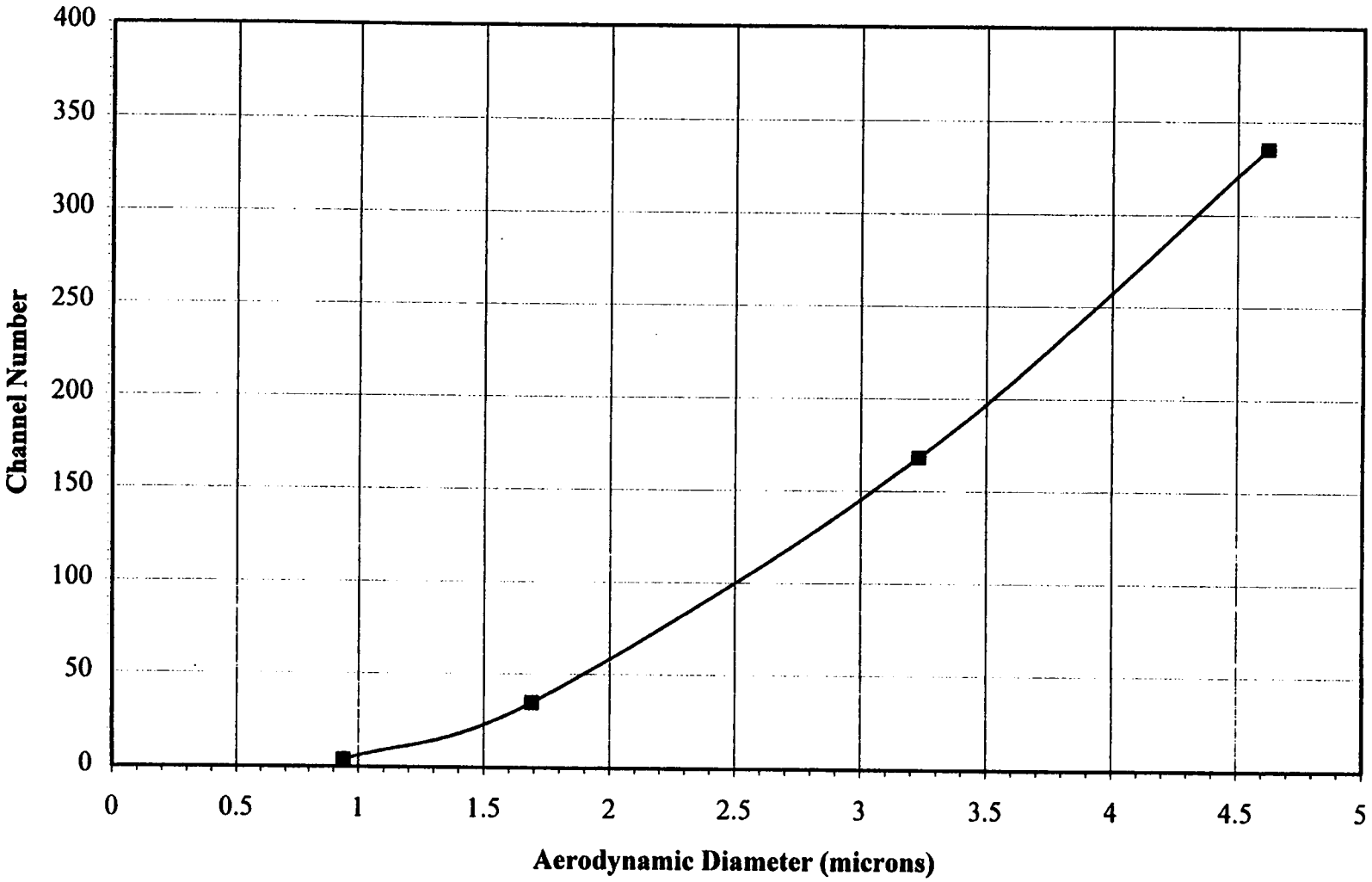

Figure A-2. Calibration Curve for Optical Particle Counter.

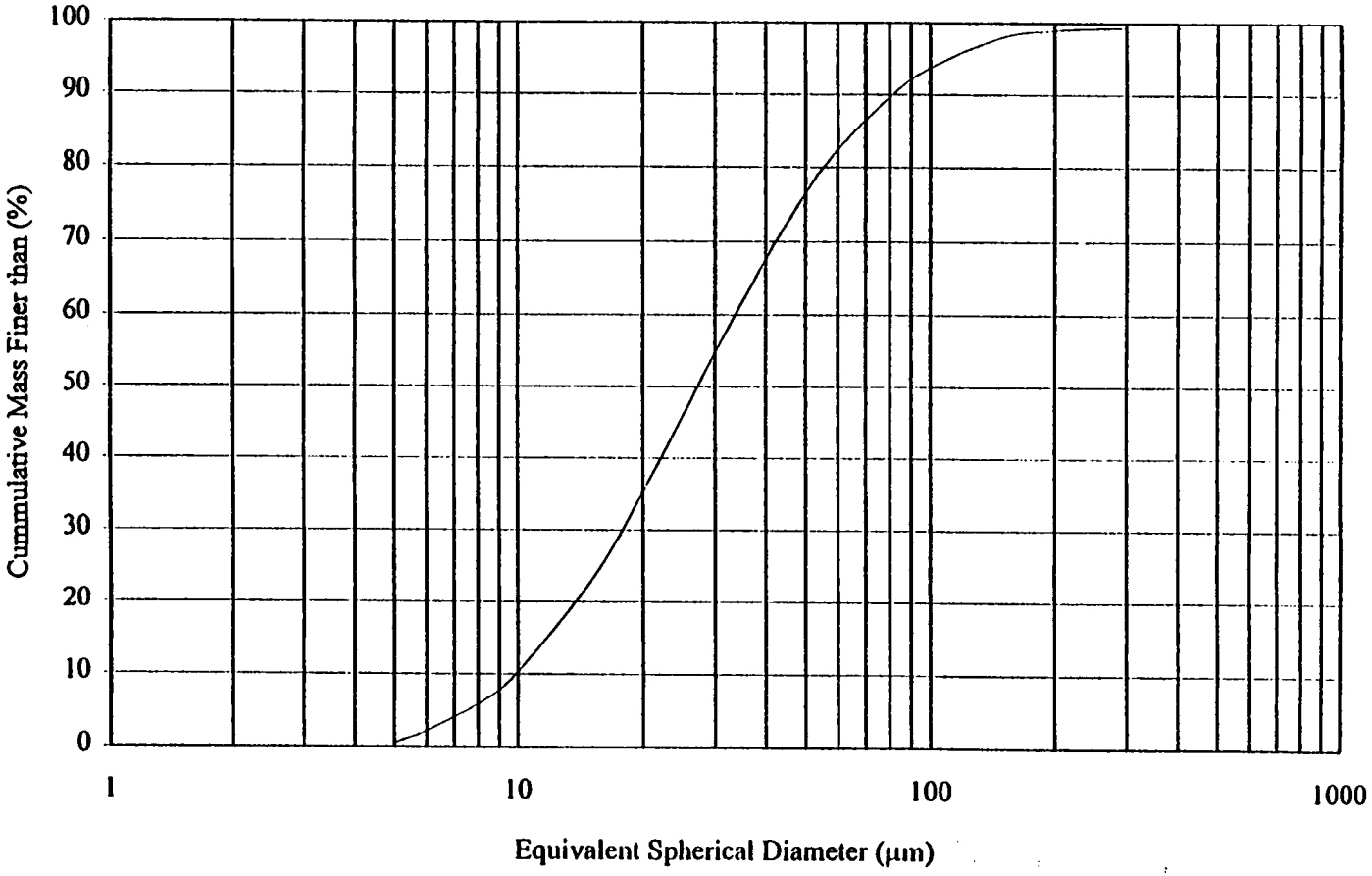

Figure A-3. Particle size distribution of flyash

APPENDIX B

TEST RESULTS

Description of Test Numbers

Each test is labeled with a series of numbers and letters which are separted by a period. Below is a sample test number and description

VV.WW.X.Y.Z

VV: describes the type of packing used in the scrubbers

2R: 2" Type-R Tellerettes were used as packing material
2K: 2" Type-K Tellerettes were used as pacing material
1R: 1" Type-R Tellerettes were used as packing material
**: this is the notation used in cases in which both packed beds contained no packing

WW: describes the gas flowrate through the system

05: gas flowrate was 500 acfm
07: gas flowrate was 700 acfm
09: gas flowrate was 900 acfm
11: gas flowrate was 1100 acfm

X: describes the type of instrument used for sampling

O: represents the optical particle counter
E: represents the electric aerosol size analyzer

Y: describes the system configuration

description of the system configuration symbols can be found on the previous page

Z: describes the test number performed under the operating conditions described

a number one represents the first test, a number two represents the second test, etc.
a letter A after the test number indicates that the test was performed by Abraham

Description of system configurations and system configuration symbols

System Configuration	Configuration Symbol
-1w---2w	A
-1w28-2w	B
-1w35-2w	C
p1w-----	D
p1w--p2-	E
p1---p2w	F
p1w--p2w	G
p1---p2-	H
p1w35---	I
p1-25p2-	J
p1-28p2-	W

System Configuration	Configuration Symbol
p1-30p2-	K
p1-35p2-	L
---20---	M
---25---	N
---30---	O
---35---	P
p1w20p2w	Q
p1w25p2w	R
p1w30p2w	S
p1w35p2w	T
wetplates*	U

System Configuration	Configuration Symbol
dryplates**	V
p1w--p2w (2:1 dilution)***	AA
p1w--p2w (4:1 dilution)***	BB
p1-35p2- (4:1 dilution)***	CC
p1w35p2w (4:1dilution)***	DD
wetplates (4:1 dilution)***	EE
p1---p2- (4:1 dilution)***	FF

Sampling was performed upstream of the pre-scrubber and downstream of the packed bed, except for the two special cases described below

The first three values describe the operation of the pre-scrubber

p1: the pre-scrubber contained packing, but scrubbing liquor was not supplied to packing
p1w: the pre-scrubber contained packing irrigated with scrubbing liquor
1w: the pre-scrubber did not contain packing, however, scrubbing liquor was supplied to the scrubber

The fourth and fifth values describe the operation of the ionizing section

20: the ionizer plates were wetted and the ionizer was operating at 20 kV
25: the ionizer plates were wetted and the ionizer was operating at 25 kV
30: the ionizer plates were wetted and the ionizer was operating at 30 kV
35: the ionizer plates were wetted and the ionizer was operating at 35 kV

The last three values describe the operation of the packed bed downstream of the ionizer

p2: the scrubber contained packing, but scrubbing liquor was not supplied to packing
p2w: the scrubber contained packing irrigated with scrubbing liquor
2w: the scrubber did not contain packing, however, scrubbing liquor was supplied to the scrubber

Special Cases

*wetplates: samples were taken immediately upstream and downstream of the wetted ionizer plates while the ionizer was operating in automatic mode with a maximum voltage of 35 kV; scrubbing liquor was supplied to the pre-scrubber

**dryplates: samples were taken immediately upstream and downstream of dry ionizer plates while the ionizer was operating in automatic mode with a maximum voltage of 32 kV; no scrubbing liquor was supplied to the pre-scrubber

*** 2:1 dilution & 4:1 dilution: during these tests, clean dried dilution air was supplied to the sampling line;
2:1 dilution indicates that there were 2 units of dilution air supplied per unit of flue gas sample
4:1 dilution indicates that there were 4 units of dilution air supplied per unit of flue gas sample

The results of the tests which are shaded are believed to be corrupt. Therefore, this data was not analyzed.

Table B-1. Test Numbers and Operating Conditions, 500acfm.

Q_g: Gas Flow Rate (acfm)
Q_{top1}: Scrubber Liquor Flow Rate to Spray Nozzles at Top of Pre-scrubber
Q_{front1}: Scrubber Liquor Flow Rate to Spray Nozzles at Front of Pre-scrubber
Q_{top2}: Scrubber Liquor Flow Rate to Spray Nozzles at Top of Packed Bed
Q_{front2}: Scrubber Liquor Flow Rate to Spray Nozzles at Front of Packed Bed

Test Number	Q_g (acfm)	Q_{top1} (gpm)	Q_{front1} (gpm)	Q_{top2} (gpm)	Q_{front2} (gpm)
**.05.O.A1	500	31.1	3.4	31.1	3.4
**.05.O.A2	500	31.1	3.4	31.1	3.4
**.05.O.A3	500	31.1	3.4	31.1	3.4
**.05.O.A4	500	31.1	3.4	31.1	3.4
**.05.O.A5	500	31.1	3.4	31.1	3.4
**.05.O.A6	500	31.1	3.4	31.1	3.4
**.05.O.B1	500	31.1	3.4	31.1	3.4
**.05.O.C1	500	31.1	3.4	31.1	3.4
**.05.O.C2	500	31.1	3.4	31.1	3.4
**.05.O.C3	500	31.1	3.4	31.1	3.4
**.05.O.C4	500	31.1	3.4	31.1	3.4
**.05.O.C5	500	31.1	3.4	31.1	3.4
**.05.O.C6	500	31.1	3.4	31.1	3.4
2R.05.O.D1	500	31.1	3.4	0	0
2R.05.O.D2	500	31.1	3.4	0	0
2R.05.O.D3	500	31.1	3.4	0	0
2R.05.O.E1A	500	31.1	3.4	0	0
2R.05.O.F1A	500	0	0	31.1	3.4
2R.05.O.G1A	500	31.1	3.4	31.1	3.4
2R.05.O.G2A	500	31.1	3.4	31.1	3.4
2R.05.O.H1A	500	0	0	0	0
2R.05.O.I1	500	31.1	3.4	0	0
2R.05.O.I2	500	31.1	3.4	0	0
2R.05.O.I3	500	31.1	3.4	0	0
2R.05.O.K1A	500	0	0	0	0
2R.05.O.M1	500	31.1	3.4	0	0
2R.05.O.P1	500	31.1	3.4	0	0
2R.05.O.P2	500	31.1	3.4	0	0
2R.05.O.P3	500	31.1	3.4	0	0
2R.05.O.P4	500	31.1	3.4	0	0
2R.05.O.P5	500	31.1	3.4	0	0
2R.05.O.R1A	500	31.1	3.4	31.1	3.4
2R.05.O.S1A	500	31.1	3.4	31.1	3.4
2R.05.O.T1	500	31.1	3.4	31.1	3.4
2R.05.O.T2	500	31.1	3.4	31.1	3.4

Table B-1. Test Numbers and Operating Conditions, 500acfm. (cont.)

Q_g: Gas Flow Rate (acfm)
Q_{top1}: Scrubber Liquor Flow Rate to Spray Nozzles at Top of Pre-scrubber
Q_{front1}: Scrubber Liquor Flow Rate to Spray Nozzles at Front of Pre-scrubber
Q_{top2}: Scrubber Liquor Flow Rate to Spray Nozzles at Top of Packed Bed
Q_{front2}: Scrubber Liquor Flow Rate to Spray Nozzles at Front of Packed Bed

Test Number	Q_g (acfm)	Q_{top1} (gpm)	Q_{front1} (gpm)	Q_{top2} (gpm)	Q_{front2} (gpm)
2R.05.O.T3	500	31.1	3.4	31.1	3.4
2R.05.O.T4	500	31.1	3.4	31.1	3.4
2R.05.O.T5	500	31.1	3.4	31.1	3.4
2R.05.O.T6A	500	31.1	3.4	31.1	3.4
2R.05.O.T7A	500	31.1	3.4	31.1	3.4
2R.05.O.U1	500	31.1	3.4	0	0
2R.05.O.U2	500	31.1	3.4	0	0
2R.05.O.U3	500	31.1	3.4	0	0
2R.05.O.V1	500	0	0	0	0
1R.05.O.G1	500	31.1	3.4	31.1	3.4
1R.05.O.G2	500	31.1	3.4	31.1	3.4
1R.05.O.G3	500	31.1	3.4	31.1	3.4
1R.05.O.T1	500	31.1	3.4	31.1	3.4
1R.05.O.T2	500	31.1	3.4	31.1	3.4
1R.05.O.T3	500	31.1	3.4	31.1	3.4
2R.05.E.BB1	500	31.1	3.4	31.1	3.4
2R.05.E.CC1	500	0	0	0	0
2R.05.E.DD1	500	31.1	3.4	31.1	3.4

Table B-2. Summary of Penetrations for Various Tests, 500 acfm.

Aerodynamic Diameter (microns)	Percent Penetration				
	**.05.O.A1	**.05.O.A2	**.05.O.A3	**.05.O.A4	**.05.O.A5
0.5	151.40	135.49	137.07	134.23	121.52
1	113.88	80.62	79.94	81.31	78.89
1.5	63.57	69.82	65.57	70.72	69.76
2	47.03	76.26	68.20	75.38	71.58
2.5	23.91	52.27	46.71	51.98	49.80
3	14.71	35.53	31.45	34.56	34.18
3.5	8.99	24.75	21.46	23.78	23.30
4	5.41	14.79	12.53	14.28	13.46
4.5	3.46	10.66	8.94	9.88	9.41
5	2.29	7.10	5.86	6.65	6.18

Aerodynamic Diameter (microns)	Percent Penetration				
	**.05.O.B1	**.05.O.C1	**.05.O.C2	**.05.O.C3	**.05.O.C4
0.5	254.42	70.58	146.79	135.43	116.27
1	214.56	38.37	37.76	34.77	32.17
1.5	105.00	5.88	10.08	9.32	8.59
2	39.98	1.10	1.95	1.93	1.60
2.5	12.31	0.15	0.30	0.28	0.22
3	2.71	0.05	0.06	0.05	0.05
3.5	0.48	0.02	0.04	0.04	0.03
4	0.11	0.01	0.03	0.02	0.02
4.5	0.05	0.00	0.02	0.02	0.02
5	0.03	0.01	0.02	0.02	0.01

Aerodynamic Diameter (microns)	Percent Penetration				
	**.05.O.C5	**.05.O.C6	2R.05.O.D1	2R.05.O.D2	2R.05.O.D3
0.5	112.92	105.36	99.94	95.51	106.46
1	29.34	26.95	68.18	69.57	72.33
1.5	7.77	7.79	78.82	81.07	77.89
2	1.59	1.58	63.39	61.45	62.52
2.5	0.23	0.22	51.74	49.08	50.99
3	0.07	0.06	44.21	40.84	42.47
3.5	0.05	0.03	39.92	45.20	38.68
4	0.03	0.03	34.89	38.99	34.32
4.5	0.03	0.02	31.82	35.35	31.37
5	0.04	0.01	28.43	31.98	29.10

Aerodynamic Diameter (microns)	Percent Penetration				
	2R.05.O.E1A	2R.05.O.F1A	2R.05.O.G1A	2R.05.O.G2A	2R.05.O.H1A
0.5	84.69	87.61	100.31	145.05	81.29
1	87.01	81.99	95.75	132.35	94.05
1.5	119.51	107.32	120.15	159.35	134.55
2	85.41	77.08	83.11	117.96	104.31
2.5	63.91	60.00	60.68	73.78	89.07
3	48.75	47.80	44.40	44.28	74.96
3.5	40.84	41.47	36.05	30.10	66.93
4	33.96	36.22	28.40	19.26	58.14
4.5	30.13	32.73	24.04	14.59	53.79
5	26.19	29.88	20.59	10.98	49.31

Table B-2. Summary of Penetrations for Various Tests, 500 acfm. (cont.)

Aerodynamic Diameter (microns)	Percent Penetration				
	2R.05.O.I1	2R.05.O.I2	2R.05.O.I3	2R.05.O.K1A	2R.05.O.M1
0.5	27.20	31.18	34.45	2.05	167.95
1	1.41	1.59	1.87	1.33	99.22
1.5	0.38	0.38	0.42	1.39	34.53
2	0.20	0.18	0.19	0.50	11.61
2.5	0.10	0.09	0.10	0.26	3.04
3	0.07	0.05	0.06	0.19	1.35
3.5	0.05	0.04	0.04	0.14	0.72
4	0.04	0.03	0.03	0.12	0.46
4.5	0.04	0.03	0.03	0.11	0.31
5	0.03	0.02	0.02	0.10	0.20

Aerodynamic Diameter (microns)	Percent Penetration				
	**.05.O.P1	**.05.O.P2	**.05.O.P3	**.05.O.P4	**.05.O.P5
0.5	60.06	51.79	56.36	52.88	52.32
1	34.01	27.36	30.36	27.42	26.60
1.5	11.67	8.36	10.39	7.90	6.89
2	5.30	2.25	5.07	2.31	1.20
2.5	1.39	0.33	1.69	0.50	0.16
3	0.18	0.08	0.29	0.10	0.05
3.5	0.05	0.04	0.08	0.03	0.03
4	0.02	0.02	0.03	0.02	0.01
4.5	0.02	0.01	0.03	0.02	0.00
5	0.01	0.00	0.02	0.01	0.01

Aerodynamic Diameter (microns)	Percent Penetration				
	2R.05.O.R1A	2R.05.O.S1A	2R.05.O.T1	2R.05.O.T2	2R.05.O.T3
0.5	40.76	41.99	25.16	27.13	25.00
1	25.14	25.56	12.91	13.71	12.61
1.5	7.78	7.50	3.61	3.63	3.40
2	2.01	1.93	0.78	0.74	0.64
2.5	0.66	0.66	0.18	0.17	0.14
3	0.22	0.19	0.06	0.05	0.05
3.5	0.10	0.09	0.04	0.04	0.03
4	0.06	0.04	0.03	0.02	0.02
4.5	0.05	0.03	0.04	0.02	0.01
5	0.03	0.02	0.03	0.01	0.02

Aerodynamic Diameter (microns)	Percent Penetration				
	2R.05.O.T4	2R.05.O.T5	2R.05.O.T6A	2R.05.O.T7A	2R.05.O.U1
0.5	25.50	30.22	40.92	38.92	15.92
1	12.99	15.99	21.24	24.66	4.94
1.5	3.47	4.01	6.37	7.37	0.37
2	0.67	0.78	1.41	1.98	0.17
2.5	0.15	0.16	0.43	0.71	0.08
3	0.06	0.05	0.22	0.21	0.06
3.5	0.04	0.04	0.17	0.08	0.04
4	0.03	0.02	0.15	0.04	0.04
4.5	0.03	0.02	0.15	0.03	0.00
5	0.02	0.02	0.15	0.03	0.12

Table B-2. Summary of Penetrations for Various Tests, 500 acfm. (cont.)

Aerodynamic Diameter (microns)	Percent Penetration				
	2R.05.O.U2	2R.05.O.U3	2R.05.O.V1	1R.05.O.G1	1R.05.O.G2
0.5	17.65	16.72	38.82	128.48	114.29
1	5.23	4.93	14.37	100.70	87.09
1.5	0.38	0.49	0.76	87.80	73.65
2	0.20	0.21	0.38	70.86	59.32
2.5	0.11	0.12	0.17	46.96	40.91
3	0.13	0.11	0.02	31.37	29.59
3.5	0.24	0.15	0.10	23.45	23.98
4	0.23	0.07	0.11	16.75	19.01
4.5	0.77	0.34	0.00	13.64	16.48
5	2.16	0.12	0.00	10.68	11.40

Aerodynamic Diameter (microns)	Percent Penetration			
	1R.05.O.G3	1R.05.O.T1	1R.05.O.T2	1R.05.O.T3
0.5	131.43	144.50	154.00	170.97
1	102.37	43.71	43.48	51.43
1.5	87.91	11.25	11.44	12.62
2	68.35	2.20	2.39	2.61
2.5	45.34	0.47	0.58	0.63
3	30.40	0.18	0.23	0.26
3.5	22.93	0.10	0.14	0.16
4	17.33	0.06	0.09	0.08
4.5	14.41	0.05	0.07	0.06
5	11.96	0.03	0.05	0.05

Aerodynamic Diameter (microns)	Percent Penetration		
	2R.05.E.BB1	2R.05.E.CC1	2R.05.E.DD1
0.021	n/a	n/a	n/a
0.038	n/a	n/a	n/a
0.067	51.56	n/a	n/a
0.118	112.77	22.18	15.84
0.210	93.15	9.41	4.55
0.375	83.20	5.29	3.11
0.669	81.48	7.61	3.87
1.182	67.16	10.32	3.21

Table B-3. Test Numbers and Operating Conditions, 700acfm.

Qg: Gas Flow Rate (acfm)
Qtop1: Scrubber Liquor Flow Rate to Spray Nozzles at Top of Pre-scrubber
Qfront1: Scrubber Liquor Flow Rate to Spray Nozzles at Front of Pre-scrubber
Qtop2: Scrubber Liquor Flow Rate to Spray Nozzles at Top of Packed Bed
Qfront2: Scrubber Liquor Flow Rate to Spray Nozzles at Front of Packed Bed

Test Number	Qg (acfm)	Qtop1 (gpm)	Qfront1 (gpm)	Qtop2 (gpm)	Qfront2 (gpm)
2R.07.O.A1	700	31.1	3.4	31.1	3.4
2R.07.O.C1	700	31.1	3.4	31.1	3.4
2R.07.O.G1A	700	31.1	3.4	31.1	3.4
2R.07.O.H1A	700	0	0	0	0
2R.07.O.U1	700	31.1	3.4	0	0
2R.07.O.U2	700	31.1	3.4	0	0
2R.07.O.U3	700	31.1	3.4	0	0
2R.07.O.V1	700	0	0	0	0
2R.07.E.BB1	700	31.1	3.4	31.1	3.4
2R.07.O.CC1	700	0	0	0	0
2R.07.O.DD1	700	31.1	3.4	31.1	3.4

Table B-4. Summary of Penetrations for Various Tests, 700 acfm.

Aerodynamic Diameter (microns)	Percent Penetration				
	2R.07.O.A1	2R.07.O.C1	2R.07.O.G1A	2R.07.O.H1A	2R.07.O.U1
0.5	130.90	79.42	154.29	90.58	15.21
1	113.75	43.10	127.60	91.33	5.13
1.5	84.51	7.13	142.84	121.29	1.70
2	57.30	1.68	97.58	106.61	1.01
2.5	32.77	0.33	62.76	93.89	0.72
3	20.57	0.14	39.97	81.37	0.69
3.5	13.04	0.05	28.95	73.16	0.86
4	8.11	0.03	19.24	63.98	0.84
4.5	5.33	0.01	15.10	57.74	1.22
5	3.51	0.00	11.23	50.86	0.79

Aerodynamic Diameter (microns)	Percent Penetration		
	2R.07.O.U2	2R.07.O.U3	2R.07.O.V1
0.5	13.85	13.02	39.33
1	4.52	4.31	14.90
1.5	1.36	1.37	2.83
2	0.84	0.80	1.71
2.5	0.64	0.57	0.87
3	0.59	0.70	0.73
3.5	0.74	0.65	0.60
4	0.95	0.81	0.68
4.5	1.83	1.05	0.00
5	2.12	1.22	0.00

Aerodynamic Diameter (microns)	Percent Penetration		
	2R.07.E.BB1	2R.07.E.CC1	2R.07.E.DD1
0.021	n/a	n/a	n/a
0.038	n/a	n/a	n/a
0.067	134.44	n/a	n/a
0.118	85.57	8.25	15.06
0.210	85.64	8.00	4.99
0.375	80.51	9.30	4.12
0.669	74.27	10.28	7.83
1.182	66.23	8.37	10.07

Table B-5. Test Numbers and Operating Conditions, 900acfm.

Qg: Gas Flow Rate (acfm)
Qtop1: Scrubber Liquor Flow Rate to Spray Nozzles at Top of Pre-scrubber
Qfront1: Scrubber Liquor Flow Rate to Spray Nozzles at Front of Pre-scrubber
Qtop2: Scrubber Liquor Flow Rate to Spray Nozzles at Top of Packed Bed
Qfront2: Scrubber Liquor Flow Rate to Spray Nozzles at Front of Packed Bed

Test Number	Qg (acfm)	Qtop1 (gpm)	Qfront1 (gpm)	Qtop2 (gpm)	Qfront2 (gpm)
**.09.O.A1	900	31.1	3.4	31.1	3.4
**.09.O.A2	900	31.1	3.4	31.1	3.4
**.09.O.A3	900	31.1	3.4	31.1	3.4
**.09.O.A4	900	31.1	3.4	31.1	3.4
**.09.O.A5	900	31.1	3.4	31.1	3.4
**.09.O.A6	900	31.1	3.4	31.1	3.4
**.09.O.B1	900	31.1	3.4	31.1	3.4
**.09.O.C1	900	31.1	3.4	31.1	3.4
**.09.O.C2	900	31.1	3.4	31.1	3.4
**.09.O.C3	900	31.1	3.4	31.1	3.4
**.09.O.C4	900	31.1	3.4	31.1	3.4
**.09.O.C5	900	31.1	3.4	31.1	3.4
**.09.O.C6	900	31.1	3.4	31.1	3.4
2R.09.O.D1	900	31.1	3.4	0	0
2R.09.O.D2	900	31.1	3.4	0	0
2R.09.O.D3	900	31.1	3.4	0	0
2R.09.O.E1A	900	31.1	3.4	0	0
2R.09.O.F1A	900	0	0	31.1	3.4
2R.09.O.G1A	900	31.1	3.4	31.1	3.4
2R.09.O.G2A	900	31.1	3.4	31.1	3.4
2R.09.O.G3A	900	31.1	3.4	31.1	3.4
2R.09.O.G4A	900	31.1	3.4	31.1	3.4
2R.09.O.G5A	900	31.1	3.4	31.1	3.4
2R.09.O.G6A	900	31.1	3.4	31.1	3.4
2R.09.O.G7A	900	31.1	3.4	31.1	3.4
2R.09.O.G8A	900	0	0	0	0
2R.09.O.G9A	900	14.6	3.4	14.6	3.4
2R.09.O.G10A	900	20.5	3.4	20.5	3.4
2R.09.O.G11A	900	28.8	3.4	28.8	3.4
2R.09.O.G12A	900	35.2	3.4	35.2	3.4
2R.09.O.G13A	900	40.61	3.4	40.61	3.4
2R.09.O.H1A	900	0	0	0	0
2R.09.O.H2A	900	0	0	0	0
2R.09.O.I1	900	31.1	3.4	0	0
2R.09.O.I2	900	31.1	3.4	0	0

Table B-5. Test Numbers and Operating Conditions, 900acfm. (cont.)

Qg: Gas Flow Rate (acfm)
Qtop1: Scrubber Liquor Flow Rate to Spray Nozzles at Top of Pre-scrubber
Qfront1: Scrubber Liquor Flow Rate to Spray Nozzles at Front of Pre-scrubber
Qtop2: Scrubber Liquor Flow Rate to Spray Nozzles at Top of Packed Bed
Qfront2: Scrubber Liquor Flow Rate to Spray Nozzles at Front of Packed Bed

Test Number	Qg (acfm)	Qtop1 (gpm)	Qfront1 (gpm)	Qtop2 (gpm)	Qfront2 (gpm)
2R.09.O.I3	900	31.1	3.4	0	0
2R.09.O.J1A	900	0	0	0	0
2R.09.O.N1	900	31.1	3.4	0	0
2R.09.O.O1	900	31.1	3.4	0	0
2R.09.O.P1	900	31.1	3.4	0	0
2R.09.O.P2	900	31.1	3.4	0	0
2R.09.O.P3	900	31.1	3.4	0	0
2R.09.O.P4	900	31.1	3.4	0	0
2R.09.O.P5	900	31.1	3.4	0	0
2R.09.O.Q1A	900	31.1	3.4	31.1	3.4
2R.09.O.Q2A	900	31.1	3.4	31.1	3.4
2R.09.O.R1A	900	31.1	3.4	31.1	3.4
2R.09.O.R2A	900	31.1	3.4	31.1	3.4
2R.09.O.S1A	900	31.1	3.4	31.1	3.4
2R.09.O.T1	900	31.1	3.4	31.1	3.4
2R.09.O.T2	900	31.1	3.4	31.1	3.4
2R.09.O.T3	900	31.1	3.4	31.1	3.4
2R.09.O.T4	900	31.1	3.4	31.1	3.4
2R.09.O.T5	900	31.1	3.4	31.1	3.4
2R.09.O.T6A	900	31.1	3.4	31.1	3.4
2R.09.O.T7A	900	31.1	3.4	31.1	3.4
2R.09.O.T8A	900	31.1	3.4	31.1	3.4
2R.09.O.T9	900	31.1	3.4	0	0
2R.09.O.T10	900	31.1	3.4	14.4	3.4
2R.09.O.T11	900	31.1	3.4	20.8	3.4
2R.09.O.T12	900	31.1	3.4	40.6	3.4
2R.09.O.U1	900	31.1	3.4	0	0
2R.09.O.U2	900	31.1	3.4	0	0
2R.09.O.U3	900	31.1	3.4	0	0
2R.09.O.V1	900	0	0	0	0
2K.09.O.G1	900	31.1	3.4	31.1	3.4
2K.09.O.G2	900	31.1	3.4	31.1	3.4
2K.09.O.G3	900	31.1	3.4	31.1	3.4
2K.09.O.T1	900	31.1	3.4	31.1	3.4
2K.09.O.T2	900	31.1	3.4	31.1	3.4

Table B-5. Test Numbers and Operating Conditions, 900acfm. (cont.)

Qg: Gas Flow Rate (acfm)
Qtop1: Scrubber Liquor Flow Rate to Spray Nozzles at Top of Pre-scrubber
Qfront1: Scrubber Liquor Flow Rate to Spray Nozzles at Front of Pre-scrubber
Qtop2: Scrubber Liquor Flow Rate to Spray Nozzles at Top of Packed Bed
Qfront2: Scrubber Liquor Flow Rate to Spray Nozzles at Front of Packed Bed

Test Number	Qg (acfm)	Qtop1 (gpm)	Qfront1 (gpm)	Qtop2 (gpm)	Qfront2 (gpm)
2K.09.O.T3	900	31.1	3.4	31.1	3.4
1R.09.O.G1	900	31.1	3.4	31.1	3.4
1R.09.O.G2	900	31.1	3.4	31.1	3.4
1R.09.O.G3	900	31.1	3.4	31.1	3.4
1R.09.O.T1	900	31.1	3.4	31.1	3.4
1R.09.O.T2	900	31.1	3.4	31.1	3.4
1R.09.O.T3	900	31.1	3.4	31.1	3.4
2R.09.E.G1	900	31.1	3.4	31.1	3.4
2R.09.E.BB1	900	31.1	3.4	31.1	3.4
2R.09.E.BB2	900	31.1	3.4	31.1	3.4
2R.09.E.CC1	900	0	0	0	0
2R.09.E.CC2	900	0	0	0	0
2R.09.E.DD1	900	31.1	3.4	31.1	3.4
2R.09.E.EE1	900	31.1	3.4	0	0
2K.09.E.CC1	900	0	0	0	0
2K.09.E.DD1	900	31.1	3.4	31.1	3.4
2K.09.E.FF1	900	0	0	0	0

Table B-6. Summary of Penetrations for Various Tests, 900 acfm.

Aerodynamic Diamter (microns)	Percent Penetration				
	**.09.O.A1	**.09.O.A2	**.09.O.A3	**.09.O.A4	**.09.O.A5
0.5	134.59	124.03	121.28	121.88	120.17
1	115.81	104.02	106.46	105.41	101.65
1.5	91.22	101.49	103.02	102.12	97..51
2	69.08	95.82	102.25	102.48	94.50
2.5	40.92	85.32	75.24	74.84	66.45
3	26.08	58.35	53.22	53.13	46.55
3.5	16.23	41.89	28.97	38.68	33.80
4	10.24	27.20	25.40	25.30	22.44
4.5	6.68	20.74	19.38	23.78	16.79
5	4.79	15.29	14.25	17.23	12.30

Aerodynamic Diameter (microns)	Percent Penetration				
	**.09.O.A6	**.09.O.B1	**.09.O.C1	**.09.O.C2	**.09.O.C3
0.5	123.27	156.42	89.95	89.55	89.31
1	108.83	115.86	50.62	17.12	16.42
1.5	105.62	39.89	9.70	5.18	4.77
2	100.91	12.78	2.97	1.53	1.32
2.5	73.31	3.06	0.82	0.54	0.39
3	61.75	0.83	0.37	0.30	0.21
3.5	38.16	0.29	0.20	0.22	0.16
4	25.08	0.13	0.09	0.13	0.10
4.5	19.39	0.07	0.08	0.10	0.08
5	14.13	0.05	0.05	0.07	0.07

Aerodynamic Diameter (microns)	Percent Penetration				
	**.09.O.C4	**.09.O.C5	**.09.O.C6	2R.09.O.D1	2R.09.O.D2
0.5	89.70	94.42	91.30	91.66	102.94
1	19.08	17.77	16.40	66.94	72.31
1.5	5.09	4.99	4.55	67.73	63.92
2	1.43	1.35	1.23	49.62	49.64
2.5	0.50	0.45	0.40	37.27	38.03
3	0.25	0.23	0.20	29.65	30.77
3.5	0.17	0.18	0.13	25.44	26.00
4	0.11	0.12	0.09	21.28	20.64
4.5	0.10	0.10	0.07	18.55	17.88
5	0.07	0.07	0.04	15.63	15.43

Aerodynamic Diameter (microns)	Percent Penetration				
	2R.09.O.D3	2R.09.O.E1A	2R.09.O.F1A	2R.09.O.G1A	2R.09.O.G2A
0.5	117.78	79.27	67.68	97.31	213.75
1	74.12	84.52	74.40	110.60	161.00
1.5	59.59	88.31	84.25	118.06	150.76
2	46.20	76.82	74.44	80.61	107.51
2.5	35.89	51.15	51.20	43.81	75.81
3	29.61	30.15	32.22	19.28	50.38
3.5	25.27	22.66	25.52	12.74	35.65
4	20.99	16.16	19.36	7.96	22.05
4.5	18.08	11.36	15.06	5.18	15.82
5	15.70	9.30	12.68	4.01	10.59

Table B-6. Summary of Penetrations for Various Tests, 900 acfm. (cont.)

Aerodynamic Diameter (microns)	Percent Penetration				
	2R.09.O.G3A	2R.09.O.G4A	2R.09.O.G5A	2R.09.O.G6A	2R.09.O.G7A
0.5	252.30	225.18	201.22	182.68	171.60
1	248.95	222.81	198.85	178.98	171.05
1.5	208.54	189.84	168.30	154.59	157.03
2	111.84	101.90	87.35	85.03	93.12
2.5	75.50	69.17	57.90	58.03	68.65
3	49.73	47.31	38.87	39.54	50.89
3.5	35.62	34.23	27.28	28.14	38.83
4	22.02	21.89	17.39	17.55	27.08
4.5	16.41	16.77	12.95	12.67	19.57
5	10.70	11.06	8.57	8.81	14.31

Aerodynamic Diameter (microns)	Percent Penetration				
	2R.09.O.G8A	2R.09.O.G9A	2R.09.O.G10A	2R.09.O.G11A	2R.09.O.G12A
0.5	133.68	150.09	167.02	130.77	158.35
1	133.94	157.95	183.06	139.51	173.09
1.5	133.97	155.87	177.17	137.78	169.31
2	130.74	100.37	102.06	82.72	94.11
2.5	129.87	75.48	71.71	58.88	63.90
3	124.76	57.57	50.30	41.97	42.36
3.5	118.13	45.54	37.98	31.61	30.06
4	106.35	31.44	25.58	20.78	18.26
4.5	97.53	24.35	19.42	15.61	12.83
5	86.61	17.46	13.72	10.70	8.61

Aerodynamic Diameter (microns)	Percent Penetration				
	2R.09.O.G13A	2R.09.O.H1A	2R.09.O.H2A	2R.09.O.I1	2R.09.O.I2
0.5	139.37	76.90	85.92	17.12	11.87
1	149.11	88.84	85.98	9.22	6.79
1.5	146.22	105.83	110.93	6.69	4.81
2	116.23	92.43	95.04	3.85	2.82
2.5	61.38	67.15	78.29	1.75	1.31
3	29.87	45.72	63.68	0.89	0.89
3.5	18.82	38.60	53.56	0.57	0.60
4	9.30	33.48	42.58	0.38	0.39
4.5	6.27	28.81	35.81	0.31	0.29
5	4.60	26.01	29.31	0.22	0.21

Aerodynamic Diameter (microns)	Percent Penetration				
	2R.09.O.I3	2R.09.O.J1A	**.09.O.N1	**.09.O.O1	**.09.O.P1
0.5	21.72	11.61	78.26	81.81	13.82
1	8.54	12.78	46.91	41.34	8.33
1.5	6.20	13.27	21.19	14.02	3.73
2	3.48	7.25	8.25	4.69	0.99
2.5	1.56	3.17	2.61	1.41	0.56
3	0.82	1.41	1.46	0.75	0.37
3.5	0.53	1.04	0.92	0.50	0.27
4	0.35	0.76	0.65	0.38	0.21
4.5	0.26	0.58	0.49	0.29	0.17
5	0.19	0.47	0.35	0.24	0.18

Table B-6. Summary of Penetrations for Various Tests, 900 acfm. (cont.)

Aerodynamic Diameter (microns)	Percent Penetration				
	**.09.O.P2	**.09.O.P3	**.09.O.P4	**.09.O.P5	2R.09.O.Q1A
0.5	13.94	13.53	14.48	11.96	36.73
1	8.31	8.03	8.93	7.01	38.51
1.5	3.63	3.35	4.16	2.93	33.47
2	1.12	0.91	1.32	0.88	17.56
2.5	0.70	0.55	0.77	0.48	7.02
3	0.50	0.34	0.47	0.31	2.15
3.5	0.40	0.27	0.33	0.21	1.19
4	0.37	0.23	0.22	0.18	0.58
4.5	0.34	0.17	0.17	0.13	0.29
5	0.33	0.19	0.17	0.09	0.19

Aerodynamic Diameter (microns)	Percent Penetration				
	2R.09.O.Q2A	2R.09.O.R1A	2R.09.O.R2A	2R.09.O.S1A	2R.09.O.T1
0.5	46.81	17.43	32.84	25.90	10.48
1	35.46	15.66	21.54	16.75	5.49
1.5	25.00	10.03	10.92	7.37	2.99
2	16.84	4.30	5.52	3.18	1.80
2.5	8.27	1.96	2.37	1.45	0.95
3	4.21	0.98	1.05	0.59	0.41
3.5	2.46	0.66	0.59	0.31	0.25
4	1.26	0.31	0.30	0.15	0.18
4.5	0.81	0.16	0.19	0.11	0.13
5	0.45	0.11	0.15	0.08	0.14

Aerodynamic Diameter (microns)	Percent Penetration				
	2R.09.O.T2	2R.09.O.T3	2R.09.O.T4	2R.09.O.T5	2R.09.O.T6A
0.5	9.14	8.00	7.03	6.69	23.01
1	4.75	4.33	3.58	3.47	12.05
1.5	2.72	2.60	2.16	2.02	5.60
2	1.58	1.38	1.10	0.97	2.32
2.5	0.85	0.66	0.50	0.46	0.85
3	0.38	0.31	0.20	0.18	0.30
3.5	0.23	0.20	0.12	0.12	0.20
4	0.16	0.12	0.08	0.10	0.13
4.5	0.12	0.09	0.06	0.07	0.08
5	0.12	0.08	0.06	0.06	0.05

Aerodynamic Diameter (microns)	Percent Penetration				
	2R.09.O.T7A	2R.09.O.T8A	2R.09.O.T9	2R.09.O.T10	2R.09.O.T11
0.5	20.87	25.06	16.56	28.03	49.04
1	15.30	15.44	7.79	16.15	31.54
1.5	8.14	5.85	1.86	3.66	6.67
2	3.56	2.79	1.16	1.44	1.79
2.5	1.86	1.53	0.49	0.62	0.38
3	1.03	0.71	0.31	0.27	0.14
3.5	0.71	0.40	0.19	0.13	0.06
4	0.34	0.20	0.13	0.07	0.04
4.5	0.16	0.14	0.11	0.04	0.02
5	0.11	0.09	0.08	0.04	0.03

Table B-6. Summary of Penetrations for Various Tests, 900 acfm. (cont.)

Aerodynamic Diameter (microns)	Percent Penetration				
	2R.09.O.T12	2R.09.O.U1	2R.09.O.U2	2R.09.O.U3	2R.09.O.V1
0.5	64.43	31.14	28.68	32.76	40.76
1	40.74	12.29	11.01	13.28	17.52
1.5	7.95	3.25	3.20	3.97	6.87
2	2.05	1.59	1.80	1.97	4.83
2.5	0.31	0.74	0.91	0.95	2.83
3	0.15	0.50	0.70	0.62	2.25
3.5	0.09	0.36	0.44	0.45	1.87
4	0.07	0.28	0.27	0.22	1.36
4.5	0.06	0.28	0.15	0.18	0.99
5	0.05	0.10	0.44	0.21	0.26

Aerodynamic Diameter (microns)	Percent Penetration				
	2K.09.O.G1	2K.09.O.G2	2K.09.O.G3	2K.09.O.T1	2K.09.O.T2
0.5	125.57	117.97	118.08	59.17	59.23
1	108.30	102.31	102.21	27.92	27.89
1.5	83.05	78.60	78.43	4.40	4.37
2	58.04	54.41	53.68	1.29	1.22
2.5	37.86	34.55	33.86	0.47	0.39
3	27.77	25.27	24.63	0.27	0.21
3.5	21.76	19.32	18.91	0.20	0.15
4	16.84	14.75	14.38	0.16	0.12
4.5	13.62	11.49	11.29	0.15	0.10
5	10.83	8.99	8.62	0.13	0.09

Aerodynamic Diameter (microns)	Percent Penetration				
	2K.09.O.T3	1R.09.O.G1	1R.09.O.G2	1R.09.O.G3	1R.09.O.T1
0.5	61.19	95.04	101.46	94.66	58.85
1	29.55	76.18	85.60	74.44	21.49
1.5	5.04	62.81	70.12	60.20	8.76
2	1.41	55.85	61.95	55.13	3.10
2.5	0.46	38.28	45.57	38.59	1.07
3	0.25	26.77	33.17	26.84	0.43
3.5	0.17	16.25	25.65	20.05	0.25
4	0.13	11.57	18.48	14.39	0.13
4.5	0.10	9.09	18.54	11.33	0.09
5	0.08	6.89	14.05	8.62	0.06

Aerodynamic Diameter (microns)	Percent Penetration	
	1R.09.O.T2	1R.09.O.T3
0.5	55.57	64.42
1	19.37	21.87
1.5	7.28	8.12
2	2.22	2.46
2.5	0.74	0.80
3	0.32	0.34
3.5	0.19	0.20
4	0.10	0.09
4.5	0.07	0.08
5	0.05	0.06

Table B-6. Summary of Penetrations for Various Tests, 900 acfm. (cont.)

Aerodynamic Diameter (microns)	Percent Penetration				
	2R.09.E.G1	2R.09.E.BB1	2R.09.E.BB2	2R.09.E.CC1	2R.09.E.CC2
0.021	n/a	n/a	n/a	n/a	n/a
0.038	n/a	n/a	n/a	n/a	n/a
0.067	98.73	n/a	n/a	n/a	n/a
0.118	116.74	83.77	89.97	15.15	5.00
0.210	110.73	71.89	73.26	12.48	10.21
0.375	106.30	64.09	63.59	16.58	10.30
0.669	99.85	67.80	55.84	18.70	15.05
1.182	104.49	60.73	59.01	9.96	4.88

Aerodynamic Diameter (microns)	Percent Penetration				
	2R.09.E.DD1	2R.09.E.EE1	2K.09.E.CC1	2K.09.E.DD1	2K.09.E.FF1
0.021	n/a	n/a	n/a	n/a	n/a
0.038	n/a	n/a	n/a	n/a	n/a
0.067	n/a	n/a	n/a	n/a	n/a
0.118	17.35	54.03	5.01	19.52	101.43
0.210	5.80	8.96	2.20	6.97	74.56
0.375	12.47	27.54	8.28	13.07	93.98
0.669	10.22	18.79	7.83	14.91	102.01
1.182	13.88	33.71	6.47	19.11	107.08

Table B-7. Test Numbers and Operating Conditions, 1100acfm.

Qg: Gas Flow Rate (acfm)
Qtop1: Scrubber Liquor Flow Rate to Spray Nozzles at Top of Pre-scrubber
Qfront1: Scrubber Liquor Flow Rate to Spray Nozzles at Front of Pre-scrubber
Qtop2: Scrubber Liquor Flow Rate to Spray Nozzles at Top of Packed Bed
Qfront2: Scrubber Liquor Flow Rate to Spray Nozzles at Front of Packed Bed

Test Number	Qg (acfm)	Qtop1 (gpm)	Qfront1 (gpm)	Qtop2 (gpm)	Qfront2 (gpm)
**.11.O.A1	1100	31.1	3.4	31.1	3.4
**.11.O.A2	1100	31.1	3.4	31.1	3.4
**.11.O.A3	1100	31.1	3.4	31.1	3.4
**.11.O.A4	1100	31.1	3.4	31.1	3.4
**.11.O.A5	1100	31.1	3.4	31.1	3.4
**.11.O.A6	1100	31.1	3.4	31.1	3.4
**.11.O.C1	1100	31.1	3.4	31.1	3.4
**.11.O.C2	1100	31.1	3.4	31.1	3.4
**.11.O.C3	1100	31.1	3.4	31.1	3.4
**.11.O.C4	1100	31.1	3.4	31.1	3.4
**.11.O.C5	1100	31.1	3.4	31.1	3.4
**.11.O.C6	1100	31.1	3.4	31.1	3.4
2R.11.O.D1	1100	31.1	3.4	0	0
2R.11.O.D2	1100	31.1	3.4	0	0
2R.11.O.D3	1100	31.1	3.4	0	0
2R.11.O.E1A	1100	31.1	3.4	0	0
2R.11.O.F1A	1100	0	0	31.1	3.4
2R.11.O.G1A	1100	31.1	3.4	31.1	3.4
2R.11.O.H1A	1100	0	0	0	0
2R.11.O.I1	1100	31.1	3.4	0	0
2R.11.O.I2	1100	31.1	3.4	0	0
2R.11.O.I3	1100	31.1	3.4	0	0
2R.11.O.P1	1100	31.1	3.4	0	0
2R.11.O.P2	1100	31.1	3.4	0	0
2R.11.O.P3	1100	31.1	3.4	0	0
2R.11.O.P4	1100	31.1	3.4	0	0
2R.11.O.P5	1100	31.1	3.4	0	0
2R.11.O.R1A	1100	31.1	3.4	31.1	3.4
2R.11.O.S1A	1100	31.1	3.4	31.1	3.4
2R.11.O.T1	1100	31.1	3.4	31.1	3.4
2R.11.O.T2	1100	31.1	3.4	31.1	3.4
2R.11.O.T3	1100	31.1	3.4	31.1	3.4
2R.11.O.T4	1100	31.1	3.4	31.1	3.4
2R.11.O.T5	1100	31.1	3.4	31.1	3.4
2R.11.O.T6A	1100	31.1	3.4	31.1	3.4

Table B-7. Test Numbers and Operating Conditions, 1100acfm. (cont.)

Qg: Gas Flow Rate (acfm)
Qtop1: Scrubber Liquor Flow Rate to Spray Nozzles at Top of Pre-scrubber
Qfront1: Scrubber Liquor Flow Rate to Spray Nozzles at Front of Pre-scrubber
Qtop2: Scrubber Liquor Flow Rate to Spray Nozzles at Top of Packed Bed
Qfront2: Scrubber Liquor Flow Rate to Spray Nozzles at Front of Packed Bed

Test Number	Qg (acfm)	Qtop1 (gpm)	Qfront1 (gpm)	Qtop2 (gpm)	Qfront2 (gpm)
2R.11.O.T7A	1100	31.1	3.4	31.1	3.4
2R.11.O.U1	1100	31.1	3.4	0	0
2R.11.O.U2	1100	31.1	3.4	0	0
2R.11.O.U3	1100	31.1	3.4	0	0
2R.11.O.V1	1100	0	0	0	0
2R.11.O.W1A	1100	0	0	0	0
1R.11.O.G1	1100	31.1	3.4	31.1	3.4
1R.11.O.G2	1100	31.1	3.4	31.1	3.4
1R.11.O.G3	1100	31.1	3.4	31.1	3.4
1R.11.O.T1	1100	31.1	3.4	31.1	3.4
1R.11.O.T2	1100	31.1	3.4	31.1	3.4
1R.11.O.T3	1100	31.1	3.4	31.1	3.4
2R.11.E.BB1	1100	31.1	3.4	31.1	3.4
2R.11.E.CC1	1100	0	0	0	0
2R.11.E.DD1	1100	31.1	3.4	31.1	3.4

Table B-8. Summary of Penetrations for Various Tests, 1100 acfm.

Aerodynamic Diamter (microns)	Percent Penetration				
	**.11.O.A1	**.11.O.A2	**.11.O.A3	**.11.O.A4	**.11.O.A5
0.5	129.19	121.81	120.28	121.90	111.48
1	111.15	109.59	105.64	106.57	93.54
1.5	87.06	105.17	100.27	101.56	88.44
2	63.21	98.37	92.19	94.11	80.76
2.5	36.06	72.03	65.94	68.13	57.91
3	22.27	61.29	45.31	47.31	40.46
3.5	13.99	38.30	33.19	34.03	29.95
4	8.71	25.73	21.90	22.33	19.95
4.5	5.95	19.65	17.12	17.14	15.40
5	4.48	14.44	12.96	12.61	11.24

Aerodynamic Diameter (microns)	Percent Penetration				
	**.11.O.A6	**.11.O.C1	**.11.O.C2	**.11.O.C3	**.11.O.C4
0.5	115.97	95.84	89.14	91.08	87.73
1	101.58	55.34	18.45	19.24	18.60
1.5	96.90	12.56	6.59	6.51	6.52
2	88.43	4.27	2.26	2.00	2.10
2.5	64.86	1.29	0.98	0.81	0.81
3	46.47	0.64	0.60	0.45	0.45
3.5	34.43	0.36	0.42	0.32	0.43
4	22.96	0.18	0.32	0.19	0.26
4.5	19.80	0.13	0.25	0.17	0.23
5	12.89	0.10	0.21	0.15	0.16

Aerodynamic Diameter (microns)	Percent Penetration				
	**.11.O.C5	**.11.O.C6	2R.11.O.D1	2R.11.O.D2	2R.11.O.D3
0.5	91.06	92.20	109.33	118.88	131.13
1	18.71	18.81	73.04	87.20	122.84
1.5	6.28	6.16	61.62	76.24	124.42
2	1.94	1.93	49.53	56.95	105.00
2.5	0.80	0.80	40.38	45.53	87.52
3	0.44	0.47	34.50	37.10	71.83
3.5	0.32	0.32	29.62	31.55	61.80
4	0.23	0.22	24.03	24.96	48.49
4.5	0.18	0.18	21.24	21.34	41.43
5	0.16	0.12	18.14	18.24	34.31

Aerodynamic Diameter (microns)	Percent Penetration				
	2R.11.O.E1A	2R.11.O.F1A	2R.11.O.G1A	2R.11.O.H1A	2R.11.O.I1
0.5	97.81	84.81	88.84	108.56	28.24
1	96.99	82.59	81.10	112.29	10.59
1.5	117.04	100.63	92.57	138.48	7.56
2	85.40	79.59	73.65	101.62	3.96
2.5	60.57	60.14	51.66	75.34	1.72
3	40.59	44.91	35.85	54.22	0.89
3.5	29.96	36.34	26.80	43.43	0.57
4	21.55	28.49	18.63	34.21	0.42
4.5	17.21	24.31	14.16	28.92	0.30
5	12.94	20.38	10.15	22.63	0.23

Table B-8. Summary of Penetrations for Various Tests, 1100 acfm. (cont.)

Aerodynamic Diameter (microns)	Percent Penetration				
	2R.11.O.I2	2R.11.O.I3	2R.11.O.P1	2R.11.O.P2	2R.11.O.P3
0.5	31.31	33.07	14.90	13.85	14.97
1	11.58	10.80	9.97	9.25	10.17
1.5	8.32	8.05	4.87	4.51	4.84
2	4.25	5.03	1.78	1.33	1.61
2.5	1.93	2.46	1.24	0.79	0.93
3	1.05	1.38	0.92	0.55	0.64
3.5	0.72	0.96	0.77	0.41	0.47
4	0.48	0.71	0.63	0.31	0.38
4.5	0.38	0.50	0.58	0.27	0.28
5	0.30	0.35	0.55	0.28	0.27

Aerodynamic Diameter (microns)	Percent Penetration				
	2R.11.O.P4	2R.11.O.P5	2R.11.O.R1A	2R.11.O.S1A	2R.11.O.T1
0.5	15.83	12.99	32.41	21.85	10.49
1	10.80	8.44	19.53	13.66	6.84
1.5	5.12	4.17	11.90	6.54	3.32
2	1.69	1.67	5.46	1.97	1.54
2.5	0.95	1.22	2.60	0.80	0.98
3	0.60	0.97	1.27	0.43	0.76
3.5	0.49	0.85	0.79	0.30	0.60
4	0.29	0.82	0.40	0.21	0.57
4.5	0.24	0.77	0.22	0.18	0.50
5	0.27	0.81	0.19	0.15	0.49

Aerodynamic Diameter (microns)	Percent Penetration				
	2R.11.O.T2	2R.11.O.T3	2R.11.O.T4	2R.11.O.T5	2R.11.O.T6A
0.5	12.59	9.69	10.80	8.83	21.57
1	8.82	6.41	7.19	5.75	12.62
1.5	4.07	3.08	3.23	2.69	4.84
2	1.70	1.27	1.24	1.02	1.61
2.5	1.01	0.75	0.74	0.56	0.78
3	0.63	0.51	0.54	0.43	0.45
3.5	0.53	0.43	0.43	0.31	0.32
4	0.42	0.37	0.39	0.27	0.21
4.5	0.44	0.34	0.39	0.29	0.18
5	0.32	0.32	0.35	0.23	0.15

Aerodynamic Diameter (microns)	Percent Penetration				
	2R.11.O.T7A	2R.11.O.U1	2R.11.O.U2	2R.11.O.U3	2R.11.O.V1
0.5	31.05	21.00	29.25	21.35	40.49
1	10.80	13.85	20.89	12.62	22.29
1.5	4.34	10.17	15.68	8.21	14.73
2	1.40	6.75	10.47	5.12	8.91
2.5	0.66	3.90	6.52	3.64	4.97
3	0.46	2.76	4.64	3.01	3.67
3.5	0.36	1.98	3.61	2.68	2.60
4	0.32	1.50	2.49	1.80	2.36
4.5	0.31	0.97	2.25	1.83	1.12
5	0.30	0.97	2.53	2.39	0.57

Table B-8. Summary of Penetrations for Various Tests, 1100 acfm. (cont.)

Aerodynamic Diameter (microns)	Percent Penetration				
	2R.11.O.W1A	1R.11.O.G1	1R.11.O.G2	1R.11.O.G3	1R.11.O.T1
0.5	19.86	94.62	90.30	101.24	60.84
1	16.46	77.10	71.66	81.41	20.40
1.5	17.51	67.78	60.59	72.41	8.78
2	8.54	58.74	50.90	62.53	3.22
2.5	4.62	39.66	34.88	42.68	1.19
3	2.85	26.47	24.16	29.01	0.51
3.5	2.18	18.84	17.99	21.06	0.30
4	1.65	12.22	12.19	13.56	0.14
4.5	1.40	8.85	9.28	7.94	0.09
5	1.22	5.85	6.49	5.23	0.05

Aerodynamic Diameter (microns)	Percent Penetration	
	1R.11.O.T2	1R.11.O.T3
0.5	50.13	72.17
1	16.50	22.10
1.5	7.07	9.15
2	2.61	2.90
2.5	1.01	1.01
3	0.46	0.41
3.5	0.27	0.22
4	0.15	0.11
4.5	0.09	0.07
5	0.06	0.04

Aerodynamic Diameter (microns)	Percent Penetration		
	2R.11.E.BB1	2R.11.E.CC1	2R.11.E.DD1
0.021	n/a	n/a	n/a
0.038	n/a	n/a	n/a
0.067	17.27	n/a	n/a
0.118	80.19	11.46	18.63
0.210	79.78	18.92	24.84
0.375	60.21	11.22	15.50
0.669	71.51	19.04	10.23
1.182	79.55	14.69	25.61

APPENDIX C

DETERMINATION OF OVERALL MASS COLLECTION EFFICIENCY

The majority of tests conducted during the study were performed using an optical particle counter (OPC) or an electric size aerosol analyzer (EASA). The OPC used light-scattering techniques in order to measure the number of particles in a gas sample. The EASA used electrostatic techniques in order to measure the number of particles in a gas sample. Both of these instruments are frequently used in the field of research to determine the concentration of particles in a gas stream, and to determine the efficiency of systems based on particle numbers. However, in the industrial and regulatory environments, efficiencies are reported on a mass basis, not a number basis. Therefore, efforts were made to conducted tests using particle sampling techniques normally employed in industrial settings.

Initial tests were conducted using an Anderson Mark III cascade impactor. However, the mass mean diameter of the flyash which was fed to the inlet gas stream was so large that most of the particles were collected on the first stage of the impactor, and virtually no particles were collected on any of the other stages. When the impactor was disassembled, particles fell through the holes on the first stage and dropped onto other stages. Therefore, it was impossible to determine which stage was responsible for the collection of the particles.

In order to reduce the mass mean diameter of the particles entering the impactor, a pre-separator was placed directly upstream of the impactor. The cut diameter of the pre-separator was 10 microns. During tests performed with the pre-separator, nearly all of the particles were removed in the pre-separator, and there was no mass gain on any of

the filters in the impactor. The sampling time of these tests ranged from 45 - 120 minutes. Calculations showed that it would be necessary to sample for approximately 5 - 7 hours upstream of the system in order to obtain an appreciable mass gain on the filters in the impactor. Sampling times downstream of the system would be 10 - 20 times longer. Therefore, it was concluded that accurate results in regards to the overall mass collection efficiency of the system would not be obtained using cascade impactors.

It was determined that EPA Method V sampling would provide better results than the cascade impactors in regards to the overall mass collection efficiency of the system. Two EPA Method V sampling trains were borrowed from Oak Ridge National Labs (ORNL) at Oak Ridge, TN. These sampling trains were calibrated by ORNL scientists. Isokinetic tests were conducted with the Method V sampling equipment when the gas flowrate in the system was 900 acfm, the pre-scrubber and packed bed were operating with liquid flowrates of 3.4 gpm and 31.1 gpm to the front and top spray nozzles, respectively, and the ionizer was operating in the automatic mode with an average operating voltage of 31.1 kV. Two consecutive tests were conducted, each with a duration of 75 minutes. Since some deposition of particles occurred in the sampling nozzle and sampling line, an acetone probe and nozzle rinse was conducted after each test. The results of these tests are shown on the following page.

Table C-1. Results of EPA Method V Tests

Duration: 75 minutes 900 acfm - 0.88 acfm in sampling train		
Test 1		
Initial Weights (g)	**Upstream**	**Downstream**
Filter	0.2400	0.2432
Can	51.4962	51.7827
Patch 1	0.4119	0.4035
Patch 2	0.3852	0.4224
Sum	52.5333	52.8518
Final Weights (g)		
Filter	0.2789	0.2473
Can & Patches	52.1541	52.3973
Sum	52.4330	52.6446
Mass of Dust Collected*	0.0389	0.0041
Penetration	10.54	
Efficiency	89.46	
* The weight of the cans and patches were disregarded since the final total weights were less than the initial total weights		

Duration: 75 minutes 900 acfm - 0.88 acfm in sampling train		
Test 2		
Initial Weights (g)	**Upstream**	**Downstream**
Filter	0.2501	0.2677
Can	49.3756	49.3846
Patch 1	0.4124	0.4150
Patch 2	0.3853	0.4030
Sum	50.4234	50.4703
Final Weights (g)		
Filter	0.2754	0.2685
Can & Patches	50.1587	50.1030
Sum	50.4341	50.3715
Mass of Dust Collected*	0.0253	0.0008
Penetration	3.16	
Efficiency	96.84	
* The weight of the cans and patches were disregarded since the final total weights were less than the initial total weights		

The term "can" which is shown in the results on the previous page, refers to the metal sampling can which was used to collect the acetone from the probe and nozzle rinse. The term "patch" refers to the cloth patches which were used to clean the probe and nozzle during the rinse. It should be noted that the final mass of the cans and patches was less than the initial mass of the cans and patches for each test. Therefore, the masses of the cans and patches were disregarded and not included in any calculations.

As shown in the results, Test 1 yielded an overall mass collection efficiency of 89.5%, while Test 2 yielded an overall mass collection efficiency of 96.8%. However, it is important to note that in Test 2, the mass of dust collected was only 0.0008 g. The error in measurement of the filter weights is probably 0.001-0.002 g. Therefore, the reported mass of dust collected is within the error of measurement, and is somewhat suspect.

The overall mass collection efficiency of particles in the aerodynamic size range of 0.5 - 5.0 microns was determined based on the average number of particles sampled upstream of the system and the average number of particles sampled downstream of the system. This test was performed at 900 acfm, the pre-scrubber and packed bed were operating with liquid flowrates of 3.4 gpm and 31.1 gpm to the front and top spray nozzles, respectively, and the ionizer was operating in the automatic mode with an average operating voltage of 31.1 kV. Using a particle density of 2.5 g/cc, the average mass of particles collected upstream of the system was 7.66E-4 grains, while the average mass of particles collected downstream of the system was 2.44E-6 grains. Therefore, the

penetration of the system on a mass basis, for particles with aerodynamic diameters from 0.5 - 5.0 microns, is 0.3%. A summary of these calculations is provided on the following page.

Table C-2. Summary of Overall Mass Collection Efficiency as Measured by an OPC

UPSTREAM						
Aerodynamic Diameter (microns)	**Log-Mean Diameter (microns)**	**Volume of Particle With d=LMD (m^3)**	**Total Number of Particles in Size Range**	**Total Volume of Particles in Size Range (m^3)**	**Total Mass ** of Particles in Size Range (g)**	**Total Mass ** of Particles in Size Range (gr)**
0.5						
	0.71	1.85E-19	105294.6	1.95E-14	4.87E-08	7.52E-07
1						
	1.22	9.62E-19	444965.4	4.28E-13	1.07E-06	1.65E-05
1.5						
	1.73	2.72E-18	373638.2	1.02E-12	2.54E-06	3.92E-05
2						
	2.24	5.85E-18	254569.2	1.49E-12	3.73E-06	5.75E-05
2.5						
	2.74	1.08E-17	182017.8	1.96E-12	4.89E-06	7.55E-05
3						
	3.24	1.78E-17	158301.2	2.82E-12	7.05E-06	1.09E-04
3.5						
	3.74	2.74E-17	135111.2	3.71E-12	9.26E-06	1.43E-04
4						
	4.24	4.00E-17	99008.2	3.96E-12	9.90E-06	1.53E-04
4.5						
	4.74	5.59E-17	79578.8	4.45E-12	1.11E-05	1.72E-04
5						
			Total		**4.96E-05**	**7.66E-04**

DOWNSTREAM						
Aerodynamic Diameter (microns)	**Log-Mean Diameter (microns)**	**Volume of Particle With d=LMD (m^3)**	**Total Number of Particles in Size Range**	**Total Volume of Particles in Size Range (m^3)**	**Total Mass ** of Particles in Size Range (g)**	**Total Mass ** of Particles in Size Range (gr)**
0.5						
	0.71	1.85E-19	6464.8	1.20E-15	2.99E-09	4.62E-08
1						
	1.22	9.62E-19	13723.8	1.32E-14	3.30E-08	5.09E-07
1.5						
	1.73	2.72E-18	6291.4	1.71E-14	4.28E-08	6.60E-07
2						
	2.24	5.85E-18	1920.4	1.12E-14	2.81E-08	4.34E-07
2.5						
	2.74	1.08E-17	553.4	5.95E-15	1.49E-08	2.30E-07
3						
	3.24	1.78E-17	242.6	4.32E-15	1.08E-08	1.67E-07
3.5						
	3.74	2.74E-17	142.4	3.91E-15	9.76E-09	1.51E-07
4						
	4.24	4.00E-17	82.8	3.31E-15	8.28E-09	1.28E-07
4.5						
	4.74	5.59E-17	55.8	3.12E-15	7.80E-09	1.20E-07
5						
			Total		**1.58E-07**	**2.44E-06**

** **BASED ON A PARTICLE DENSITY OF 2.5 g/cc**

APPENDIX D

RESULTS OF FLUORESCENT SPHERE TESTS

As summarized in previous tables, tests were performed with the optical particle counter at locations directly upstream and downstream of the ionizing plates. These tests are referred to as the "wetplate" tests. Since the sampling nozzles were placed only 12 inches upstream and downstream of the plates, it was necessary to use nozzles which were constructed of an insulating material in order to eliminate the possibility of arcing from the plates to the nozzle. Therefore, two identical sampling nozzles were constructed of glass and mounted in the ionizing section.

Although there was no visible evidence of particle build-up or particle collection in the sampling nozzles, there was concern that collection of the highly charged sub-micron particles may be occurring in the sampling nozzles. Therefore, a second, independent method of testing was employed in order to verify the results of the tests conducted with the optical particle counter. The second method involved mounting identical open-faced Teflon filters in the ionizing section at the same locations as the sampling nozzles. The filters were mounted so that their faces were perpendicular to the direction of gas flow. Each of the filters was connected to an EPA Method V sampling train which had been previously calibrated and leak-checked, and operated at a flowrate of 0.83 acfm. Approximately 60 ml of monodisperse fluorescent- green polystyrene latex (PSL) spheres with a diameter of 2 microns and a solids content of 1 percent were mixed with 300 ml of deionized-distilled water. The solution was placed in a TSI single-jet atomizer, and the atomized solution was injected into the inlet gas stream at a location upstream of the pre-scrubber. The gas flowrate during the tests was 900 acfm. Some of

the spheres in the gas stream impacted on the faces of the filters as they passed thru the ionizing section of the system. The filters were then later analyzed to determine the number of spheres which had been collected, and ultimately determine the collection efficiency of the ionizing section.

After a period of 15 minutes, the atomizer was removed from the system, the EPA sampling trains were disconnected, and the filters were removed from the filter holders and placed in clean petri dishes. The filter holders were then washed thoroughly, and the test was repeated. Three consecutive tests were performed at these conditions.

After the tests were conducted, the filters were taken to the lab and analyzed with a 10X microscope under a black light. The black light caused the spheres on the filters to fluoresce, and the number of spheres were physically counted at 10 random locations on each of the filters. The overall penetration based on the number of spheres collected on the filters was determined by the following equation:

$$\text{Fractional Penetration} = 1 - \text{Fractional Efficiency} = \frac{\text{Sum of Spheres Counted Downstream of Ionizer}}{\text{Sum of Spheres Counted Upstream of Ionizer}}$$

As shown in the results on the following pages, penetrations of 2.98%, 3.33%, and 2.51% were calculated for Test 1, Test 2, and Test 3, respectively for the 2 micron fluorescent spheres. The results of the three tests conducted with the optical particle counter at the same operating conditions yielded penetrations of 1.59%, 1.80%, and

1.97% for particles with an aerodynamic diameter of 2 microns. These tests are refered to as tests 2R.09.O.U1, 2R.09.O.U2, and 2R.09.O.U3 in the prior sections. It should be noted that the density of the monodisperse polystyrene latex spheres was 1 g/cc. Therefore, the aerodynamic and physical diameters of those spheres were equivalent.

In conclusion, the results of the tests performed with the fluorescent spheres validate the results that were obtained when testing was conducted with the optical particle counter under the same operating conditions. Therefore, it was concluded that the method of sampling directly upstream and downstream of the ionizing plates using glass nozzles in conjunction with the optical particle counter was valid.

Table D-1. Results of Fluorescent Sphere Tests

Duration: 15 minutes each
2 micron spheres - 900 acfm - directly upstream and downstream of plates with open-faced Teflon filters
60 ml of spheres (1% solids) in approximately 300 ml of distilled-dionized water

Test 1		
Location on Filter	**Upstream Counts**	**Downstream Counts**
1	37	3
2	66	2
3	74	3
4	72	2
5	51	2
6	57	1
7	84	1
8	72	2
9	60	3
10	64	0
Sum	637	19
Penetration	2.98	
Efficiency	97.02	

Test 2		
Location on Filter	**Upstream Counts**	**Downstream Counts**
1	64	2
2	58	5
3	73	1
4	62	2
5	76	2
6	64	3
7	74	1
8	88	2
9	70	1
10	62	4
Sum	691	23
Penetration	3.33	
Efficiency	96.67	

Test 3		
Location on Filter	**Upstream Counts**	**Downstream Counts**
1	57	1
2	67	3
3	61	3
4	70	2
5	78	1
6	47	0
7	64	2
8	54	1
9	54	1
10	85	2
Sum	637	16
Penetration	2.51	
Efficiency	97.49	

APPENDIX E

DETERMINATION OF GRAIN LOADING

The dust loading upstream of the pre-scrubber was calculated for particles with aerodynamic diameters in the range of 0.5 - 5.0 microns, at a gas flowrate in the system of 900 acfm. The optical particle counter was used to sample the flue gas stream upstream of the pre-scrubber. The loading was determined by summing the number of particles in a given size range, and using the log-mean diameter of each of those size ranges to calculate the total volume of particles collected in each size range. The total mass of particles was then determined by using the particle density of 2.5 g/cc. Finally, the masses of particles in each size range were summed to give a total mass of particles collected. Based on a sample volume of 0.25 ft^3, the particle loading at the inlet of the pre-scrubber was determined. A summary of these calculations is provided in Table E-1. The results yield an inlet grain loading to the system of 3.1E-3 gr/ft^3.

Table E-1. Determination of Dust Loading at 900 acfm

Aerodynamic Diameter (microns)	Log-Mean Diameter (microns)	Volume of Particle With d=LMD (m^3)	Total Number of Particles in Size Range	Total Volume of Particles in Size Range (m^3)	Total Mass ** of Particles in Size Range (g)	Total Mass ** of Particles in Size Range (gr)
0.5						
	0.71	1.85E-19	105294.6	1.95E-14	4.87E-08	7.52E-07
1						
	1.22	9.62E-19	444965.4	4.28E-13	1.07E-06	1.65E-05
1.5						
	1.73	2.72E-18	373638.2	1.02E-12	2.54E-06	3.92E-05
2						
	2.24	5.85E-18	254569.2	1.49E-12	3.73E-06	5.75E-05
2.5						
	2.74	1.08E-17	182017.8	1.96E-12	4.89E-06	7.55E-05
3						
	3.24	1.78E-17	158301.2	2.82E-12	7.05E-06	1.09E-04
3.5						
	3.74	2.74E-17	135111.2	3.71E-12	9.26E-06	1.43E-04
4						
	4.24	4.00E-17	99008.2	3.96E-12	9.90E-06	1.53E-04
4.5						
	4.74	5.59E-17	79578.8	4.45E-12	1.11E-05	1.72E-04
5						
			Total		**4.96E-05**	**7.66E-04**

Sample Volume = 0.25 ft^3

Inlet Loading $\frac{\text{7.66E-4 gr}}{\text{0.25 ft}^3} = \text{3.1E-3 gr/ft}^3$

** BASED ON A PARTICLE DENSITY OF 2.5 g/cc

APPENDIX F

SUB-MICRON DROPLET CARRYOVER RESULTS

Droplet carryover from the scrubber downstream of the ionizing section could have a significant negative impact on the overall mass collection efficiency of the IWS unit if the droplets contained dissolved and/or suspended solids. If the concentrations of the total suspended solids (TSS) and the total dissolved solids (TDS) in the sump of the scrubbers were high, and droplet carryover was significant, increased concentrations of particulates downstream of the second scrubber would be present as the droplets began to dry. Therefore, it was important to determine whether droplet carryover occurred in the system, and what effect this carryover had on the overall mass collection efficiency of the system.

During these tests, the particle feed system was disconnected and the ports used with the particle feed system were sealed in order to minimize the number of particles entering the system from the ambient air. The sump of the IWS was spiked with a known quantity of table salt, which yielded a dissolved solids concentration equivalent to the sum of the dissolved and total suspended solids concentration which was measured in the IWS recycle loop at the TSCA incinerator at Oak Ridge, TN during the trial burn in 1989. Measurements were taken upstream and downstream of the system with a TSI Model 3030 Electric Aerosol Size Analyzer (EASA) used in conjunction with a dilution system. The dilution system caused the droplets in the flue gas sample to dry before entering the EASA. Any dissolved salt which was present in the droplets crystallized as the droplets dried, and those salt crystals were measured as particles. Therefore, a direct measurement of the particle loading at the outlet of the IWS due to droplet carryover was made. These

studies were conducted on particles ranging in physical diameter from 0.032 - 0.320 microns

During tests performed at the pilot plant, the pre-scrubber operated with liquid flowrates of 3.4 gpm and 31.1 gpm to the front and upper spray headers respectively. These are the normal operating liquid flowrates in the pilot plant system. Fresh makeup water was supplied to the pre-scrubber sump. The packed bed downstream of the ionizing section operated at the same liquid flowrates as the pre-scrubber. However, makeup water was not supplied to the packed bed, and the sump of the packed bed was spiked with table salt. The amount of table salt added to the sump was determined using the operating conditions at the TSCA incinerator trial burn in 1989:

TSCA Conditions:

TDS = 3360 mg/l
TSS = 315 mg/l
3360 mg/l + 315 mg/l = 3675 mg/l total solids

This solids loading was used to determine the amount of table salt which needed to be added to the sump of the packed bed as follows:

UT Pilot Plant:

primary sump: 79 gals
secondary sump: 83 gals
total: 162 gals

$$3675\frac{mg}{l}solids \times \frac{1g}{1000mg} \times \frac{lb}{453.6g} \times \frac{3.79l}{gal} \times 162gal = 4.48lb$$

Therefore, approximately 4.5 lbs of salt was required to obtain a total solids concentration in the sump equivalent to the total solids concentration in the sump of the TSCA system during the trial burn. Approximately 4.9 lbs of non-iodized table salt was added to the secondary sump of the IWS. The IWS operated for a period of 30 minutes before testing began in order to ensure complete mixing and uniform concentration of the dissolved salt in the water. It is important to once again note that fresh makeup water was not supplied to the packed bed, and there was no blowdown from the packed bed. This ensured a constant concentration of salt in solution.

The EASA was set up at the sampling port downstream of the packed bed. Since the flue gas stream was saturated at this location, and because moisture in the gas stream adversely affected the operation of the EASA, it was necessary to dilute the flue gas sample which was taken from the duct with clean dried air. This was achieved using a desiccant and particulate filter connected to a compressed air line which was then connected to the sampling line. The clean dried dilution air was supplied to the flue gas sample immediately downstream of the sampling nozzle. The EASA sampled 8.2 L/hr. However, 6.56 L/hr of dilution air was supplied to the sampling line, therefore only 1.64 L/hr of flue gas was sampled. The ratio of dilution air to flue gas sample was 4:1.

Droplets which carried over from the packed bed had a concentration of dissolved salt equivalent to the concentration of salt in the sump. When the flue gas sample was

taken from the duct, the droplets dried out after the sample mixed with the clean dried dilution air. Any dissolved salt which was present in the droplet crystallized as the droplet dried, and form a particle. The concentration of these salt crystals in the sample was then used to determine the effect of droplet carryover (i.e. particle carryover) of the system. The results of the droplet carryover studies are shown in Table F-1 and Table F-2.

Table F-1. Mass carryover at p1wp2w and 900 acfm.
Pre-scrubber and packed bed were operating under normal liquid flowrates, and ionizer was not operating.

Particle Diameter (microns)	Outlet Loading* (g particles/cm^3 flue gas)	Outlet Loading* (grains particles/ft^3 flue gas)
0.042	8.52E-14	3.72E-8
0.075	7.21E-13	3.15E-7
0.133	5.67E-11	2.48E-5
0.237	3.82E-11	1.67E-5
Total	**9.57E-11**	**4.18E-5**

Table F-2. Mass carryover at p1w35p2w and 900 acfm.
Pre-scrubber and packed bed were operating under normal liquid flowrates, and ionizer was operating at 35 kV.

Particle Diameter (microns)	Outlet Loading* (g particles/cm^3 flue gas)	Outlet Loading* (grains particles/ft^3 flue gas)
0.042	2.27E-13	9.93E-8
0.075	4.80E-13	2.10E-7
0.133	3.15E-11	1.38E-5
0.237	9.76E-11	4.27E-5
Total	**1.3E-10**	**5.67E-5**

* These outlet loading account for the 4:1 dilution used during sampling, and assume that the density of the salt used in the tests was 2.5 g/cc.

Table F-1 shows the outlet loading of the system when the pre-scrubber was operating under normal conditions with fresh water at 900 acfm, and the packed bed downstream of the ionizer was operating with water that had been spiked with table salt. The ionizer was not operating during these tests. The results show an outlet loading of 4.18E-5 gr/ft^3.

Table F-2 shows the outlet loading of the overall system when the pre-scrubber, ionizer, and packed bed were operating under normal conditions at 900 acfm. The pre-scrubber was operating with fresh water. The ionizer was operating at an average voltage of 31.1 kV, while the packed bed downstream of the ionizer was operating with water that had been spiked with table salt. There was no blowdown from the packed bed, and no makeup water was supplied to the packed bed. This assured a constant concentration of salt in solution. As indicated, the outlet loading in the size range of 0.032 - 0.320 microns was 5.67E-5 gr/ft^3.

In conclusion, the mass carryover from the system in the sub-micron size range appears to be negligible. Although the total numbers of droplets which carry over from the packed bed may be high, the effect on the overall mass collection efficiency is negligible since the concentration of solids in the IWS sump is relatively low.

Since the sump of the pre-scrubber was not spiked, only the effect of droplet carryover from the packed bed downstream of the ionizer was studied. However, even if droplet carryover from the pre-scrubber was significant, the effect on the overall mass

collection efficiency of the system would be negligible since the droplets which carried over would be collected in the IWS unit.

APPENDIX G

DROPLET CARRYOVER RESULTS FOR 0.5 - 5.0 MICRON DIAMETERS

Droplet carryover in the aerodynamic size range of 0.5 - 5.0 microns was measured with the optical particle counter. This test was performed at 900 acfm, the pre-scrubber and packed bed were operating with liquid flowrates of 3.4 gpm and 31.1 gpm to the front and top spray nozzles, respectively, and the ionizer was operating in the automatic mode with an average voltage of 31.1 kV. The pre-scrubber and packed bed were filled with 2" Type-R Tellerettes. The particle feed system was disconnected and the ports used with the particle feed system were sealed. The sumps of the pre-scrubber and packed bed were drained and subsequently filled with fresh water in order to minimize the amount of solids in the scrubbing water.

Measurements were taken with the OPC upstream and downstream of the system. The measurements taken upstream of the system provided a background concentration of particles in the system. The background concentration of particles in the system was negligible. The total volume of droplets was determined by summing the number of droplets in given size ranges, and using the average diameter of each of those size ranges to calculate the total volume of droplets collected in each size range. The volumes of droplets in each size range were summed to determine a total volume of droplet carryover. The total volume of droplets collected in a 0.25 ft^3 sample was 3.5E-12 m^3.

As discussed in the section on sub-micron droplet carryover, the TSCA incinerator at Oak Ridge, TN had a total solids loading in the IWS recycle loop of 3,675 mg/L during the 1989 trial burn. Based on this concentration of solids in the sump, the amount of mass which would carry over in the form of dissolved and/or suspended solids

in the droplets is 1.29E-5 mg. Based on a sample volume of 0.25 ft^3, the outlet loading was determined to be approximately 8E-7 gr/ft^3. This loading due to droplet carryover is negligible, and would not have an impact on the overall mass collection efficiency of the TSCA incinerator.

A summary of the calculations is provided in Table G-1. Figure G-1 shows the inlet and outlet counts as a function of channel number for aerodynamic diameters of 0.5 - 5.0 microns.

Table G-1. Results of Droplet Carryover Measurements

900 acfm - p1w35p2w - 2" Type-R Tellerettes - no dust feed into inlet				
Aerodynamic Diameter of Droplet (microns)	**Average Diameter of Droplet (microns)**	**Average Number of Droplets Measured in Size Range**	**Volume of a Single Droplet (m3)**	**Total Volume of Droplets in Size Range (m3)**
0.5				
	0.75	130752.8	2.20893E-19	2.89E-14
1				
	1.25	289814.4	1.02265E-18	2.96E-13
1.5				
	1.75	161523	2.80616E-18	4.53E-13
2				
	2.25	89917.4	5.96411E-18	5.36E-13
2.5				
	2.75	49527.2	1.08892E-17	5.39E-13
3				
	3.25	30833.8	1.79741E-17	5.54E-13
3.5				
	3.75	17813.2	2.76116E-17	4.92E-13
4				
	4.25	8401	4.01944E-17	3.38E-13
4.5				
	4.75	4891.6	5.6115E-17	2.74E-13
5				
		Total Volume of Droplets Sampled		**3.51E-12**

Based on a TSCA Sump Loading = 3675 mg/L

$$3.51E\text{-}12\ m3 \times \frac{1000\ L}{1\ m3} \times \frac{3675\ mg}{L} = 1.29E\text{-}5\ mg$$

Total Flue Gas Volume Sampled = 0.25 ft3

Outlet Loading

$$1.29E\text{-}5\ mg \times \frac{1\ g}{1000\ mg} \times \frac{7000\ gr}{453.6\ g} \times \frac{1}{0.25\ ft3}$$

$$= 7.96E\text{-}7\ gr/ft3$$

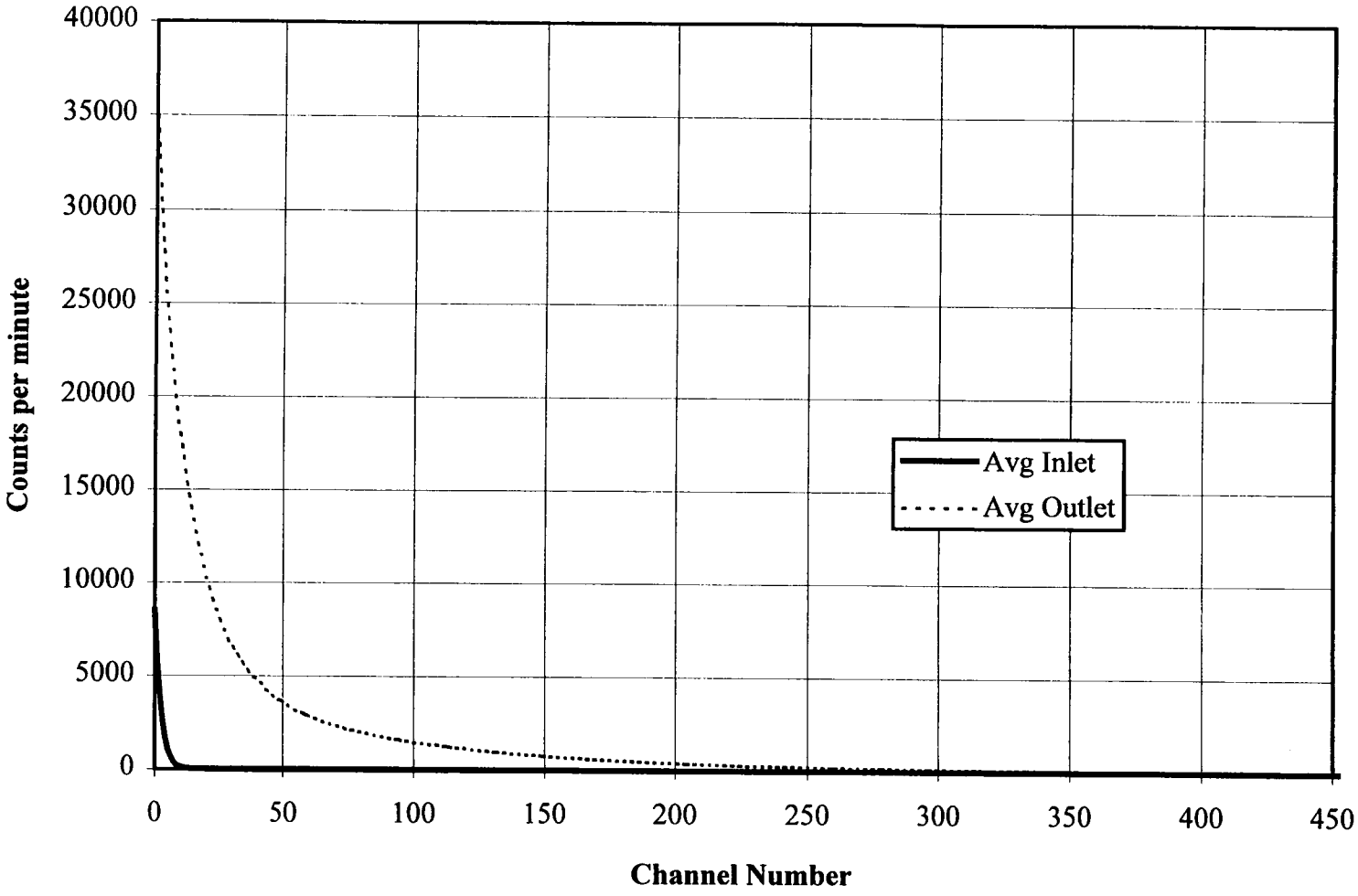

Figure G-1. Inlet and Outlet Counts VS Channel Number for 0.5 - 5.0 micron Particles at p1w35p2w, 2" Type-R Tellerettes, No Dust Feed into Inlet

VITA

Thomas C. Morse was born in Kankakee, Illinois on February 1, 1970. He attended the public school system in Momence, Illinois, and graduated from Momence Community High School in May 1988. After high school, he worked as a technician for the Sangamon County Highway Department in Springfield, Illinois, and also studied pre-engineering at Lincoln Land Community College. In August, 1992 he entered Southern Illinois University and received a Bachelor's degree in May, 1995 in mechanical engineering. He joined the Master's program in environmental engineering at the University of Tennessee at Knoxville in June, 1995. He completed the requirements for his Master's degree in September, 1996.

He is currently a member of the Air and Waste Management Association, the American Society of Mechanical Engineers, and a member of Tau Beta Pi, the national honor society. He will be employed as an environmental engineer specializing in particulate control at Precision Combustion Incorporated in New Haven, Connecticut.